DEPARTMENT OF PHYSICS
UNIVERSITY OF JYVÄSKYLÄ
RESEARCH REPORT No. 1/2018

HYDROGEN PLASMA INDUCED PHOTOELECTRON EMISSION FROM METAL SURFACES

BY

JANNE LAULAINEN

Academic Dissertation
for the Degree of
Doctor of Philosophy

To be presented, by permission of the
Faculty of Mathematics and Science
of the University of Jyväskylä,
for public examination in Auditorium FYS1 of the
University of Jyväskylä on January 19th, 2018
at 12 o'clock noon

Jyväskylä, Finland
January 2018

ABSTRACT

Laulainen, Janne
Hydrogen plasma induced photoelectron emission from metal surfaces
Jyväskylä: University of Jyväskylä, 2018, 70 p. (+included articles)
Department of Physics Research Report No. 1/2018
ISSN 0075-465X
ISBN 978-951-39-7327-8 (paper copy)
ISBN 978-951-39-7328-5 (PDF)
Diss.

Low temperature hydrogen plasmas are strong sources of vacuum ultraviolet radiation. The properties of laboratory plasmas can be influenced by surface processes induced by photons with their energies exceeding the surface work function of the wall material.

In this work, the plasma induced photoelectron emission has been studied with different ion sources. The emission depends on the mechanical design of the plasma device, plasma heating method and the discharge power (density). Parametric studies include the quantifying of the emission from different metal surfaces, commonly used as plasma facing materials in ion sources, as well as alkali metal covered surfaces. Experimental studies suggest that low temperature hydrogen plasma induced photoelectron emission from metal surfaces can reach an order of magnitude of 1 A per kW of plasma heating power. Furthermore, the emission can increase 2–3.5 times when the metal surface is coated with a thin layer of alkali metal reducing the work function. The free electrons produced by the photoelectron emission can influence various plasma processes and especially the plasma sheath structure, which has been studied using a one-dimensional analytical model.

Keywords: low temperature hydrogen plasma, photoelectron emission, ion source

Author

Janne Laulainen
Department of Physics
University of Jyväskylä
Jyväskylä, Finland

Supervisor

Dr. Olli Tarvainen
Department of Physics
University of Jyväskylä
Jyväskylä, Finland

Reviewers

Dr. Jacques Lettry
Beams Department
European Organization for Nuclear Research (CERN)
Geneva, Switzerland

Prof. Katsuyoshi Tsumori
Plasma Heating Physics Research Division
National Institute for Fusion Science (NIFS)
Oroshi Toki, Gifu, Japan

Opponent

Dr. Dan Faircloth
Low Energy Beams Group
ISIS, Rutherford Appleton Laboratory
Oxfordshire, United Kingdom

TIIVISTELMÄ (ABSTRACT IN FINNISH)

Matalan lämpötilan vetyplasman tuottama ultraviolettisäteily aiheuttaa metallipinnoilla valosähköistä ilmiötä, mikä tuottaa vapaita fotoelektroneja kaikissa laboratorioplasmoissa. Tässä väitöskirjassa tutkitaan valosähköisen ilmiön merkitystä ionilähteiden plasman kannalta. Väitöskirjassa raportoidaan valosähköisen ilmiön voimakkuus ionilähdeolosuhteissa sekä arvioidaan ilmiön merkitystä ionilähteiden toiminnan kannalta kokeellisiin havaintoihin pohjautuen.

Erityyppisillä ionilähteillä suoritettujen mittausten perusteella ilmiön on havaittu riippuvan ionilähteen mekaanisesta suunnittelusta, plasman lämmitystavasta sekä plasmaan syötetystä tehosta. Mittauksia suoritettiin tyypillisesti ionilähteissä käytettävillä metalleilla, mukaan lukien alkalimetallilla päällystetyillä pinnoilla.

Kokeellisten tulosten perusteella plasmakammion seiniltä irtoavien fotoelektronien kokonaisvirran plasmaan syötettyä tehoa kohden voidaan todeta olevan suuruusluokaltaan 1 A/kW. Negatiivisissa vetyionilähteissä käytetään tyypillisesti cesiumia pienentämään konversiopinnan irrotustyötä, mikä parantaa ionilähteiden toimintaa. Päällystämällä metallipinta ohuella alkalimetallikerroksella valosähköisen ilmiön voimakkuus voi mittausten perusteella kasvaa 2–3,5-kertaiseksi.

Valosähköisen ilmiön tuottamat vapaat elektronit voivat osallistua useisiin eri reaktioihin ja vaikuttaa sitä kautta plasman ominaisuuksiin. Plasmakammion seiniltä irtoavien elektronien avaruusvaraus voi myös muuttaa seinän ja plasman välille muodostuvan rajakerroksen, niin sanotun plasmavaipan rakennetta. Tässä työssä määritettyä suuruusluokkaa valosähköiselle ilmiölle voidaan soveltaa esimerkiksi simulaatioissa, joilla tutkitaan ionilähteiden toimintaa.

PREFACE

The work reported in this thesis has been carried out at the accelerator laboratory of the Department of Physics of the University of Jyväskylä during the years 2013–2017.

First of all, I want to sincerely thank my supervisor Dr. Olli Tarvainen for all the help and guidance that I have received over the years. This work would not have been possible without the valuable instructions and great ideas. I want to express my gratitude to Dr. Hannu Koivisto for introducing me to the world of ion sources already back in 2011 and for the possibility to work in the ion source group.

I would like to thank Prof. Panagiotis Svarnas and Dr. Spyridon Aleiferis for the fruitful collaboration and the possibility to visit their laboratory in Patras, Greece. I want to thank Dr. Jacques Lettry and Prof. Katsuyoshi Tsumori for reviewing my thesis.

I want to thank all the past and current ion source group members. Special thanks goes to Dr. Jani Komppula for all the help during the time we shared the basement laboratory. Dr. Taneli Kalvas is gratefully acknowledged for all the help with simulations and experimental work. I want to thank Dr. Ville Toivanen and Mr. Risto Kronholm for collaboration and enjoyable time. I would also like to express my most sincere thanks to all the friends and colleagues at the Department.

Finally, I want to thank all my family and friends outside the University for the unforgettable moments and spare time activities. I am especially thankful to my mother, who has always supported and encouraged me in my studies. Last but not least, Anne, thank you for everything.

Jyväskylä, January 2018

Janne Laulainen

ACKNOWLEDGEMENTS

This work has been supported by the Academy of Finland under the Finnish Centre of Excellence Programme 2012–2017 (Nuclear and Accelerator Based Physics Research at JYFL) and the European Union's Horizon 2020 research and innovation programme under Grant Agreement No. 654002.

LIST OF INCLUDED ARTICLES

PI Janne Laulainen, Taneli Kalvas, Hannu Koivisto, Jani Komppula, and Olli Tarvainen. Photoelectron emission from metal surfaces induced by VUV-emission of filament driven hydrogen arc discharge plasma. *AIP Conference Proceedings* ***1655****, 020007 (2015)*.

PII Janne Laulainen, Taneli Kalvas, Hannu Koivisto, Jani Komppula, Risto Kronholm, and Olli Tarvainen. Photoelectron emission from metal surfaces induced by radiation emitted by a 14 GHz electron cyclotron resonance ion source. *Review of Scientific Instruments* ***87****, 02A506 (2016)*.

PIII Janne Laulainen, Taneli Kalvas, Hannu Koivisto, Risto Kronholm, Olli Tarvainen, Spyridon Aleiferis, and Panagiotis Svarnas. Photoelectron emission experiments with ECR-driven multi-dipolar negative ion plasma source. *AIP Conference Proceedings* ***1869****, 020012 (2017)*.

PIV Janne Laulainen, Spyridon Aleiferis, Taneli Kalvas, Hannu Koivisto, Risto Kronholm, and Olli Tarvainen. Hydrogen plasma induced photoelectron emission from low work function cesium covered metal surfaces. *Physics of Plasmas* ***24****, 103502 (2017)*.

PV Janne Laulainen, Taneli Kalvas, Hannu Koivisto, Risto Kronholm, and Olli Tarvainen. Photoelectron emission induced by low temperature hydrogen plasmas. *Accepted for publication in AIP Conference Proceedings (2018)*.

The author of this thesis has performed most of the experimental work and the data analysis and has written the manuscripts in all of the publications. The publications listed above are included in the appendices of the thesis.

CONTENTS

1 INTRODUCTION

This work discusses the photoelectric effect in H^+/H^- (D^+/D^-) ion sources. Positive hydrogen and deuterium ions are straightforward to produce in comparison to negative ions. Maximum (pulsed) currents extracted from modern single aperture H^+/D^+ ion sources can reach values of 500 mA [1], while maximum H^- currents of 100 mA have been reached to date [2]. Positive hydrogen ions are used in high current accelerators and, for example, in long pulse spallation neutron production [3] and in materials irradiation studies for fusion machine development [4]. Also, positive ions are used for neutral beam injection into fusion machines at beam energies less than 100 keV [5].

Negative ions are attractive for the same reason they are difficult to produce, i.e. the ease of detaching the electron from the ion. Negative hydrogen and deuterium ion sources, in which the ions are produced in the plasma volume or on a surface in interaction with the plasma, are used for a variety of applications. For example, at the Department of Physics of the University of Jyväskylä (JYFL), H^-/D^- ions are used in accelerator based nuclear physics with two cyclotrons (K130, MCC30/15), because they allow more efficient ion beam extraction in comparison to protons through charge exchange [6]. At JYFL, negative ions are also used in tandem accelerator (Pelletron), whose operation principle is based on stripping electrons from energetic negative ion beam [7]. Injection of very fast neutral atoms at energies around 1 MeV is an effective method for heating large thermonuclear fusion machine plasmas to ignition temperatures and for non-inductive current drive [8, 9]. Negative ions are used in large-scale accelerator facilities using charge exchange injection into circular accelerators and storage rings e.g. in spallation neutron sources [10], and in isotope production with cyclotrons [11]. In addition to ion sources, low temperature hydrogen plasmas are used, for example, in plasma thrusters [12, 13] and material processing [14, 15].

The motivation for this study arises from the observation that low temperature

hydrogen plasmas are strong sources of vacuum ultraviolet (VUV) radiation. Up to 30 % of the plasma heating power is dissipated through VUV emission in low temperature hydrogen plasmas of positive (H^+/D^+) and negative (H^-/D^-) ion sources [16, 17, 18, 19]. This raises questions about the importance of surface processes induced by radiation emitted from the plasma with energy exceeding the work function of the surface. Plasma induced photoelectron (PE) emission is a fundamental process, which acts as a source of free electrons in all laboratory plasmas. The question about the role of PE emission in ion sources has persisted at least three decades [20], but experimental results for plasma induced PE emission in ion source relevant conditions have not been available prior to this work. The objective of this study is to quantify the PE yield in low temperature hydrogen plasma sources and identify the effects of plasma induced PE emission on the plasma properties and performance of ion sources.

In addition to the intense VUV photon flux from hydrogen plasmas, negative hydrogen ion sources are attractive for PE emission studies, because surface properties and surface–plasma interactions play a fundamental role in their operation principle. In particular, cesium is commonly used to enhance the surface production of negative ions. Lowering the work function by a thin layer of cesium can enhance not only the negative ion production, but also all other processes related to a low work function, such as the PE emission. In positive ion sources, the plasma wall material has an important role as well, since it influences dissociation, ionization, and recombination of the plasma, and thereby affects the $H^+/H_2^+/H_3^+$ species fraction [21].

The plasma induced PE emission can be measured using a remote sample illuminated by light emitted from the plasma. The total magnitude of the PE emission from the internal surfaces determined from the experimental studies can be used to evaluate the influence of PEs on the plasma properties. Depending on the intensity and the energy distribution of the emitted electrons, free electrons produced by the PE emission can contribute to various electron impact processes and additional space charge caused by the PE emission can change the plasma sheath structure, thereby affecting the negative ion yield.

The thesis is outlined as follows. The physical background related to the study of PE emission induced by low temperature hydrogen plasmas is briefly introduced in Chapter 2. The experimental methods used for PE emission measurements are described in Chapter 3. The experimental results for PE emission from clean metal surfaces and alkali metal covered surfaces are presented in Chapter 4 and 5, respectively. The effect of PEs on the properties of low temperature hydrogen plasmas is evaluated in Chapter 6. Finally, the relevance and implications of the work are discussed in Chapter 7.

2 HYDROGEN ION SOURCES AND PHOTOELECTRIC EFFECT

This chapter discusses basic plasma processes relevant for hydrogen ion source plasmas. As plasma physics is an extensive topic the reader is referred to standard textbooks, e.g. References [22, 23, 24, 25], for more detailed discussion on the topic in wider context.

2.1 Plasma ion sources

The basic operation principle of a plasma ion source is to create a plasma containing the desired ion species and extract them from the plasma chamber. Ion sources are typically categorized by the plasma or ion formation mechanism. In this work, emphasis is on low temperature ion source plasmas, which are sustained either by transferring energy to the plasma by thermionic emission from a biased filament or through an interaction between the electrons and the microwave radiation. Other methods for sustaining the plasma include, for example, cold cathodes and radiofrequency (RF) radiation. Due to particle and radiative losses, constant heating is required to sustain the plasma by inelastic collisions between the plasma particles and hot electrons with energies exceeding the ionization potential of the neutral gas (atoms or molecules). Schematic illustrations of a filament-driven (negative) hydrogen ion source and a microwave-driven (positive) hydrogen ion source are presented in Figure 2.1.

In filament-driven arc discharge, free electrons, capable of ionizing or exciting neutral atoms or molecules from their ground states, are produced by thermionic emission from a hot cathode. The emitted electrons are accelerated by applying a negative potential to the filament with respect to the plasma chamber and the

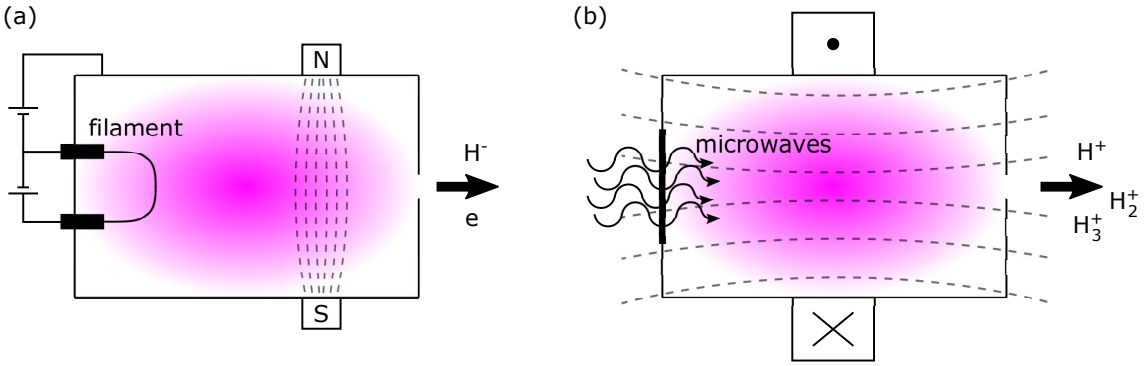

FIGURE 2.1 Schematic illustration of (a) a filament-driven (negative) hydrogen ion source and (b) a microwave-driven (positive) hydrogen ion source. Plasma is illustrated with magenta and the dashed lines represent the magnetic field lines.

plasma itself. In ion sources, the most commonly used filament materials are metals with high melting temperatures, such as tantalum and tungsten. The filament material is constantly evaporated and accumulates onto the plasma chamber walls, which complicates the use of filament-driven sources for surface production of negative hydrogen ions (see Section 2.1.3). Multi-cusp magnetic field structure is typically utilized to confine the plasma. Permanent magnets, with alternating polarities facing towards the plasma, are placed on the plasma chamber wall. As a result, there is a strong magnetic field close to the walls and a low magnetic field in a relatively large volume at the center of the chamber. The use of the cusp field allows the electrons emitted from the filament(s) to be confined and effectively dissipate their energy, thus improving the power efficiency of the discharge.

Plasma heating with microwave radiation is typically based on electron cyclotron resonance (ECR). Electrons, heated by the electric field of the microwaves, move on helical trajectories around magnetic field lines in between Coulombic collisions affecting their trajectories. The microwave power is efficiently transferred to the electrons, when the electrons pass through so-called resonance zone (magnetic field isosurface) in correct phase with respect to the microwave electric field [26]. The ECR condition is satisfied when the microwave frequency ω_{RF} equals the electron gyrofrequency ω_{ce} in the static external magnetic field, i.e.

$$\omega_{\mathrm{RF}} = \omega_{\mathrm{ce}} = \frac{eB}{m_{\mathrm{e}}}, \tag{2.1}$$

where e is the electron charge, m_{e} the electron mass, and B the magnetic field strength. For example, the magnetic field strength of 87.5 mT fulfills the resonance condition for 2.45 GHz, which is a commonly used microwave frequency in hydrogen ion sources. The microwave power can be injected to the plasma directly from a waveguide or using antennas. Often microwave-driven ion sources (especially

H^+ sources) operate in so-called overdense mode, in which case up to 100–500 mA proton beams can be extracted [1, 27]. Microwave sources have been used for H^- production with variable results [28].

Low temperature hydrogen plasmas are sustained by inelastic electron–atom and electron–molecule collisions. Sources of free electrons in laboratory plasmas are ionization, cathodes and the surfaces of the plasma chamber, where electrons can be emitted by secondary electron or PE emission. The surfaces can also be sources of ions and neutrals through secondary ion emission, wall sputtering, and surface conversion of negative ions, for example. In low temperature plasmas, the electron temperature is relatively low (< 15 eV), and the plasma is sustained by the high energy tail of the electron distribution (see Section 2.1.1). Due to energy dissipation and plasma confinement, it can be assumed that the average energy of electrons escaping the plasma and impinging on the chamber walls is low (in the order of few eV). In this case, the secondary electron emission yield is practically zero [29]. The secondary electron emission can be considered as a source of electrons only when the yield exceeds unity, for which the energy of the primary electrons has to be at least several tens of eV, and the absolute yield depends on the surface condition [29, 30]. However, in Reference [29], the reflection coefficient of low energy electrons (on copper surface in low temperature) is reported to be considerable. This thesis concentrates on the PE emission, which can be considered to be the prevailing electron emission process from the walls exposed to radiation and particle fluxes of low temperature hydrogen plasmas.

2.1.1 Electron energy distribution

In low temperature plasmas, the volumetric rates of most plasma processes, such as ionization, excitation and dissociation, are dominated by inelastic collisions between hot electrons and other plasma particles. In these processes, the energy of the colliding electron is of paramount significance as outlined below. The electron population of the plasma can be described by the electron energy distribution function (EEDF), which yields the number density of electrons at a given energy range.

Microwave heated plasmas are often considered to follow the Maxwell-Boltzmann distribution [22, 31], also referred to as Maxwellian, or the Druyvesteyn distribution [32], which assumes that the electron temperature is much greater than the ion and neutral temperature and that the primary interactions occur between electrons and neutral particles. As the Maxwellian distribution is mathematically more simple, it is used as an example in the following. The Maxwellian distribution $f_{\mathrm{M}}(E_{\mathrm{e}})$ represents an electron population in thermodynamic equilibrium and

is written as

$$f_{\mathrm{M}}(E_{\mathrm{e}})\mathrm{d}E_{\mathrm{e}} = \frac{2}{\sqrt{\pi}} \frac{\sqrt{E_{\mathrm{e}}}}{(k_{\mathrm{B}}T_{\mathrm{e}})^{\frac{3}{2}}} \exp\left(\frac{-E_{\mathrm{e}}}{k_{\mathrm{B}}T_{\mathrm{e}}}\right) \mathrm{d}E_{\mathrm{e}}, \tag{2.2}$$

where k_{B} is the Boltzmann constant, T_{e} the electron temperature, E_{e} the electron energy. Only in the case of Maxwellian distribution, the designation of a temperature can be used in a thermodynamic meaning. If the electron energy distribution follows the Maxwell-Boltzmann distribution, the definition of temperature corresponds to the width of the distribution. For other distibutions, the concept of temperature corresponds to the mean particle energy

$$\langle E_{\mathrm{e}} \rangle_{\mathrm{M}} = \frac{3}{2} k_{\mathrm{B}} T_{\mathrm{e}}. \tag{2.3}$$

Typically in ECR plasmas operating in low pressure, two electron populations with $T_{\mathrm{e,cold}}$ and $T_{\mathrm{e,hot}}$ are found [33, 34]. The resulting bi-Maxwellian distribution $f_{\mathrm{bi-M}}(E_{\mathrm{e}})$ is written as

$$\begin{aligned} f_{\mathrm{bi-M}}(E_{\mathrm{e}})\mathrm{d}E_{\mathrm{e}} =& (1-\beta)\frac{2}{\sqrt{\pi}} \frac{\sqrt{E_{\mathrm{e}}}}{(k_{\mathrm{B}}T_{\mathrm{e,cold}})^{\frac{3}{2}}} \exp\left(\frac{-E_{\mathrm{e}}}{k_{\mathrm{B}}T_{\mathrm{e,cold}}}\right) \mathrm{d}E_{\mathrm{e}} \\ &+ \beta\frac{2}{\sqrt{\pi}} \frac{\sqrt{E_{\mathrm{e}}}}{(k_{\mathrm{B}}T_{\mathrm{e,hot}})^{\frac{3}{2}}} \exp\left(\frac{-E_{\mathrm{e}}}{k_{\mathrm{B}}T_{\mathrm{e,hot}}}\right) \mathrm{d}E_{\mathrm{e}}, \end{aligned} \tag{2.4}$$

where the population with $T_{\mathrm{e,hot}}$ is assigned to contribute to the total electron density with a fraction β [33]. For example, in Reference [35], a bi-Maxwellian EEDF is measured from an ECR plasma using a Langmuir probe. Typical temperatures of the cold and hot electron populations of the ECR plasma are 1–5 eV and $\geq$ 10 eV, respectively. The cold electron population is produced mainly by ionization and the hot population is heated locally by the resonant interaction with the microwaves.

In arc discharge, the EEDF typically spans from very low energies up to the energy corresponding to the potential difference between the plasma and the cathode $E_{\mathrm{e,max}}$, thus forming a rather uniform distribution [36]. The uniform distribution $f_{\mathrm{U}}(E_{\mathrm{e}})$ can be described mathematically as

$$f_{\mathrm{U}}(E_{\mathrm{e}}) = \begin{cases} \frac{1}{E_{\mathrm{e,max}}} & \text{when } E_{\mathrm{e}} \leq E_{\mathrm{e,max}} \\ 0 & \text{when } E_{\mathrm{e}} > E_{\mathrm{e,max}}. \end{cases} \tag{2.5}$$

For uniform distribution the mean energy is given by

$$\langle E_{\mathrm{e}} \rangle_{\mathrm{U}} = \frac{1}{2} E_{\mathrm{e,max}}. \tag{2.6}$$

The power efficiency of the arc discharge is typically higher in comparison to the microwave discharge. This is because all the hot electrons are accelerated

by the filament potential directly to an energy of several tens of eV, which is optimal for the ionization of the hydrogen gas. In a multi-cusp confinement, the electrons, which are not actively heated in the plasma volume, deposit their energy efficiently in multiple inelastic collisions before escaping to the chamber walls. In the microwave discharge, on the other hand, the electrons released via ionization processes initially have low energies and are heated in the plasma volume with only a small fraction of them gaining enough energy for ionization.

The probability for an electron impact process is described by the cross section σ_k for reaction k. The cross section is a function of the kinetic energy of the incident electron. The rate coefficient k_k for a collision process k is defined as the average of the product of the collision cross section and the relative velocity of the colliding particles. When electrons collide with heavy particles (neutral atoms or ions), the rate coefficient can be calculated treating the heavy particles as a stationary background and only using the electron velocity. The rate coefficients for excitation and ionization processes can be calculated by weighting the electron velocity according to the EEDF:

$$k_k = \int_0^\infty \sigma_k(E_\mathrm{e}) \sqrt{\frac{2eE_\mathrm{e}}{m_\mathrm{e}}} f(E_\mathrm{e})\, \mathrm{d}E_\mathrm{e}. \tag{2.7}$$

The volumetric reaction rate R_k of a two-body collision process can be calculated by multiplying the rate coefficient with the densities of the two colliding species n_i and n_j:

$$R_k = n_\mathrm{i} n_\mathrm{j} k_k. \tag{2.8}$$

2.1.2 Electron impact ionization

The predominant electron impact processes leading to the formation of positive ions in hydrogen plasmas are [37]

$$\mathrm{e} + \mathrm{H} \rightarrow \mathrm{H}^+ + 2\mathrm{e} \tag{2.9}$$
$$\mathrm{e} + \mathrm{H_2} \rightarrow \mathrm{H}^+ + \mathrm{H} + 2\mathrm{e} \tag{2.10}$$
$$\mathrm{e} + \mathrm{H_2} \rightarrow \mathrm{H_2^+} + 2\mathrm{e} \tag{2.11}$$
$$\mathrm{e} + \mathrm{H_2^+} \rightarrow \mathrm{H}^+ + \mathrm{H} + \mathrm{e} \tag{2.12}$$
$$\mathrm{H_2} + \mathrm{H_2^+} \rightarrow \mathrm{H_3^+} + \mathrm{H} \tag{2.13}$$
$$\mathrm{e} + \mathrm{H_3^+} \rightarrow \mathrm{H}^+ + 2\mathrm{H} + 2\mathrm{e}. \tag{2.14}$$

Cross sections of reactions (2.9)–(2.11) are presented in Figure 2.2. In typical hydrogen ion sources, the main production channel of protons is considered to be process (2.10). Although this process has a low cross section in comparison to other reactions, such as (2.9) and (2.11), the molecular H_2 is most often the dominant gas species which explains the importance of the given dissociative

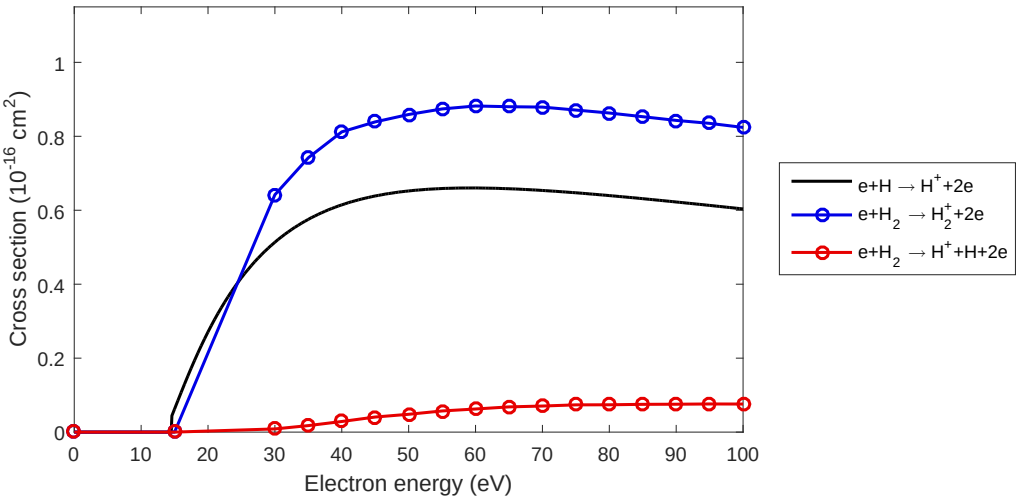

FIGURE 2.2 Cross sections of electron impact ionization of hydrogen. Cross section data is from References [38, 39].

ionization process. The reaction rates of other processes are smaller due to the relatively low densities of neutral hydrogen atoms and molecular ions.

Figure 2.3 presents the rate coefficients calculated from Equation (2.7) for total ionization of hydrogen molecule (defined as sum of cross sections for reactions (2.10) and (2.11)) assuming Maxwellian distribution and a uniform distribution representing the microwave and arc discharge plasmas. The threshold energy for molecular ionization is 16 eV. The rate coefficients for ionization (and excitation) reactions depend strongly on the EEDF. For the Maxwellian EEDF of low tempera-

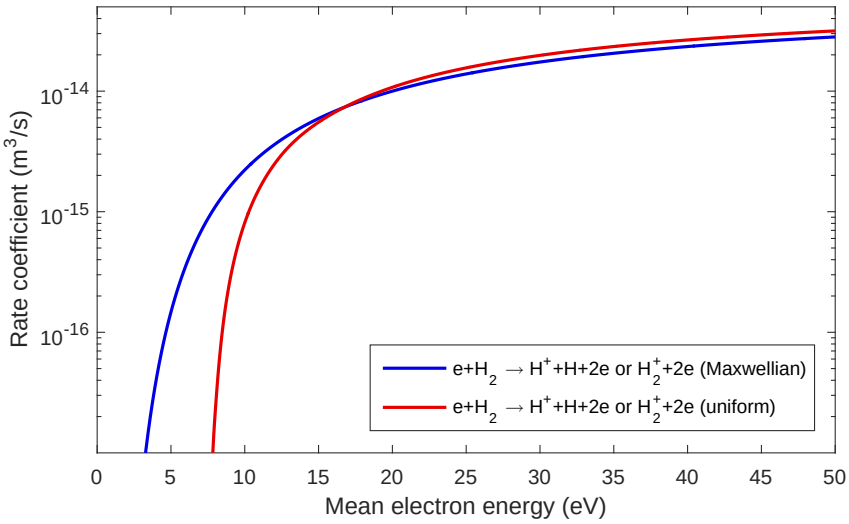

FIGURE 2.3 The rate coefficient for electron impact ionization of a hydrogen molecule as a function of mean electron energy for Maxwellian and uniform EEDF. Calculated using the total ionization cross sections of hydrogen molecule from Reference [39].

ture plasmas, the density of hot electrons in the tail of the distribution decreases exponentially at energies higher than the ionization threshold. For the uniform EEDF, the rate coefficient is higher when mean electron energy exceeds 17 eV (filament potential 34 V). However, this does not automatically mean that the ionization efficiency would be better in filament-driven sources, since other processes and particle densities need to be taken into account, which requires global collisional radiative modelling.

2.1.3 Negative hydrogen production

Negative hydrogen ion sources are often categorized by the dominant negative ion production channel, i.e. volume or surface production. Although both plasma–volume and plasma–surface processes are always involved in negative ion sources, the desired process can be enhanced by the source design.

Volume production of negative ions is a process in which negative ions are formed by electron–molecule and electron–ion collision processes in the volume of the discharge plasma [40]. The predominant volume production channel of negative hydrogen ions is dissociative electron attachment (DEA) by a collision between a cold electron and a vibrationally excited H_2 molecule in the ground electronic $X^1\Sigma_g^+$ state:

$$e_{cold} + H_2(X^1\Sigma_g^+; v'') \rightarrow H_2^-(^2\Sigma_u^+) \rightarrow H^- + H. \tag{2.15}$$

An effective source of vibrationally excited molecules with $v'' > 8$ is radiative decay from $B^1\Sigma_u^+$ and $C^1\Pi_u$ singlet states, excited by collisions of ground state molecules with energetic primary electrons [41]:

$$e_{hot} + H_2 \rightarrow H_2(B^1\Sigma_u^+ \text{ or } C^1\Pi_u) \rightarrow H_2(X^1\Sigma_g^+; v'') + h\nu. \tag{2.16}$$

Also the plasma chamber walls contribute to volume produced negative ion yield by affecting the production of vibrationally excited molecules via recombinative desorption [40, 42].

In tandem-type negative ion sources, a transverse magnetic filter field is used to separate the discharge chamber to so-called driver and negative ion production / extraction regions, as illustrated in Figure 2.4. The warm and dense plasma in the driver produces electrons and vibrationally excited molecules. Low energy electrons and vibrationally excited neutral molecules diffuse through the transverse filter field to the region, where negative ions are produced predominantly via DEA and further extracted from the ion source. The average energy of the electrons diffusing through the filter field is considerably lower than that of electrons in the driver-volume, which is advantageous for DEA and for the survival of negative ions from electron detachment. The volume production can be enhanced by increasing the densities of low energy electrons and hydrogen molecules on high

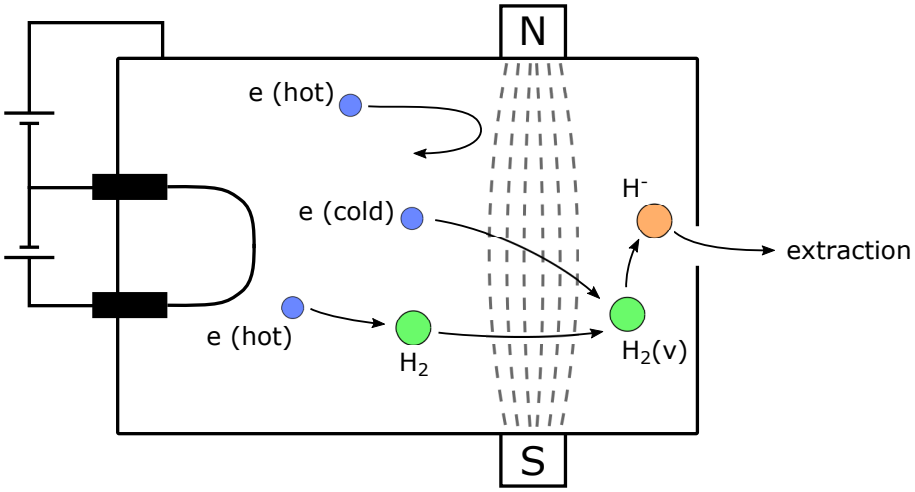

FIGURE 2.4 Schematic illustration of negative hydrogen ion formation in volume production ion source. The dashed lines indicate the transverse filter field.

vibrational levels [40]. The filter field decreases the electron to negative ion ratio of the extracted beam and can also lead to formation of a strongly electronegative plasma in the filter region, especially when the negative ion density is increased by surface production [43, 44, 45].

The surface production of negative hydrogen ions is based on electron tunneling from the conduction band of a metal to the affinity level of a hydrogen atom [46]. Surface production is illustrated in Figure 2.5. Negative ions are produced via the surface conversion process, where hydrogen atoms or ions obtain one or more electrons from the surface:

$$e_{surface} + H \rightarrow H^- \tag{2.17}$$

$$2e_{surface} + H_x^+ \rightarrow H^- + H_{x-1}, \quad x = 1, 2, 3. \tag{2.18}$$

Ions impinging on the surface are neutralized before the formation of a negative ion by resonant electron transfer from the metal and subsequent Auger de-excitation. The neutral atom picks up an additional electron from the conduction band of the metal via a resonant electron transfer (Figure 2.5). Close to the surface, the electron affinity level is lowered by the induction of a positive image charge in the metal, which can lead to electron tunneling from the conduction band of the metal to the affinity level of the hydrogen atom. The finite lifetime of the electron within the hydrogen atom is accompanied by a broadening of the affinity level, which increases the tunneling probability. [46, 47]

The yield of the surface production depends on the work function ϕ of the metal. This is because the probability of the tunneling process depends on the height (and width) of the surface potential barrier. Furthermore, the work function affects the survival probability of the H^- ion emitted from the surface. The negative ion yield

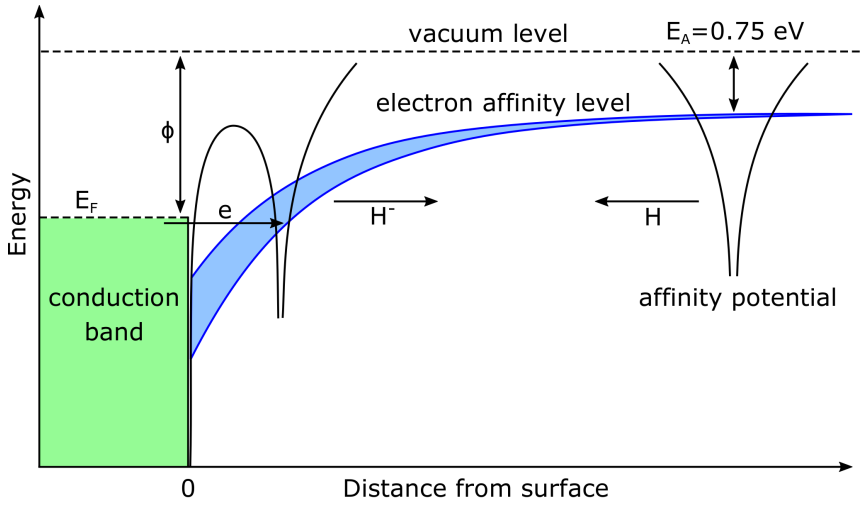

FIGURE 2.5 Illustration of the surface conversion process of a hydrogen atom to a negative ion. Modified from Reference [47].

can be described by two models: an amplitude model and a probability model [46]. In the amplitude model, the negative ion formation/survival probability P is described as

$$P \propto \exp\left(-\frac{\phi - E_{\mathrm{A}}}{v_{\mathrm{H^-}}}\right), \tag{2.19}$$

where $E_{\mathrm{A}} = 0.75$ eV is the electron affinity far from the surface, and $v_{\mathrm{H^-}}$ negative ion escape velocity normal to the surface. In the probability model, the probability is described as

$$P \propto \frac{v_{\mathrm{H^-}}}{\phi - E_{\mathrm{A}} - \Delta E_{\mathrm{A}}}, \tag{2.20}$$

where ΔE_{A} is the electron affinity level shift near the surface. According to both models the surface production of negative ions can be enhanced by lowering the work function of the surface. In negative ion sources, this is typically realized by covering the metallic conversion surface with a thin layer of cesium with an ideal thickness of less than a monolayer [48, 49, 50]. Lowering the work function can also enhance the PE emission, which makes PE emission more relevant in cesiated negative ion sources.

2.2 Hydrogen plasma light emission

Light is emitted by hydrogen plasmas as a consequence of electronic transitions from excited states to lower states of neutral atoms and molecules. Excitation to higher states is typically caused by electron impact collisions and the excited states decay spontaneously. Low temperature hydrogen plasmas are often considered to be in corona equilibrium, which implies that the excitation and de-excitation rates

of excited states are equal. This is valid for so-called ionizing plasmas (as opposed to recombining plasmas) found in the plasma devices discussed here.

The level scheme of hydrogen atom can be described using the Bohr model. Electrons occupy quantized orbitals labeled with principal quantum number n, which gives the total energy of the state. The atomic energy levels have a fine structure splitting the energy levels due to interaction between the electron spin and the orbital angular momentum, but the magnitude of the fine structure is negligible in comparison to the energy of the electronic excitation (eV vs µeV). When the excited state n_2 decays to lower state n_1, the energy difference ΔE of the two states is transferred to the emitted photon, i.e.

$$\Delta E = h\nu = \frac{hc}{\lambda} = \frac{\mu e^4}{8h^2\varepsilon_0^2}\left(\frac{1}{n_1^2} - \frac{1}{n_2^2}\right) \approx -13.6\left(\frac{1}{n_1^2} - \frac{1}{n_2^2}\right) \text{ eV}, \tag{2.21}$$

where h is the Planck constant, ν frequency of the emitted photon, c the speed of light in vacuum, λ wavelength of the emitted photon, μ the reduced mass of hydrogen atom, and ε_0 the vacuum permittivity. Transitions between all principal quantum levels are optically allowed. Transitions ending up to $n_1 = 1$, 2, and 3 are referred to historically as Lyman, Balmer and Paschen series, respectively.

In hydrogen molecule, the electronic states can also be described by orbitals. The diatomic hydrogen molecule has two electrons, which causes splitting into singlet and triplet systems. Electron has a half-integer spin which can point up or down. The total spin S can thus be either 1 (parallel) or 0 (antiparallel). $S = 0$ corresponds to singlet states and $S = 1$ to triplet states.

Molecular electronic states can be labeled by the following notation:

$$N^{2S+1}\Lambda_{u/g}^{+/-}, \tag{2.22}$$

where N is the united atom principal quantum number denoted with upper and lower case letters (X, B, C, D,...), $2S+1$ the multiplicity, Λ the total orbital angular momentum quantum number denoted with Greek letters (Σ, Π, Δ,... for $\Lambda = 0, 1, 2,...$), $+/-$ the parity of the state, and u/g the wavefunction symmetry (ungerade/gerade). Optically allowed transitions between electronic states follow selection rules:

1. $g \leftrightarrow u$
2. $\Delta S = 0$
3. $\Delta\Lambda = 0, \pm 1$.

In addition to electronic excitation of molecules, the two nuclei of the diatomic hydrogen molecule can vibrate against each other and rotate around their center of

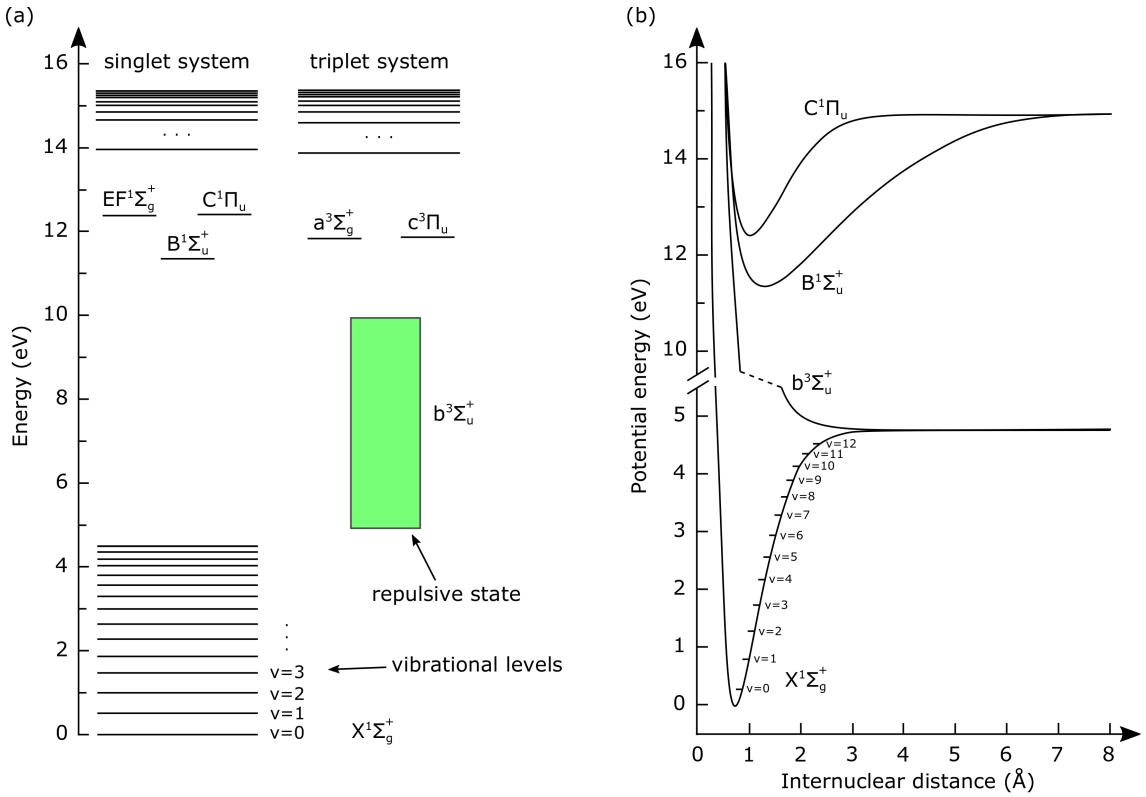

FIGURE 2.6 (a) Energy level diagram of hydrogen molecule. Modified from Reference [51]. (b) Potential diagram for certain singlet and triplet states of hydrogen molecule. Data is from Reference [52].

mass, both motions containing a quantized energy. The total energy of a molecule consists of the electronic energy E_e, vibrational energy E_{vib} and rotational energy E_{rot} (and kinetic energy). The orders of magnitude of energies associated to each degree of freedom are $E_e \gg E_{vib} \gg E_{rot}$. Each electronic energy level has vibrational levels and each vibrational level has rotational levels, and thus the light emission spectrum of molecular hydrogen consists of bands instead of discrete lines, contrary to atomic hydrogen.

The energy level diagram of hydrogen molecule is shown in Figure 2.6 (a) and the potential energy as a function of internuclear distance for $X^1\Sigma_g^+$, $B^1\Sigma_u^+$, $C^1\Pi_u$ singlet and $b^3\Sigma_u^+$ triplet states is presented in Figure 2.6 (b). The lowest triplet state $b^3\Sigma_u^+$ is repulsive, which has a significant effect on the plasma composition and the plasma light emission spectrum. The repulsive state is unbound, i.e. the potential energy does not have a minimum, and thus a molecule at the repulsive state dissociates spontaneously.

Cross sections for electron impact excitation from ground state to certain excited states of hydrogen atoms and neutral molecules are presented in Figure 2.7. The rate coefficients for electron impact excitation to the lowest singlet and triplet states with Maxwellian and uniform electron energy distributions are presented

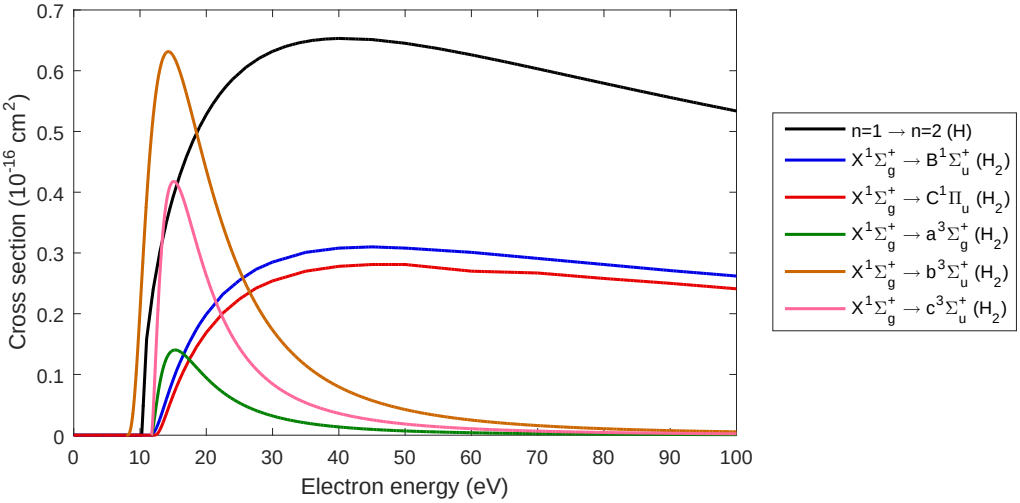

FIGURE 2.7 Cross sections for electron impact excitation of hydrogen atoms and molecules. Cross section data is from References [39, 53, 54].

in Figure 2.8. When the mean electron energy exceeds 20 eV, excitations to singlet states start to dominate over the dissociative triplet excitations. Typically in microwave heated plasmas the mean electron energy is lower in comparison to filament heated plasmas, which means that excitations to triplet states dominate, and thus the dissociation rate is higher. The dissociation rate has been observed to be considerably higher in microwave-driven ion sources [18], whereas the EEDF in the arc discharge leads to dominance of molecular excitation. The dissociation rate (together with wall recombination effects) affects the atomic to molecular

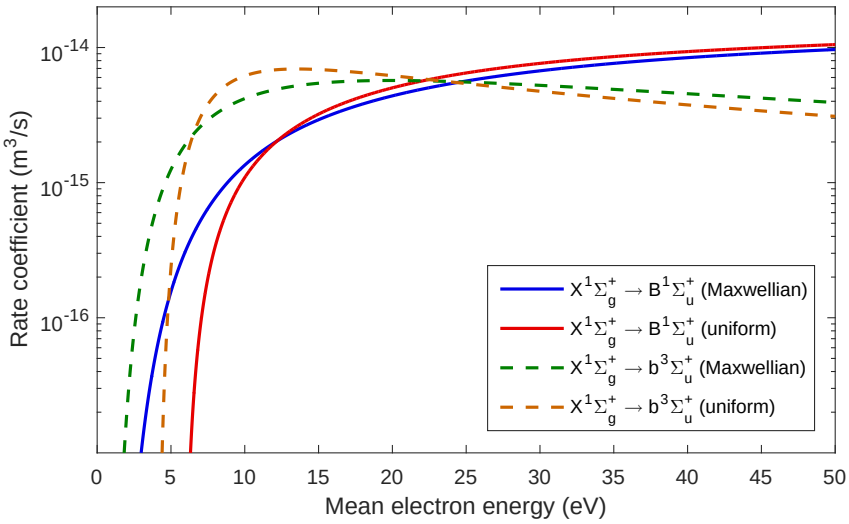

FIGURE 2.8 The rate coefficient for singlet $X^1\Sigma_g^+ \rightarrow B^1\Sigma_u^+$ and triplet $X^1\Sigma_g^+ \rightarrow b^3\Sigma_u^+$ electron impact excitation reactions as a function of mean electron energy for Maxwellian and uniform EEDF. Calculated using cross sections from References [39, 54].

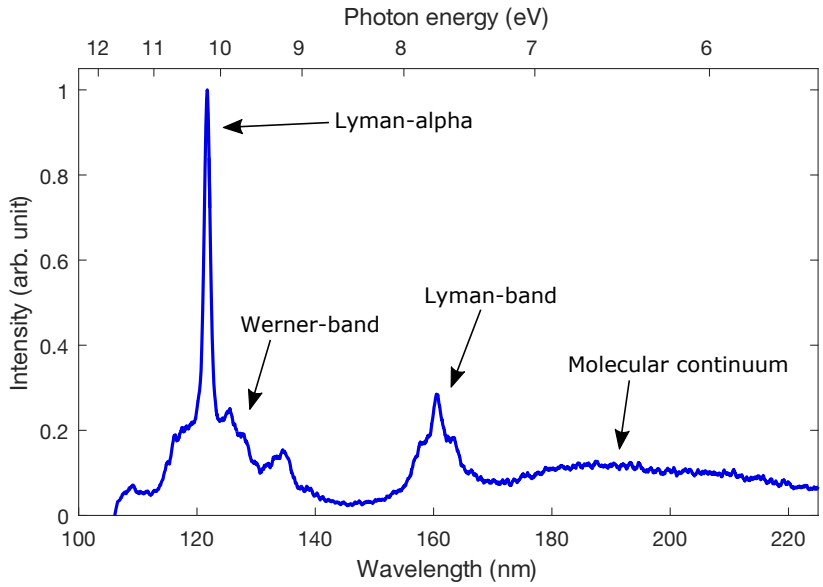

FIGURE 2.9 Typical VUV emission spectrum of hydrogen plasma. The spectrum is not calibrated for spectral response.

hydrogen fraction of the discharge and, therefore, plays a crucial role on the plasma emission spectrum.

Typical VUV emission spectrum from a hydrogen plasma is presented in Figure 2.9. The VUV spectrum is measured with a spectrometer consisting of a monochromator (McPherson model 234/302), holographic grating, and photomultiplier tube (ET Enterprises 9406B). The Lyman-alpha line at 121.6 nm corresponds to the transition from the first excited state to the ground state of atomic hydrogen ($n = 2 \rightarrow n = 1$). The Werner-band originates from the resonant $C^1\Pi_u \rightarrow X^1\Sigma_g^+$ transitions in the singlet system of the hydrogen molecule, the dominant part of the emission being found at wavelengths shorter than 130 nm. The dominant part of Lyman-band emission originating from $B^1\Sigma_u^+ \rightarrow X^1\Sigma_g^+$ transitions is in the wavelength range of 130–170 nm. The molecular continuum from the $a^3\Sigma_g^+ \rightarrow b^3\Sigma_u^+$ transition of the triplet system is assigned to wavelengths longer than 170 nm.

Theoretical calculations based on fundamental conservation laws and reaction cross sections show that at least 10 % of plasma heating power is dissipated via photon emission in low temperature hydrogen plasmas [16]. The theoretical result is supported by experimental evidence showing that low temperature hydrogen plasmas are strong sources of VUV radiation with up to 15–30 % of the discharge power radiated at wavelengths of 120–250 nm in filament-driven arc discharge [17], up to 8 % of the injected microwave power at 80–250 nm in ECR discharge [18] and up to 21 % of the RF power at 117–280 nm in RF discharge [19].

2.3 Photoelectric effect

In plasmas enclosed by metallic walls, photons emitted from the plasma impinge on metal surfaces and can induce PE emission. Photoelectric effect is a three stage process where an electron is excited by absorbing a photon, transported to the surface, and then escapes from the material. The mechanism of the photoelectric effect was famously explained by Albert Einstein [55] suggesting that energy is exchanged in discrete amounts ($h\nu$), which was pivotal to the early development of the quantum theory. Einstein was awarded the 1921 Nobel Prize in Physics "for his services to theoretical physics, and especially for his discovery of the law of the photoelectric effect" [56]. In this thesis, the discussion on the photoelectric effect is restricted to metal surfaces. More detailed presentation of the photoelectric effect can be found from textbooks, e.g. References [57, 58].

2.3.1 Work function

Electrons in the conduction band of a metal follow the Fermi-Dirac distribution. The energy of the highest occupied state is referred to as the Fermi level E_F. The potential immediately outside the surface is called vacuum level E_V, where "immediately outside" means a distance that is large enough for the image force to be negligible but small compared to the physical dimensions of the surface. The minimum energy required to remove an electron from the surface of a solid is referred to as the work function. The work function corresponds to the energy difference between the Fermi level and the vacuum level:

$$\phi = E_\mathrm{V} - E_\mathrm{F}. \tag{2.23}$$

The concept of work function is illustrated in Figure 2.10. For common metals typically used as technical surfaces in ion sources the work function is 4–5 eV [59, 60].

The energy distribution of PEs extends from zero to the maximum, which corresponds to the difference between the energy of the incident photon and the work function, i.e.

$$0 \leq E_\mathrm{PE} \leq h\nu - \phi. \tag{2.24}$$

The maximum energy corresponds to a PE emitted from the Fermi level. The kinetic energy of a PE emitted from an energy level with binding energy E_B below the Fermi level is given by

$$E_\mathrm{PE} = h\nu - E_\mathrm{B} - \phi. \tag{2.25}$$

Energy of the emitted electrons is distributed between zero and the maximum due to photon interaction with electrons deeper (than the Fermi level) in the conduction

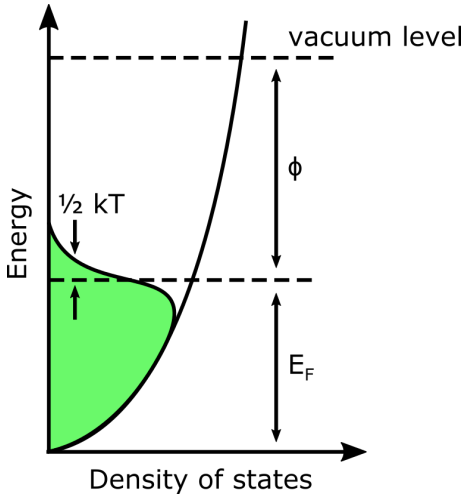

FIGURE 2.10 Density of occupied and empty states in a metal with definition of the Fermi level E_F and the work function ϕ. Modified from Reference [57].

band and due to energy losses of excited electrons in inelastic scattering during the transport to the surface. In plasma devices, the electrons emitted from the plasma chamber walls are further accelerated across the plasma–surface boundary by the positive plasma potential as discussed thoroughly in Section 2.4.

2.3.2 Quantum efficiency

The quantum efficiency (QE) Y of the PE emission is an energy and material dependent conversion factor defined as follows

$$Y = \frac{\text{emitted electrons}}{\text{incident photons}}. \tag{2.26}$$

When the energy of the incident photon is close to the work function, only electrons near the surface are excited and the electron transport inside the metal does not affect the QE. In this case, the QE can be described by the Fowler's theory [61]:

$$\begin{aligned} Y &\propto \frac{(h\nu - \phi)^2}{(U_0 - h\nu)^{1/2}}, && \text{when } h\nu \geq \phi, \\ &= 0, && \text{when } h\nu < \phi, \end{aligned} \tag{2.27}$$

where $h\nu$ is the energy of the photon, ϕ the work function, and U_0 the potential step at the surface–vacuum boundary.

At higher photon energies, the QE is affected by the electron transport inside the metal and increased probability for competing interaction mechanisms. At higher energies, the Fowler's theory is not valid, and the QE has to be determined experimentally. The wavelength dependence of experimentally determined QE is presented in Figure 2.11 for certain common metals. Close to the work function,

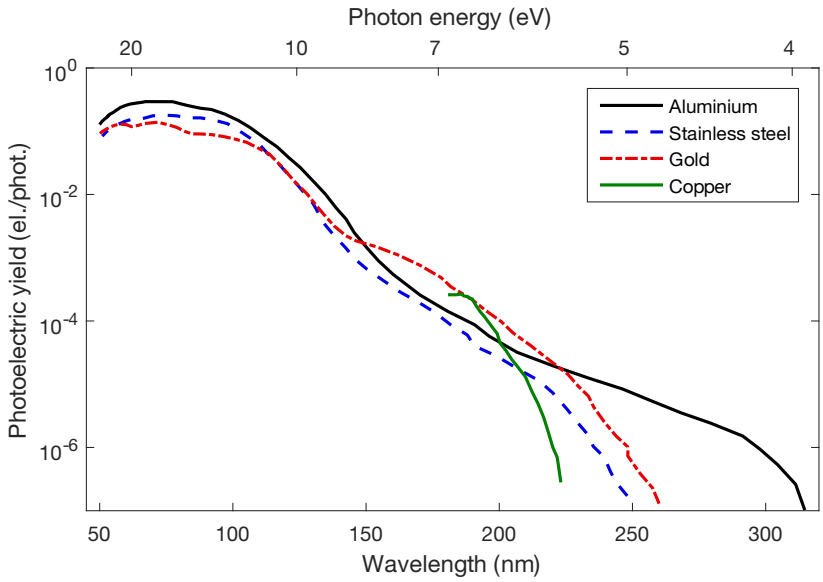

FIGURE 2.11 Experimentally determined photoelectric yield quantum efficiencies for aluminium, stainless steel, gold (from Reference [62]), and copper (from Reference [63]).

the QE of the PE emission is rather low, but increases strongly towards higher energies. The QE can increase up to an order of magnitude per eV. At energies higher than 20 eV, the QE decreases because of the decreasing absorption cross section for photons, which results in an increased probability for excitation of an electron lying deeper inside the metal and, hence, a reduced probability for the PE to reach the surface and escape [62].

2.3.3 Alkali metals

The work function of a metal surface can be lowered by adsorbing a thin layer of an alkali metal on the surface. Adsorption of electropositive cesium atoms on a metal surface takes place by transfer of a valence electron to the conduction band of the metal [64]. As the cesium coverage on the surface increases, the work function decreases due to dipole field caused by the displacement of the electron clouds reaching a minimum value at 0.5–0.7 monolayer thickness. Beyond this, bonds between nearest neighbour cesium atoms decrease the dipole field, which leads to an increasing work function saturating to a value corresponding to bulk cesium at one monolayer thickness. One monolayer of cesium corresponds to a surface density of 5.5×10^{14} cesium atoms per cm^2 [65].

The maximum change of the work function $\Delta\phi_\mathrm{m}$ caused by alkali metal (and alkaline earth metal) adsorption can be described by an empirical relation [64]

$$\Delta\phi_\mathrm{m} \cong -1.24 \left[\phi_0 - \frac{1}{2} \left(I_\mathrm{A} + E_\mathrm{A} \right) \right], \tag{2.28}$$

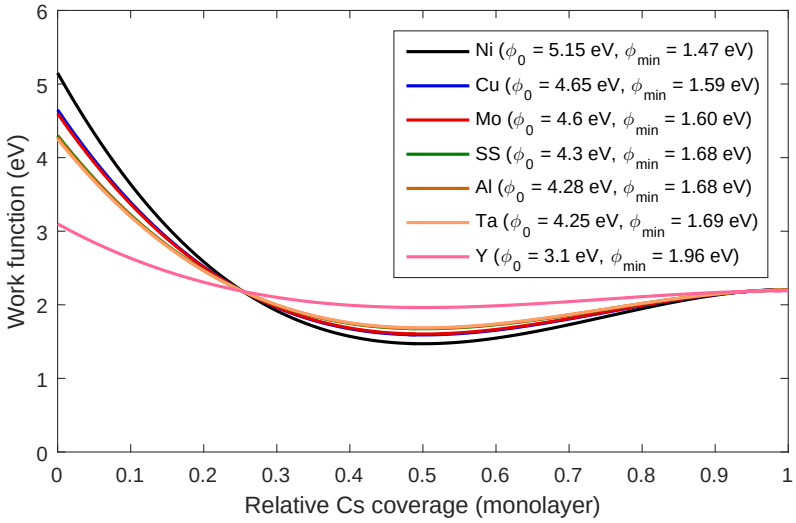

FIGURE 2.12 Semiempirical relationship for the work function as a function of relative Cs coverage in monolayers on different substrates. Calculated using semiempirical model from Reference [64].

where ϕ_0 is the intrinsic work function of the substrate material, I_A the first ionization potential, and E_A the electron affinity of the adsorbate. Higher ϕ_0 results to lower ϕ_{min}, which is due to stronger electric field on the surface. For example, for cesium $I_A = 3.894$ eV and $E_A = 0.472$ eV [66], and thus the minimum work function ϕ_{min} of a cesiated metal surface can be estimated by

$$\phi_{min} = 2.707 - 0.24\phi_0. \tag{2.29}$$

The functional dependence of the work function on surface coverage θ can be described as [64]

$$\phi(\theta) \simeq \phi_0 + \frac{6\,\Delta\phi_m}{(3-\theta_m)\theta_m}\theta - \frac{3\,\Delta\phi_m(\theta_m+1)}{(3-\theta_m)\theta_m^2}\theta^2 + \frac{2\,\Delta\phi_m}{(3-\theta_m)\theta_m^2}\theta^3, \tag{2.30}$$

where θ_m is the relative coverage corresponding to the minimum work function. Work function values suggested by Equation (2.30), which has been shown to be in good accuracy with experimental data [64], are plotted in Figure 2.12 for different substrates with variable ϕ_0 [59, 60] with a choice of $\theta_{min} = 0.5$.

In addition to ion sources, cesium covered surfaces are used in other applications, such as photocathodes having spectral responses from UV to visible light. The QE of cesium covered surfaces has been studied by Jensen et al. [67], but the wavelength range used in their experiment does not cover the VUV range.

2.3.4 Ion source relevant conditions

Experimental surface physics is typically performed in ultra-high vacuum (UHV) conditions ($< 10^{-9}$ mbar[1]). For example, experimental values for the work function of cesium covered metals are usually measured in UHV conditions [60, 68, 69, 70]. However, ion sources usually have high vacuum background pressures of 10^{-7}–10^{-5} mbar. In addition to higher neutral particle fluxes, the surfaces are exposed to plasma bombardment and UV radiation. Typical vacuum contaminants, such as residual gases, water vapour, sputtered elements, oxides, and even pump oil, are present on all surfaces. Therefore, the real work function and QE of technical surfaces covered with their natural oxide and contaminants, typically found in ion sources, can be different to literature values.

Alkali metals are highly reactive. The high reactivity of cesium leads to formation of compounds, e.g. CsOH and Cs_2O, with the impurities present in all low temperature ion source plasmas, i.e. cesium acts as a getter for O_2 and H_2O for example. The thickness of the cesium layer and the level of surface impurities is determined by the balance between their deposition and adsorption rates. Hence, the surface conditions can have significant temporal variation especially in pulsed high power discharges [71, 72]. Usually a continuous evaporation of cesium into the source is used to keep the surfaces "clean" [47, 73, 74]. Experimental results from a Penning type ion source showing notable transient lines of cesium compounds in the VUV spectra after plasma ignition have been reported [75]. It has been suggested that the involvement of cesium compounds in the cesium dynamics of the ion source is significant or even dominating in ion sources for neutral beam injection [47]. The minimum work function measured under ion source relevant conditions is typically higher in comparison to work function values derived from the measurements performed at UHV conditions [76]. However, work function less than 1.91 eV, which is below the work function of solid cesium, has been measured with a 650 nm laser from a negative ion source converter surface with simultaneous plasma operation [77]. Altogether, this means that the PE emission has to be studied in ion source relevant conditions in order to apply the results to ion source plasmas.

2.4 Plasma boundaries

Instead of sharp boundaries, plasmas surrounded by walls of solid material create a sheath between the plasma and the wall. The plasma sheath structure is very important for surface production of negative ions, and also for transport of the

[1] In this work, mbar is used as the unit of pressure. Conversion to SI units is made as 1 mbar = 100 Pa. The unit mbar is also used in the peer-reviewed publications included in the thesis.

emitted PEs into the plasma.

The mobility μ_{q} of charged particles can be expressed as

$$\mu_{\mathrm{q}} = \frac{q}{m\nu_{\mathrm{m}}}, \tag{2.31}$$

where q is the charge of the species, m the particle mass, and ν_{m} the momentum transfer collision frequency. Electrons have much smaller mass in comparison to ions and, thus, electrons have higher mobility. Therefore, the initial flux of electrons to the wall is higher during the ignition of the plasma. The plasma is left with excess positive charge, which results to positive potential in the bulk plasma with respect to the chamber walls. The electric field $\vec{E}$ created between the plasma and the chamber walls is described as the gradient of the potential Φ:

$$\vec{E} = -\nabla\Phi. \tag{2.32}$$

The positive plasma potential reduces the electron flux and increases the positive ion flux leaving the plasma. In equilibrium, the fluxes of positive and negative charges are equal resulting to a quasineutral condition, i.e.

$$\sum_{\mathrm{i}} q_{\mathrm{i}} n_{\mathrm{i}} = n_{\mathrm{e}}, \tag{2.33}$$

where q_{i} are the charge states of ion species, n_{i} the densities of ion species, and n_{e} is the electron density.

If there is no negative charge emitted from the wall, the electric field at the wall is positive i.e. points towards the wall. As the flux of negative charge from the wall increases, the electric field decreases. At a certain situation, the field will fall to zero, which is the Child-Langmuir limit, i.e. the space charge limited condition. Further increase of the current density from the wall exceeding the space charge limit will result to a formation of a virtual cathode. The situation is illustrated in Figure 2.13. If the virtual cathode exists, it limits the transport of the negative ions and the emitted PEs into the plasma depending on their energies. However, the energy of the particles that are transported through the sheath corresponds to the initial emission energy superimposed on the energy corresponding to the plasma potential.

In ion sources relying on the surface production of negative ions, the presence of a virtual cathode has been predicted by one-dimensional and two-dimensional particle in cell (PIC) codes [78, 79]. A one-dimensional analytical, collisionless model (of a two-dimensional, infinite and uniform surface) for the sheath structure in negative ion sources has been developed by McAdams et al. [80, 81, 82], based on the work of Amemiya et al. [83]. In the model, the sheath structure, including the formation of a virtual cathode, is described by solving the one-dimensional Poisson's equation in the region between the wall and the sheath edge. The

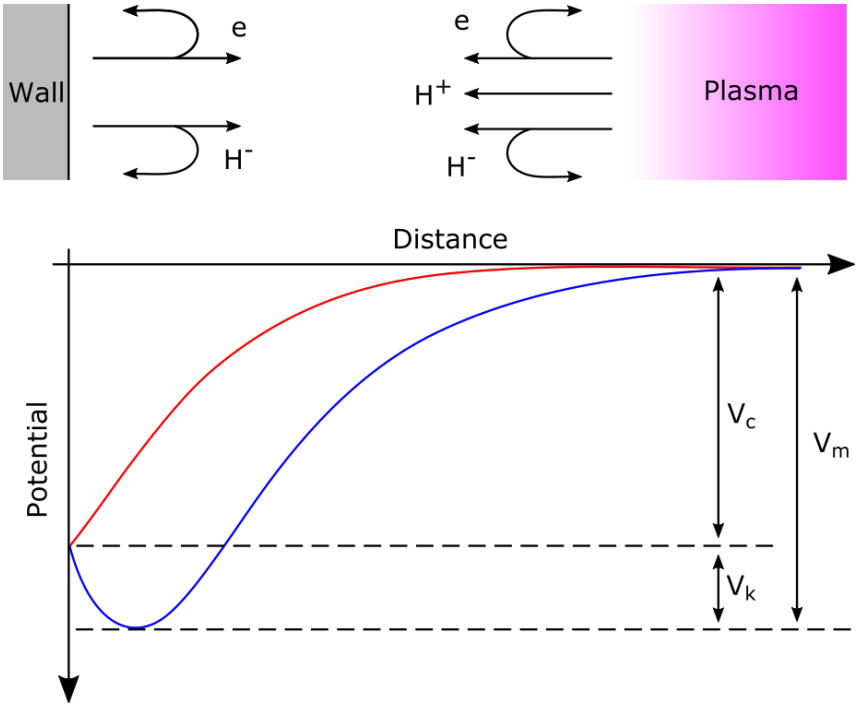

FIGURE 2.13 Illustration of the plasma sheath structure. The red line presents the sheath without a virtual cathode between the cathode at potential $-V_c$ and the sheath edge at zero potential. The blue line shows the sheath with a virtual cathode, which has a depth of V_k relative to the cathode, and the potential minimum in the sheath is at $-V_m$ relative to the sheath edge.

potential in the plasma sheath is given by the Poisson's equation, which is written as

$$\frac{\mathrm{d}^2\Phi}{\mathrm{d}x^2} = -\frac{e}{\varepsilon_0}\sum_j n_j, \tag{2.34}$$

where n_j are the plasma particle densities. The Poisson's equation is impossible to solve analytically, and thus even the one-dimensional equation has to be solved numerically. The effect of PEs on the plasma sheath structure is discussed in Section 6.2.

3 EXPERIMENTAL APPROACH FOR PHOTOELECTRON EMISSION STUDIES

The experimental setup and apparatus used in the PE emission measurements, including the PE meter specifically designed for this work and the applied ion sources, are presented in this chapter.

Parametric studies for plasma induced PE emission were performed for materials typically used in ion sources. Aluminium, copper, and stainless steel are widely used as chamber materials [84, 85, 86], tantalum is used as filament material [87, 88] and is often accumulated on the plasma chamber walls, molybdenum is used as a plasma grid material [89], and molybdenum and stainless steel are used as so-called collar materials [2, 90]. Nickel and yttrium were chosen for the experimental studies as high and low work function materials, respectively. The measurements were also realized on cesium covered samples. Cesium covered surfaces are widely used in ion sources optimized for surface production of negative hydrogen ions. Also, PE emission from rubidium covered surfaces was studied and compared to cesium.

3.1 Photoelectron meter

The measurement setup for plasma induced PE emission studies is presented schematically in Figure 3.1. The principle of measuring the PE emission is to illuminate a metal surface and count the emitted electrons.

As a default there is a direct view from the plasma to the sample, i.e. there is no optics in between them. The PE meter with rotatable discs, presented in Figure 3.2 (a), can be equipped with windows and filters, e.g. to study the

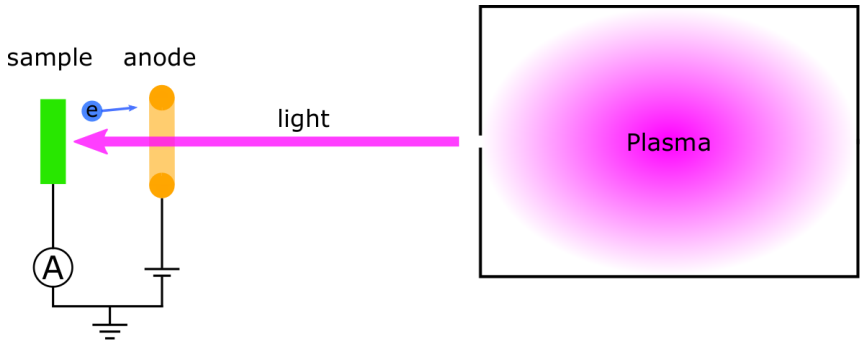

FIGURE 3.1 Schematic illustration of the experimental setup for photoelectron emission measurements.

wavelength dependence of the PE emission. The PE meter can also be equipped with multiple samples in order to study different materials without compromising the vacuum. The PE current is measured from the sample with a picoammeter. The emitted electrons are collected with an anode ring typically biased to +150 V with respect to the cathode, i.e. laboratory ground, which is sufficient to overcome space charge effects at the emitting surface. The required anode voltage depends on the measurement setup and the emitted current. An example of the measured PE current as a function of the anode voltage is shown in Figure 3.3, which shows that, in this case, the PE current saturates when the anode voltage exceeds 20 V, and the 150 V voltage is well above the space charge limitation.

The plasma induced PE emission has to be measured using a remote sample. Measuring the PE emission directly inside the plasma chamber is not possible, since the measured current would be affected by particle currents from various sources, such as plasma losses and secondary electron emission, making it impossible to determine the origin of collected charges. However, inside a plasma source, the surfaces emitting electrons are in direct contact with the plasma, which has a cleaning effect that most likely affects the initial conditioning phase of the surfaces and hence the PE emission. Low energy hydrogen ion beams, in addition to UV-drive lasers, are used for the cleaning of the photocathodes, in which the QE increases as a result of exposure to hydrogen ion beam [63]. Thus, the PE emission inside a plasma source might be higher than the emission measured from a remote sample. Also, due to possible attenuation of the VUV by residual gas on the line-of-sight, the PE current measured from a remote sample can be argued to correspond to the lower limit of the actual PE emission.

The samples, similar to surfaces in ion sources, are technical materials, which are rough in the nanoscale. The dimensions of the sample have to be large enough compared to the peak-to-peak surface roughness and characteristic dimensions of the crystal face domains etc. in order to measure the average emission. The illuminated sample surface area is determined by the size of the collimator, which

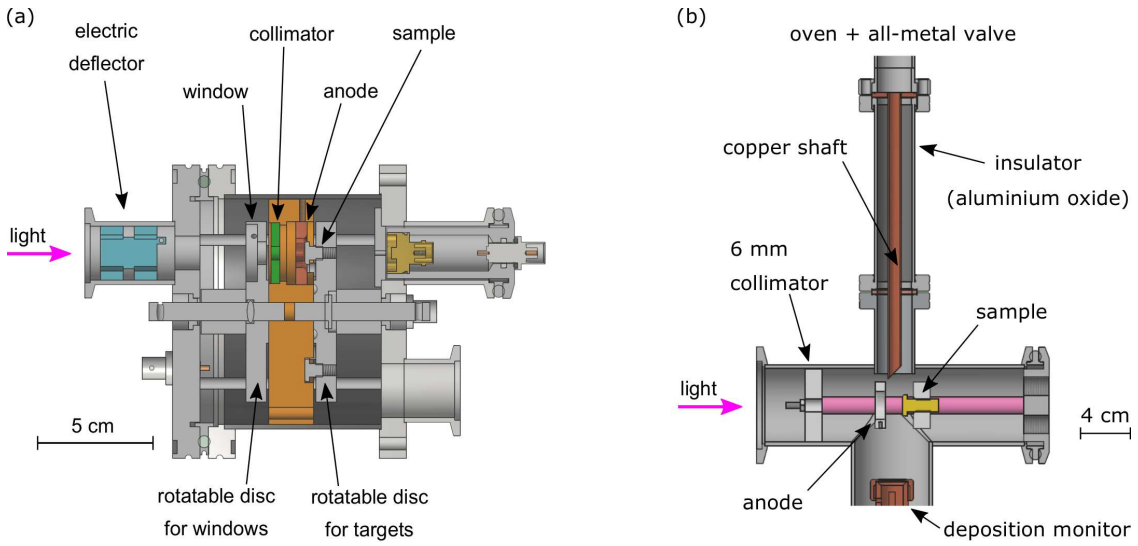

FIGURE 3.2 (a) Photoelectron meter with multiple samples and windows/filters. (b) Photoelectron meter with an integrated oven.

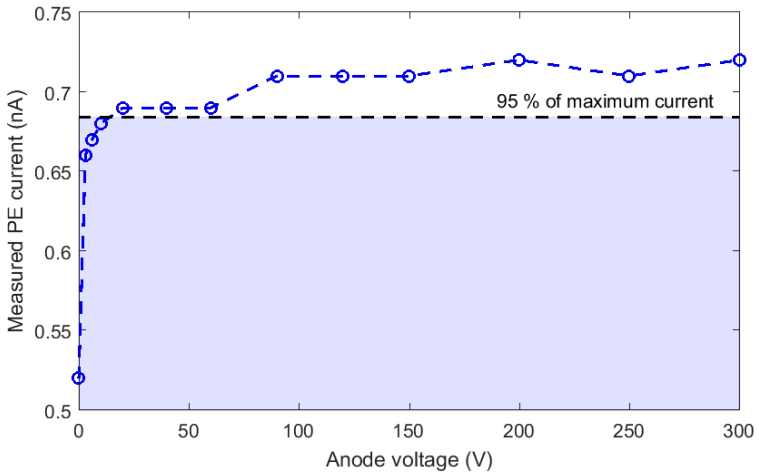

FIGURE 3.3 An example of the photoelectron current as a function of the anode voltage.

typically has a diameter of few mm. The photons are impinging on the macroscopic sample surface on normal incidence. The angle of incidence does not affect the measured PE current since the peak-to-peak roughness of the sample surface is over 100 nm, which exceeds the mean free path for VUV photons and the escape depth of the PEs and, therefore, effectively randomizes the photon angle of incidence in the microscale, as discussed in Reference [PIII]. Sample preparation, which included mechanical and chemical cleaning, was performed in atmospheric pressure, and thus the surfaces were covered with their natural oxides and typical vacuum contaminants. With the remote sample, VUV induced surface aging (accumulation of contaminants or cleaning, chemical surface reactions etc.) was observed to affect the PE emission slightly. This is demonstrated in Figure 3.4 showing the PE emission as a function of time for different setups: filament source

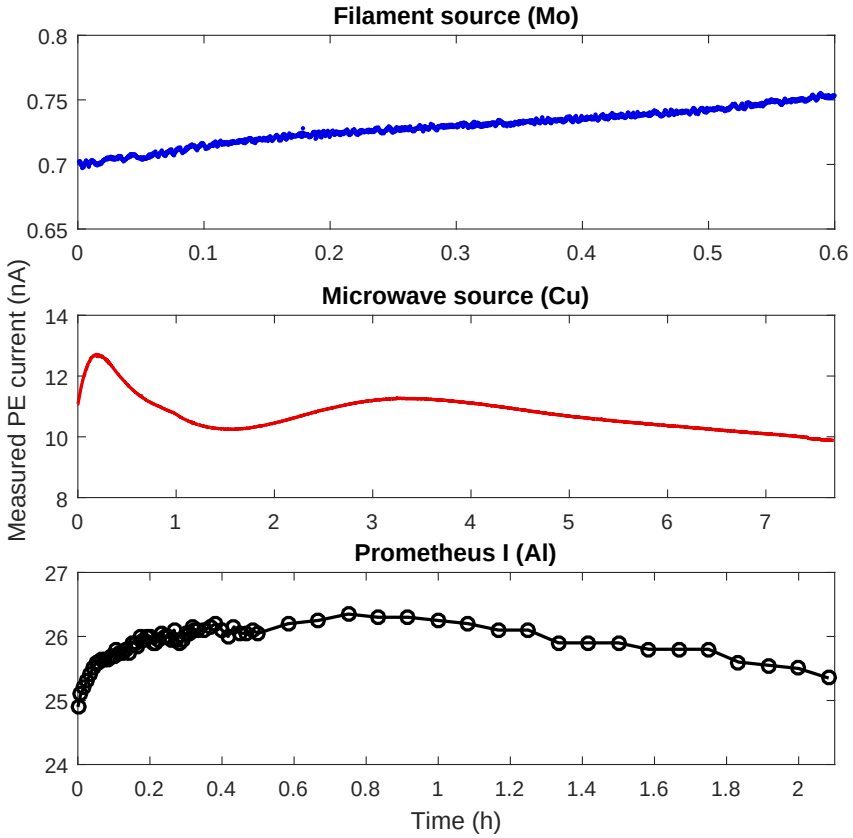

FIGURE 3.4 Examples of VUV induced surface aging with different setups: filament source with molybdenum sample, 2.45 GHz microwave source with copper sample, and Prometheus I with aluminium sample. The aging effect was observed with all hydrogen ion sources and materials, thus different materials are chosen for the example.

(described in Section 3.2.1) with molybdenum sample, 2.45 GHz microwave source (described in Section 3.2.2) with copper sample, and Prometheus I (described in Section 3.2.3) with aluminium sample. Although the aging was observed with all materials and all hydrogen ion sources, the time scale and magnitude of the effect varies. The difference is considered to be attributed to, for example, vacuum conditions such as residual gas pressure and composition. Due to the VUV induced surface aging, the samples were protected from the plasma light when measurements were not actively conducted.

The PE meter with an integrated oven, presented in Figure 3.2 (b), was utilized for the study of PE emission from alkali metal covered surfaces. The oven is based on the Los Alamos design [71]. The deposited material is evaporated from the oven consisting of a flexible bellows and an all-metal valve. The alkali metal ampoule is broken inside the vacuum by bending the bellows. The oven is connected to the vacuum system with a thermal insulator and the evaporated material is supplied through a copper shaft. The oven is heated up to ca 200 °C and kept at

constant temperature as cesium or rubidium evaporate onto the metal sample in the PE detector. Inficon XTM/2 deposition monitor, placed next to the sample, was utilized for verifying the accumulation of the evaporated material, but absolute layer thickness on the sample was not measured.

The remote sample is irradiated with the light emitted from a restricted plasma volume. The total PE current (density), emitted from the walls of the plasma chamber, is possible to be derived from the measured PE current by using Monte Carlo methods. The probability for a single photon to reach the sample surface was calculated and the measured current was divided with the given probability. To simulate the light emission profile, the spatial distribution of the plasma must be approximated. Assuming homogeneous and isotropic light emission profile across the plasma chamber volume, the maximum value for the PE emission is calculated with the simulation. In reality, the spatial distribution of the plasma light emission rate depends on the plasma density and temperature profiles. For example, in microwave discharges, the light emission distribution depends on the magnetic field configuration, incident microwave power, and neutral gas pressure [91]. Without accurate information about the density and temperature profiles, the total PE emission can only be estimated. Due to the topology of the magnetic field in the ion sources used in the measurements, it can be argued that the total VUV emission, and hence the PE emission, is most often 50–100 % of the given maximum [17].

3.2 Ion sources

The ion sources used in the study are filament and microwave driven ion sources designed for positive and negative hydrogen ion and multiply charged, heavy ion production. These ion sources differ by plasma heating mechanisms and operational pressures.

3.2.1 Filament-driven multi-cusp arc discharge ion source

The LIISA (Light Ion Ion Source Apparatus) ion source at JYFL, presented in Figure 3.5, is a TRIUMF-type DC (tantalum) filament-driven multi-cusp arc discharge volume production H^-/D^- ion source. LIISA is designed to provide up to 3 mA of H^- at 5.9 keV injection energy to the JYFL K130 cyclotron [87]. Typical extracted beam current of approximately 1 mA is reached with 70 V / $<$ 10 A discharge voltage / current. The optimum pressure for H^- beam current is 3.5×10^{-3} mbar measured in the plasma chamber. The cylindrical plasma chamber is tantalum-coated copper with 9.8 cm diameter and 32 cm length. The plasma chamber

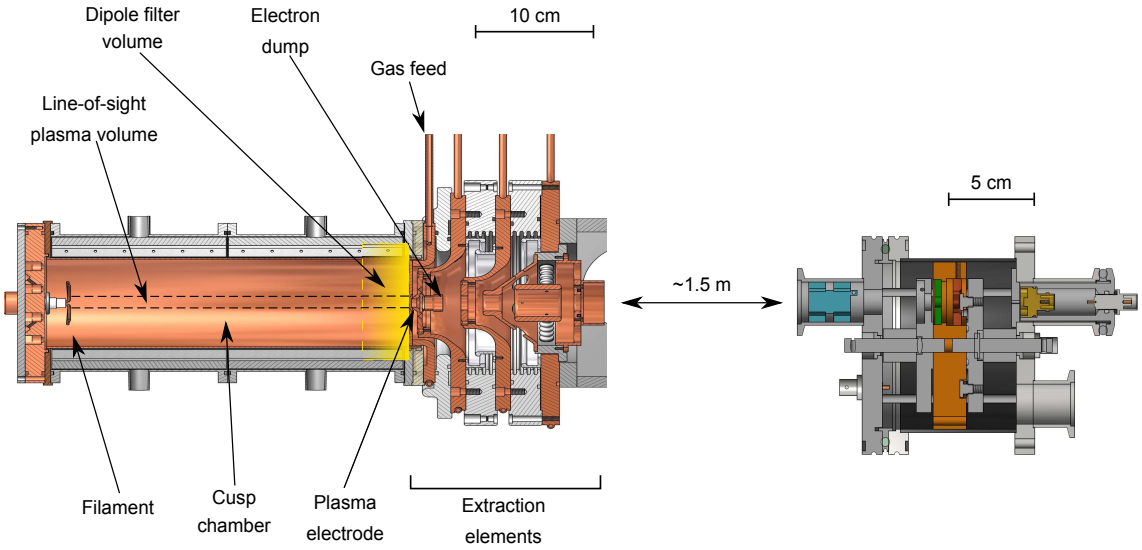

FIGURE 3.5 The experimental setup with the filament-driven multi-cusp arc discharge H^- ion source (LIISA).

pressure varies between 5×10^{-4} mbar and 1×10^{-2} mbar and the arc discharge power between 200 W and 1000 W in operational conditions. The parametric dependencies of the extracted beam current and VUV emission on the discharge power and neutral gas pressure are reported in Reference [17].

Another filament-driven ion source (see Publication [PIV]) was also used in the experimental studies. The main difference to LIISA is a shorter plasma chamber (11 cm) and the absence of the filter field.

3.2.2 2.45 GHz microwave-driven ion source

The 2.45 GHz microwave-driven ion source designed for positive ion production is presented schematically in Figure 3.6. The microwave coupling system includes a 2.45 GHz magnetron, circulator, three stub tuners for impedance matching and a ridged waveguide section. The cylindrical plasma chamber with 10 cm diameter

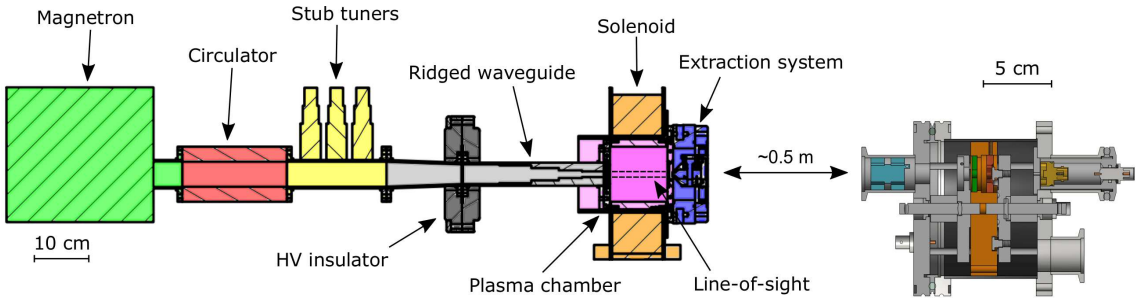

FIGURE 3.6 The experimental setup with the 2.45 GHz microwave-driven ion source.

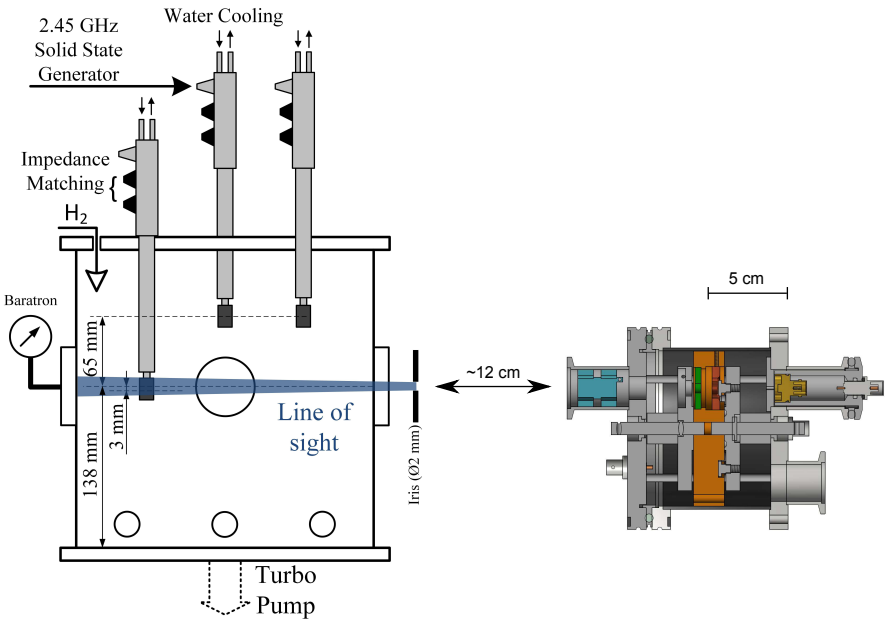

FIGURE 3.7 The experimental setup with the 2.45 GHz multi-dipolar microwave-driven ion source (Prometheus I).

and 10 cm length is made of aluminium. The waveguide is in atmospheric pressure and the vacuum chamber is sealed with a quartz window covered by a boron nitride disc. A single solenoid coil around the plasma chamber forms the ECR surface at the magnetic field strength of 87.5 mT directly in front of the window. Typical operation conditions are 300–1200 W of injected microwave power in 2×10^{-3}–2×10^{-1} mbar neutral gas pressure. The ion source has an extraction system designed for positive ions. A parametric study of the VUV emission of the microwave source is reported in Reference [18].

3.2.3 2.45 GHz multi-dipolar microwave-driven ion source

Prometheus I, presented in Figure 3.7, is a microwave-driven multi-dipolar plasma source designed for H^- production [92]. The source has been built and is operated in the High Voltage Laboratory of the Electrical and Computer Engineering Department of the University of Patras in Greece. The plasma is sustained by a two-dimensional network of ECR plasma sources [93, 94]. Each elementary source consists of two parts: a cylindrical samarium-cobalt (Sm_2Co_{17}) permanent magnet, magnetized along its axis, and a coaxial line parallel to the magnetization vector, with an open end at the rear of the magnet. The magnetic field creates the ECR surface (depicted in Reference [92]) and works as the magnetic filter of the source by confining hot electrons in the vicinity of the magnets. The sources are driven individually at 2.45 GHz by five solid state power supplies (0–180 W/elementary source). The plasma chamber pressure in operational conditions is 1×10^{-3}–

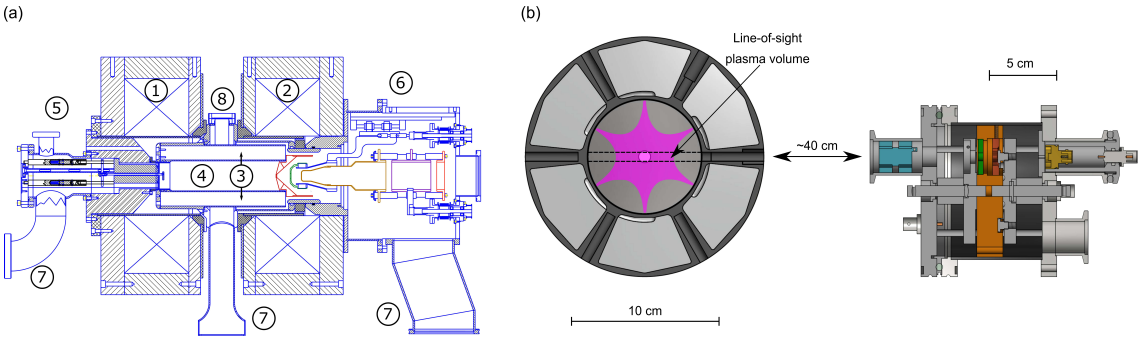

FIGURE 3.8 (a) The JYFL 14 GHz ECR ion source. (1) Injection and (2) extraction coils, (3) NdFeB hexapole, (4) plasma chamber ($\ell = 270$ mm, $\varnothing = 76$ mm), (5) iron plug, biased disc, gas and microwave injection, (6) extraction system, (7) pumping, (8) vacuum gauge. (b) ECR ion source plasma chamber and the measurement setup.

3×10^{-2} mbar. The cubic plasma chamber (edge length 24 cm) is made of stainless steel. The vertically movable elementary sources allows to study the ECR zone and the H^- production region separately. A parametric study of VUV emission of Prometheus I is reported in Reference [95].

3.2.4 14 GHz ECR ion source

The room-temperature AECR-U type JYFL 14 GHz ECR ion source [96, 97], designed for highly charged ions production, is presented in Figure 3.8. The magnetic field in the plasma chamber forms a so-called minimum-B configuration which is created by a set of two room-temperature solenoids (axial field) and permanent magnet hexapole (radial field). The source is typically operated with less than 1 kW microwave power in 1×10^{-7}–1×10^{-6} mbar neutral gas pressure. In the experiments, the ion source was operated with a single frequency (14.085 GHz) in continuous mode.

The 14 GHz ion source plasma operates in lower neutral gas pressure range in comparison to typical low temperature hydrogen discharges, which means that the intensity of the VUV emission is weaker. Furthermore, the electron energies in the high frequency ECR ion source are significantly higher in comparison to the afore-mentioned hydrogen ion sources. The ECR plasma also emits X-rays by characteristic electronic transitions, by wall bremsstrahlung, and by recombination of highly charged ions at the walls. Common metals have a high PE yields at the X-ray range as well [98], which motivated the study of the PE emission with the 14 GHz ion source.

4 PLASMA INDUCED PHOTOELECTRON EMISSION FROM METAL SURFACES

The plasma induced PE emission from clean metal surfaces has been experimentally studied with the methods described in the previous chapter. The experimental results obtained with different ion sources and plasma heating methods are summarized in this chapter. The data were originally presented in Publications [PI], [PII], [PIII], and [PV].

4.1 Parametric dependence of photoelectron emission

As an example, the parametric dependence of the plasma induced PE emission studied with the filament-driven arc discharge is summarized here for aluminium, copper, stainless steel (SAE 304), molybdenum and tantalum surfaces. The experiments are discussed in detail in Reference [PI]. The PE currents from different metals measured as a function of neutral hydrogen pressure vary less than 20 % in the range of typical operation pressures as presented in Figure 4.1. In the given example the discharge power was kept constant at 500 W (50 V / 10 A). Similarly to the PE emission measurements, the VUV emission in the filament discharge has been reported to exhibit only minor dependence on the neutral gas pressure [17]. Difference of the PE currents from the metals are also shown in Figure 4.1. The PE current from aluminium is always about 20–50 % higher in comparison to other metals measured here. This is most likely due to the wavelength dependence of the QE in the VUV range. However, the emission from all metals is in the same order of magnitude.

The PE currents from different metals measured as a function of discharge power are presented in Figure 4.2. The current increases linearly as a function of the

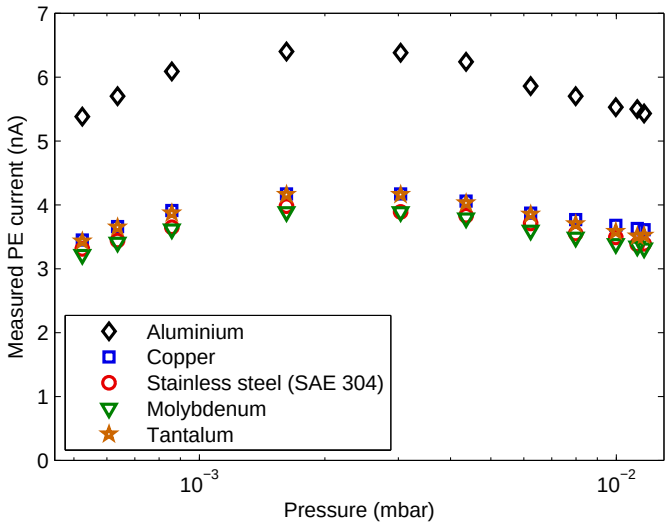

FIGURE 4.1 Measured photoelectron currents as a function of neutral hydrogen (H_2) pressure. Measured with LIISA ion source at 500 W discharge power (50 V/10 A). The figure is from Reference [PI].

discharge power, which can be explained by the confinement of hot electrons and their energy dissipation via inelastic collisions. In other words, the emitted electrons dissipate their energy through inelastic collisions and escape the confinement at low energies. Linear proportionality to the discharge power has been reported for the intensities of Lyman-alpha, Lyman-band and Werner-band emission in the filament discharge, while molecular continuum emission is proportional to the discharge current [17].

It is also shown in Figure 4.2 that the estimated total PE current from the plasma chamber walls is in the order of 1 A per kW of discharge power. However, the flux of PEs transported to the plasma might be smaller than the total emission due to the magnetic fields typically applied in ion sources. For example, the cusp magnetic field of the filament discharge limits the PE flux from the wall to the plasma, since the cross field diffusion of the emitted electrons in transverse magnetic field is significantly slower than their propagation along the field lines. The emitted electrons are more likely to be transported to the plasma at the poles of the cusp field.

The wavelength dependence of the PE emission was studied by placing a sapphire window between the sample and the hydrogen plasma. In this case, all wavelengths shorter than 150 nm were filtered out. As a result, the PE current decreased three orders of magnitude in comparison to measurements without the filter as shown in Figure 4.3. The decrease is most likely caused by the lower QE at longer wavelengths as discussed in Section 2.3.2. It is therefore concluded that the PE emission is predominantly caused by plasma light emission at wavelengths shorter than 150 nm.

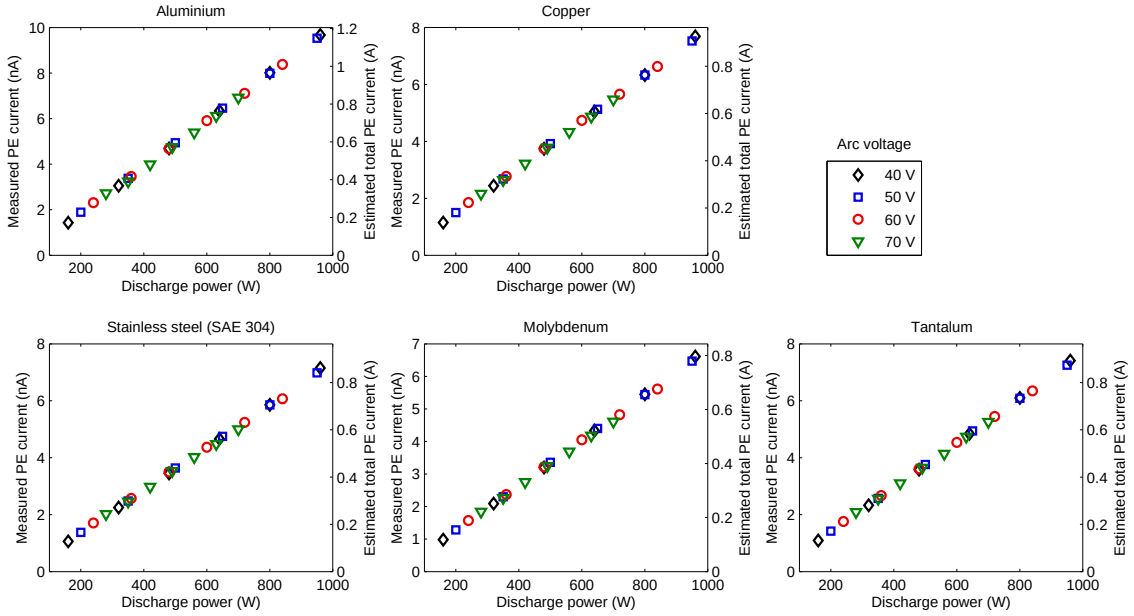

FIGURE 4.2 Measured photoelectron currents and estimated total photoelectron currents emitted from the plasma chamber walls as a function of discharge current and voltage. Measured with LIISA ion source at 3.8×10^{-3} mbar pressure. The figure is from Reference [PI].

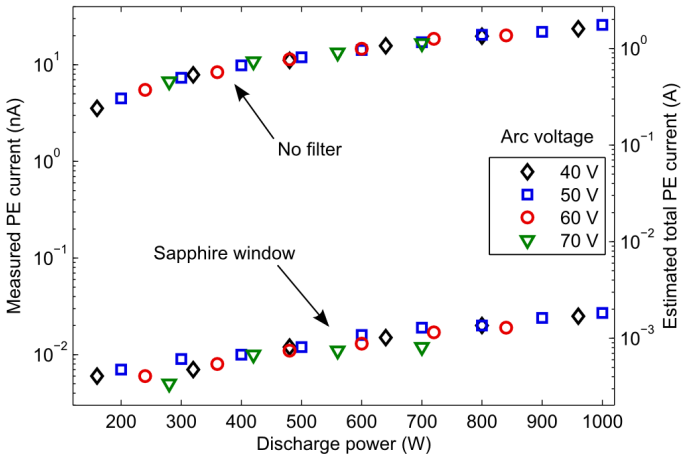

FIGURE 4.3 Difference between photoelectron currents from aluminium without filter and with sapphire window. Measured with LIISA ion source at 4.2×10^{-3} mbar pressure. The figure is from Reference [PI].

4.2 Comparison of plasma heating methods

The total PE currents normalized with the discharge power and measured with various ion sources are summarized in Table 4.1. The presented range corresponds to measured PE current variations with different metals, with the exception of the range given for the 14 GHz ion source corresponding to different values of

TABLE 4.1 Estimated total photoelectron emission for various ion sources. The presented range corresponds to measured PE current variations with different metals (aluminium, tantalum, molybdenum, copper, and stainless steel). For the 14 GHz ECR ion source, the range corresponds to different magnetic field strengths. The data is originally presented in Publications [PI], [PII], [PIII], and [PV].

Ion source	**Total PE current (AkW^{-1})**
2.45 GHz microwave	0.9–1.6
filament-driven multi-cusp	0.8–1.2
Prometheus I, ECR zone	0.5–1.0
Prometheus I, H^- production region	0.08–0.14
14 GHz ECR	0.002–0.007

the magnetic field (average for different samples). Linear dependence on the discharge power is observed with all the ion sources. The measured PE current with the 2.45 GHz microwave ion source deviates from linear dependence at high incident powers (see Figure 4.4). However, the Lyman-alpha emission has been reported to depend linearly on the microwave power [18]. Therefore, the deviation from linear power dependence is interpreted as the VUV induced surface aging effect and increased power losses in the waveguide at high incident powers. The measurement was conducted by going from high microwave power towards lower power, and thus the aging effect increased the current while the lower microwave power decreased it. By going back to the initial value with high power after the campaign, the current was increased by 14 % on average. The aging effect was observed to proceed most rapidly with the 2.45 GHz microwave source.

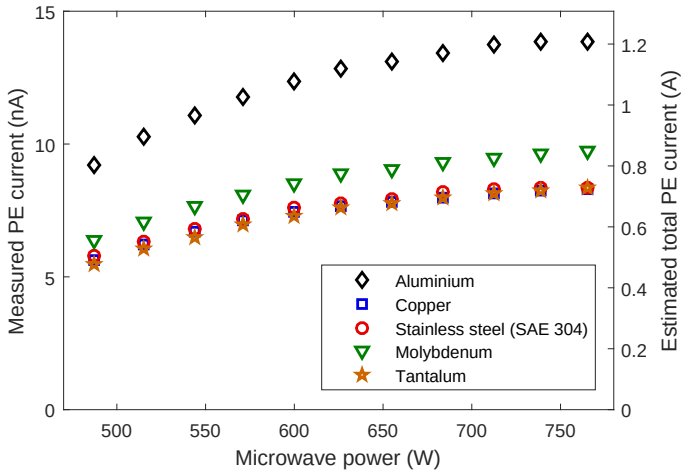

FIGURE 4.4 Photoelectron currents as a function of microwave power measured with the 2.45 GHz microwave ion source at 1.2×10^{-2} mbar pressure.

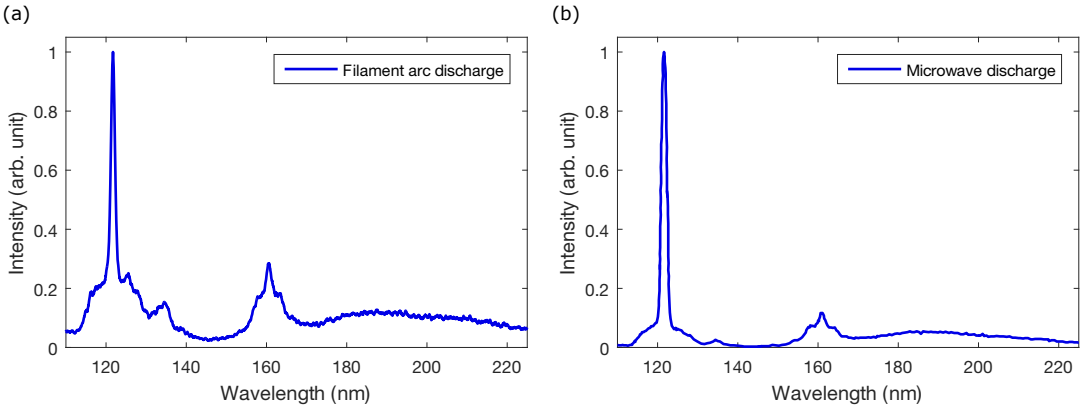

FIGURE 4.5 (a) Typical VUV emission spectrum of hydrogen plasma of a filament arc discharge (from Reference [PI]) and (b) of a microwave discharge (from Reference [18]). The spectra are not corrected for spectral transmittance.

The order of magnitude for the total PE emission is 1 A per kW of heating power for the 2.45 GHz microwave source and the filament source. For example, in filament discharge, 1 A corresponds to almost 10 % of typical discharge current. The small difference between the sources could be due to different plasma heating methods. The EEDF in the microwave source results to preferential excitation to the triplet states, which leads to molecule dissociation via the $b^3\Sigma_u^+$ state. In the 2.45 GHz microwave discharge, the volumetric dissociation rate via triplet $b^3\Sigma_u^+$ state is calculated to be 2.2–8.5 $\times$ 10^{16} $cm^{-3}s^{-1}$ at 1 kW discharge power. The upper limit is slightly higher in comparison to the filament arc discharge (LIISA), where the corresponding value is 2.5–5.8 $\times$ 10^{16} $cm^{-3}s^{-1}$. However, in the filament arc discharge, the dissociation rate via singlet $B^1\Sigma_u^+$ and $C^1\Pi_u$ states is 1.8–2.0 $\times$ 10^{16} $cm^{-3}s^{-1}$, while the corresponding value is 0.3–0.4 $\times$ 10^{16} $cm^{-3}s^{-1}$ in the microwave discharge [99]. The total dissociation rate in both discharges is similar, but the contribution of the atomic Lyman-alpha emission on the total VUV emission is higher in the microwave discharge. The VUV emission spectra measured from both types of ion sources are presented in Figure 4.5, where it is seen that in the spectrum of the microwave discharge the Lyman-alpha peak is higher than the Werner-band and Lyman-band emissions in the relative intensities in comparison to the filament discharge. This implies that the differences between the filament arc discharge and the microwave discharge are not only contributed by plasma processes but also by plasma–wall interactions. In the microwave source, the boron nitride disc (dielectric material) facing the plasma effectively increases the atomic hydrogen fraction in the plasma due to lower wall recombination rate [21]. The higher atomic fraction and the subsequent Lyman-alpha emission can explain the higher PE emission observed in the microwave source due to high QE at Lyman-alpha wavelength. It is also worth noting that, based on the total photon emission power, the power efficiency of the filament source can be considered higher in comparison to the microwave source [99]. Therefore, it

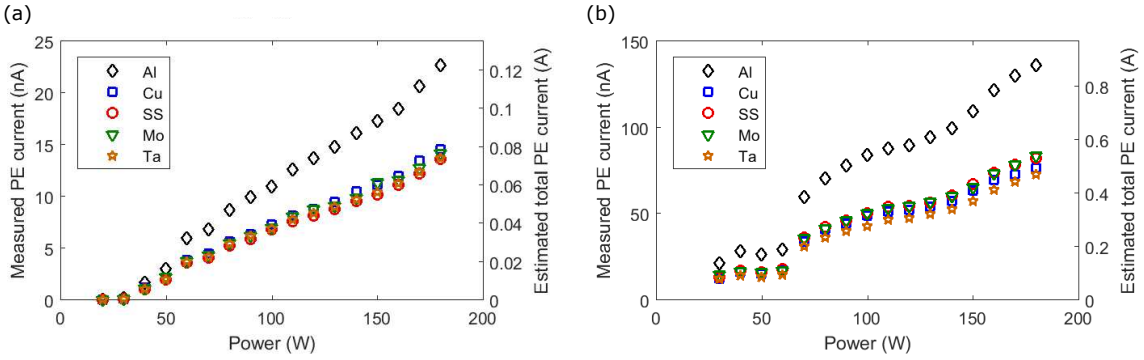

FIGURE 4.6 Photoelectron currents as a function of microwave power per elementary source measured with Prometheus I at 1.6×10^{-2} mbar pressure. (a) The photoelectron meter is viewing the H^- production region and (b) the ECR zone. The figures are from Reference [PIII].

is assumed that the results presented in Table 4.1 correspond to the minimum difference in the PE emission between these two sources.

The experimental setup with Prometheus I allowed to measure the PE current induced by light emission from the ECR zone and the H^- production region separately. This was realized by moving the ECR modules vertically with respect to the diagnostics port of the PE meter. As an example, the PE currents measured as a function of the elementary microwave source power with Prometheus I at 1.6×10^{-2} mbar pressure are presented in Figure 4.6. Detailed information on the experiments with Prometheus I can be found from Publication [PIII]. The total light emission from the ECR zone is much more intense in comparison to the H^- production region [95]. In the ECR discharge, the EEDF has to be determined locally, since the heating power is dissipated predominantly in the close proximity of the ECR surface and, consequently, the hot electron density is higher near the ECR zone. In the ECR zone, the electron temperature is higher, which results to higher Lyman-band and Werner-band emission in comparison to the H^- production region as shown in Figure 2.8. In the H^- production region, the lower electron temperature leads to higher dissociation degree and relative dominance of the Lyman-alpha emission in comparison to the ECR zone. The estimated total PE current for the H^- production region is in the order of 0.1 A, which is considered as the lower limit for the total PE emission. The estimated total PE emission reaches values of 1 A, when the ECR zone is in the line-of-sight, which is considered as the upper limit of the PE current. The lower and upper limits are obtained assuming that the whole plasma chamber volume emits light corresponding to H^- production region and ECR zone, respectively. The total emission of 1 A is in the same order of magnitude in comparison to other hydrogen ion sources studied in this work. In Prometheus I, it can be assumed that most of the electrons emitted from the walls are transported to the plasma, since the transverse magnetic field intensity is low near the walls and the emitted electrons

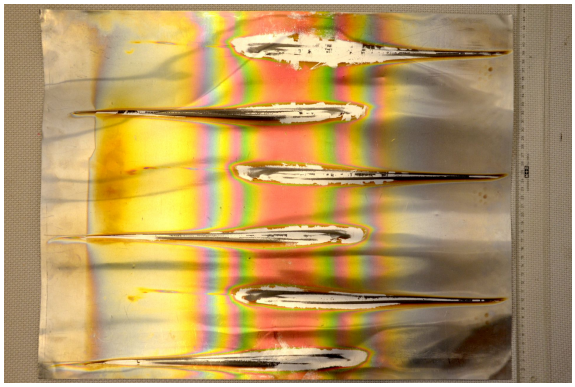

FIGURE 4.7 A cylindrical plasma chamber liner of the 14 GHz ECR ion source opened to a plane showing the radial electron flux making contact with the liner at the poles of the radial magnetic field.

are accelerated towards the plasma by the positive plasma potential.

The presented range for the PE emission in the 14 GHz ECR source in Table 4.1 corresponds to PE emission measured using residual gas, which is mainly oxygen from water and nitrogen from an air leak, at the pressure of 1×10^{-6} mbar. The estimated total PE emission is in the order of few mA per kW of injected microwave power, which is orders of magnitude lower in comparison to the low temperature plasma sources. However, this has to be put in perspective. The estimated total PE current from the plasma chamber walls can be over 10 % of the electron current leaving the plasma, as discussed in Publication [PII], where detailed information on the experiments can be found. The transport of PEs emitted from the walls is restricted by the magnetic field of the ECR ion source, which is order of magnitude higher in comparison to the low temperature plasma sources. Electrons are most probably transmitted to the plasma from the area where plasma can touch the walls, which covers approximately 5 % of the total plasma chamber area, as illustrated in Figure 4.7. Electron fluxes from the 14 GHz ECR plasma have been discussed in Reference [100]. The emission was found to be predominantly caused by radiation at 8 eV–1 keV energy range, whereas the X-ray emission at energies higher than 1 keV seems insignificant for the PE emission. However, the experiments left some open questions regarding the influence of the X-ray range on the PE emission. Due to the measurement geometry, where the line-of-sight was between the poles of the permanent magnet hexapole, the contribution of direct wall bremsstrahlung and radiation emitted due to recombination of highly charged ions near the plasma chamber walls was not completely taken into account. Also, the characteristic K_α for carbon (277 eV), nitrogen (392.4 eV), and oxygen (524.9 eV) lie between the probed range of 8 eV–1 keV. Thus, it remains unclear if the PE emission is dominated by VUV or X-ray ranges of radiation.

In the high-frequency ECR ion sources producing multi-charged ions, the hot

electron temperature is significantly higher in comparison to low temperature plasma sources. Therefore, the secondary electron emission from the plasma chamber walls is of considerable importance. It is known that the output of highly charged ions is drastically enhanced by coating the inner surface of the plasma chamber with aluminium (oxide) [101]. In ECR ion sources, the beneficial effect of wall coating was discovered when the current of highly charged oxygen ion beam increased by a factor of two after the plasma chamber had been covered by a silicon oxide layer [102]. Also carbon contamination on the plasma chamber walls has been seen to affect the plasma potential and the oxygen ion beam current significantly [103]. Altogether this implies that surface properties including electron emission play a significant role in the operation of high-frequency ECR ion sources.

5 PLASMA INDUCED PHOTOELECTRON EMISSION FROM ALKALI METAL COVERED SURFACES

Hydrogen plasma induced PE emission from cesium and rubidium covered metal surfaces was studied experimentally. The transient PE currents measured during alkali metal deposition and desorption processes are presented in this chapter. The experiments with alkali metal covered surfaces were originally presented in Publications [PIV] and [PV].

5.1 Cesium

The transient PE current measured as a function of cesium (99.99 % purity) coverage on a molybdenum sample is presented in Figure 5.1. As the cesium deposition starts, the PE current is immediately enhanced. As the cesium coverage increases, the PE current exhibits a double hump structure before reaching the maximum value. The decreasing PE current finally saturates to a value lower than the current from the clean substrate.

The observations can be qualitatively explained by the decreasing work function of the surface with the build-up of the cesium coverage, and by comparison of the photon penetration depth within the cesium layer and the metal substrate to the escape depth of the PEs. It is clearly noticeable that the work function change shown in Figure 2.12 does not alone explain the observed behavior of the PE emission. The mean free path for 10 eV VUV photons, which is the average energy for the predominant part of the spectrum, is 10 nm in molybdenum while the penetration depth in cesium is 39 µm [104]. This means that photons interact predominantly with the molybdenum substrate even at considerable cesium layer thickness. The work function is lowered by the accumulation of cesium, and

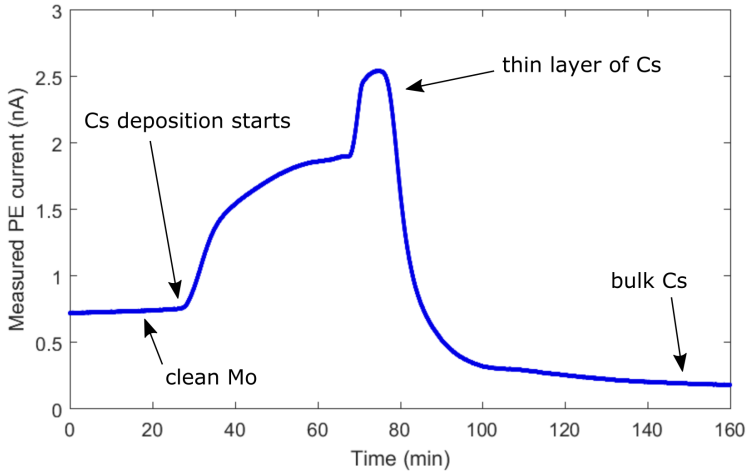

FIGURE 5.1 Measured photoelectron current from molybdenum sample as a function of time (i.e. cesium coverage on the surface). The data is originally presented in Publication [PIV].

TABLE 5.1 Penetration depths for 10 eV photons in different materials [104].

Material	**Penetration depth (nm)**
Aluminium	8
Tantalum	8
Molybdenum	10
Nickel	12
Copper	13
Yttrium	24
Rubidium	1900
Cesium	3900

thus the PE yield is higher, as long as the emitted electrons are able to propagate through the deposited layer with sufficient energy. Typical escape depth of PEs with energies of a few eV is 1–3 nm [105]. If the cesium layer is too thick, the PE current is limited by the short escape depth of the electrons, although the work function is lower for bulk cesium in comparison to molybdenum.

With different substrate materials, the maximum PE current is measured to be 2–3.5 times higher in comparison to clean substrate as shown in Figure 5.2. With all the substrates the PE current saturates to the same value, which corresponds to emission from bulk cesium. Depending on the substrate the saturation current is 60–80 % lower than the initial value measured for the bare metal. The penetration depth for 10 eV photons varies in the range of 8–24 nm for all the substrates, while the penetration depth in cesium and rubidium is two orders of magnitude longer

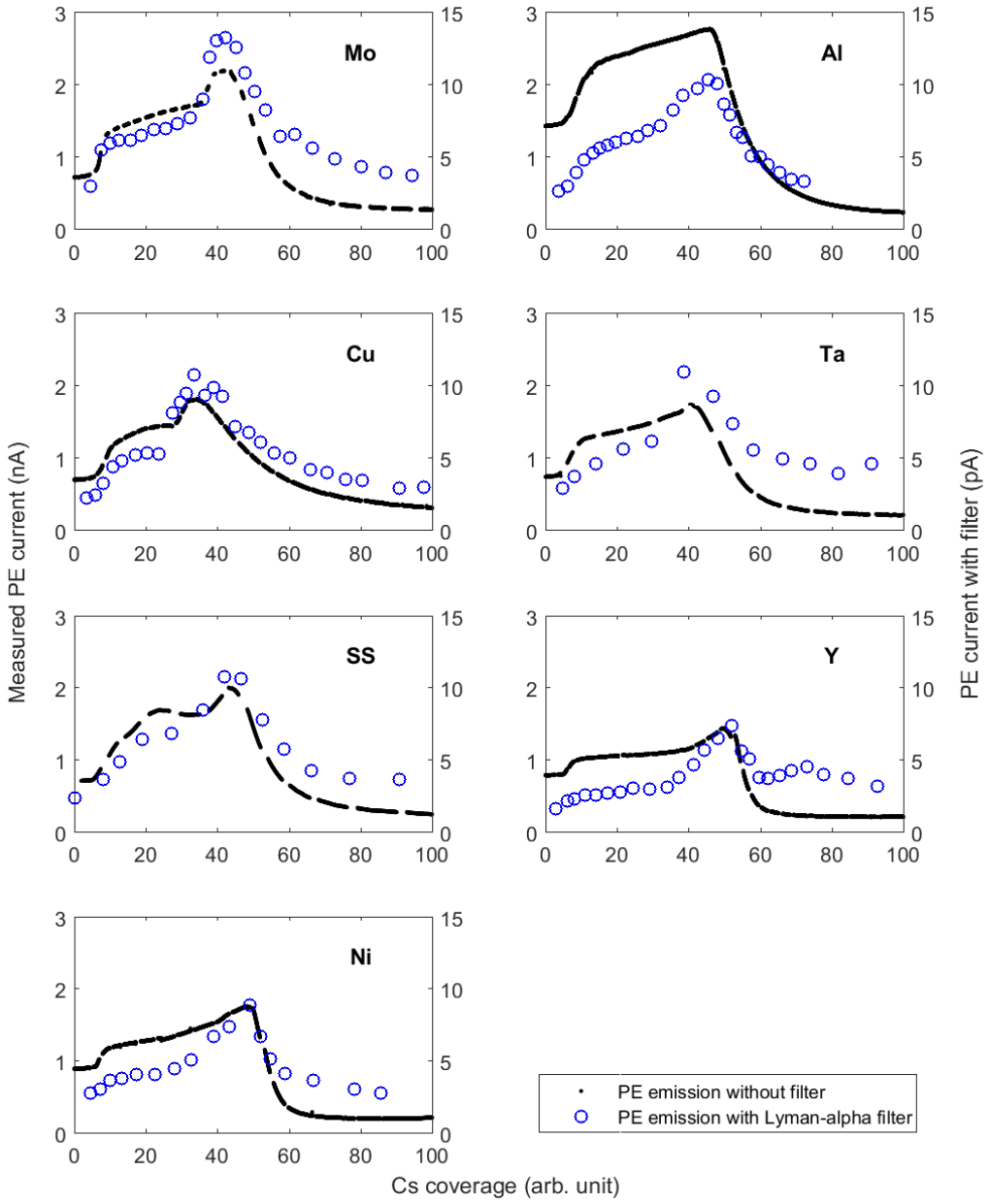

FIGURE 5.2 Measured photoelectron currents from different substrates (molybdenum aluminium, copper, tantalum, stainless steel (SAE 304), yttrium, and nickel) as a function of cesium coverage by exposing the sample to the whole emission spectrum of the hydrogen plasma (left axes) and by applying the Lyman-alpha filter (right axes). The figure is from Reference [PIV].

as listed in Table 5.1. Figure 5.2 also shows the measured PE current by applying a bandpass filter corresponding to Lyman-alpha (eSource Optics 25122FNB, 122 nm, FWHM 20 nm), which is the predominant contributor of the VUV spectrum on the PE emission. The transmittance of the filter is in the order of a few percent. The PE current measured with the Lyman-alpha filter shows similar behavior as a function of cesium as the current measured without the filter. For different substrates, the

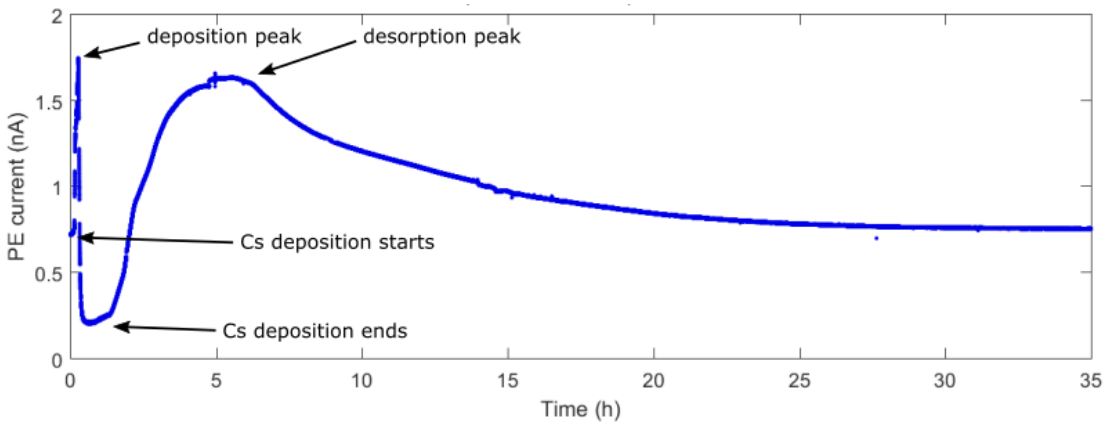

FIGURE 5.3 Measured photoelectron current from cesium covered tantalum sample showing the deposition and desorption peaks. The data is originally presented in Publication [PV].

relative difference in the PE current measured with the Lyman-alpha filter in proportion to the PE current measured without the filter is somewhat different. The ratio also changes as a function of the cesium coverage. This is believed to be due to the functional dependence of the QE on the photon energy with varying work function.

It is worth noting, that in Reference [106] an increase by two orders of magnitude in the PE current arising from 3.94 eV photons was observed during deposition of cesium on a stainless steel surface in ion source relevant conditions. At around 10 eV photon energy, the initial QE of metals is about 2–5 % as shown in Figure 2.11. Therefore, an increase by two orders of magnitude in the total emission throughout the VUV wavelength range would be unnatural, since PE emission is a process between a single photon and a single electron and the QE cannot exceed 100 % by definition. The initial QE is orders of magnitude lower at 3.94 eV photon energy, and thus the effect of cesium on the PE current can be greater at energies close to the work function.

Time evolution of the PE current from the cesium covered tantalum sample is shown in Figure 5.3. As the alkali metal deposition ceases the PE current starts to increase again reaching another maximum, almost as high as the deposition peak, before saturation. The so called desorption peak is also observed with photocathodes and is believed to be caused by diffusion and desorption of cesium [107]. The surface can have patches (due to different crystal faces, roughness, contamination, etc.) with different QE and different bond strength between the substrate and cesium atoms. When the cesium deposition is stopped, cesium starts to diffuse on the micron scale required to traverse these patches resulting to a more optimal cesium coverage, and thus increased PE emission. When more than a monolayer is deposited on the surface, cesium evaporates faster from portions where the layer is thicker due to weaker bond strength between cesium atoms in comparison

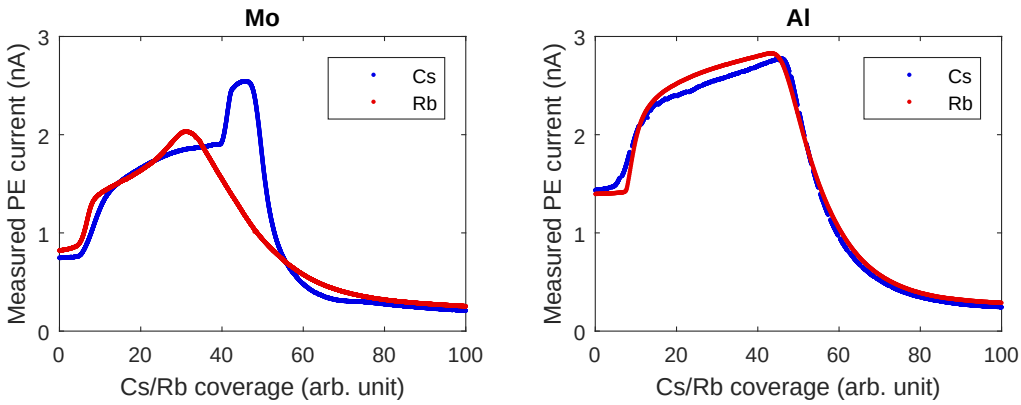

FIGURE 5.4 Measured photoelectron currents from molybdenum and aluminium substrates as a function of cesium and rubidium coverage. The figure is from Reference [PIV].

to bond strength between cesium and the substrate atoms, which evens out the overall coverage and hence increases the QE. In addition, the desorption peak can be contributed by gradual accumulation of impurities and formation of chemical compounds on the surface with time.

5.2 Rubidium

Rubidium was used for confirming the results obtained with cesium. The work function of rubidium (2.16 eV) is almost as low as the work function of cesium (2.14 eV) [59]. A comparison of PE emission from molybdenum and aluminium substrates as a function of cesium and rubidium coverage, presented in Figure 5.4, shows almost identical behavior. The PE current saturates to the same value with both alkali metals, i.e. low temperature hydrogen plasma induced PE emission from bulk cesium and bulk rubidium are identical. The comparison of the two alkali metals also suggests that their impurity compounds with different chemical properties play a minor role in determining the PE current.

6 THE EFFECT OF PHOTOELECTRONS ON PLASMA PROPERTIES

The PE emission may have a considerable effect on ion source plasma properties depending on the intensity and the energy distribution of the emitted electrons. In low temperature hydrogen plasmas, the rate coefficient for ionization shown in Figure 2.3 is within the same order of magnitude with excitation to radiative states indicated in Figure 2.8. Therefore, the magnitude of PE emission as a source of free electrons is not comparable to ionization due to relatively low QE of metals as shown in Figure 2.11. Thus, PEs influence on the total electron density of the plasma can be considered minute. However, the PE emission potentially has considerable local effects on the plasma chemistry, which can be affected even by a small stimulus altering the equilibrium, and the plasma sheath structure, which are discussed in this chapter.

6.1 Plasma chemistry

The effect of PEs on the plasma chemistry is largely dependent on the energy distribution of the emitted electrons. The energy distribution of the emitted electrons extends from zero to the maximum energy which corresponds to the difference between the energy of the incident photon and the work function of the surface material. The PEs are further accelerated across the plasma sheath by the positive plasma potential. There are hundreds of possible electron impact processes in hydrogen plasmas, but their cross sections differ by orders of magnitude [54].

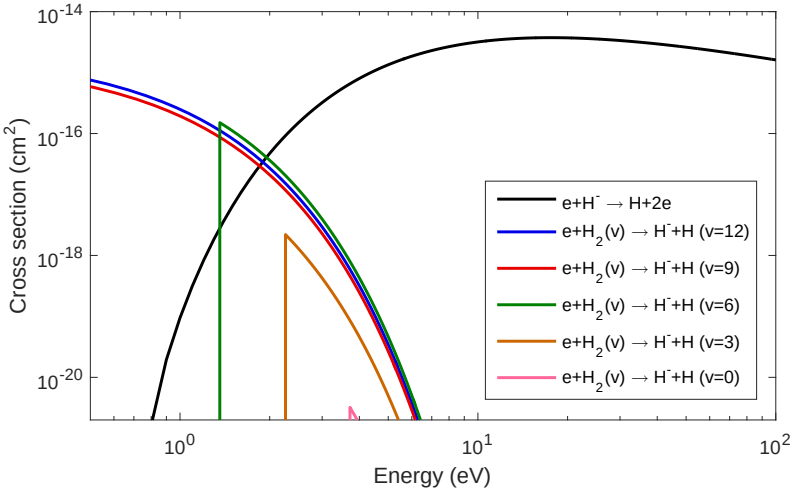

FIGURE 6.1 Cross sections for electron detachment and vibrational dependence of dissociative electron attachment. Cross section data is from Reference [54].

Some ion source relevant plasma processes potentially affected by the PEs are

$$\mathrm{e} + \mathrm{H}_2(\mathrm{X}^1\Sigma_g^+; v'') \rightarrow \mathrm{H}_2^- (^2\Sigma_u^+) \rightarrow \mathrm{H}^- + \mathrm{H}(n=1) \tag{6.1}$$

$$\mathrm{e} + \mathrm{H}^- \rightarrow \mathrm{H} + 2\mathrm{e} \tag{6.2}$$

$$\mathrm{e} + \mathrm{H}_2(\mathrm{X}^1\Sigma_g^+) \rightarrow \mathrm{H}_2(\mathrm{b}^3\Sigma_u^+) \rightarrow \mathrm{H} + \mathrm{H} + \mathrm{e} \tag{6.3}$$

$$\mathrm{e} + \mathrm{H}_2(\mathrm{X}^1\Sigma_g^+) \rightarrow \mathrm{H}_2(\mathrm{a}^3\Sigma_g^+) \tag{6.4}$$

$$\mathrm{e} + \mathrm{H}_2(\mathrm{X}^1\Sigma_g^+) \rightarrow \mathrm{H}_2(\mathrm{B}^1\Sigma_u^+) \tag{6.5}$$

$$\mathrm{e} + \mathrm{H}_2(\mathrm{X}^1\Sigma_g^+) \rightarrow \mathrm{H}_2(\mathrm{C}^1\Pi_u) \tag{6.6}$$

$$\mathrm{e} + \mathrm{H} \rightarrow \mathrm{H}^+ + 2\mathrm{e} \tag{6.7}$$

$$\mathrm{e} + \mathrm{H}_2 \rightarrow \mathrm{H}_2^+ + 2\mathrm{e}. \tag{6.8}$$

Low energy electrons are required for dissociative electron attachment (6.1), which has a large cross section for vibrationally excited molecules at electron energies around 1 eV [54], as illustrated in Figure 6.1. Higher energy electrons can be "poisonous" for negative ions, since electron detachment (6.2) cross section increases rapidly with the electron energy from the threshold energy of 0.75 eV to 10 eV [54], which is also presented in Figure 6.1. Molecular excitation from the ground state to triplet states is peaked around the threshold, which is 8 eV for excitation to the repulsive $\mathrm{b}^3\Sigma_u^+$ (6.3) state and 12 eV for excitation to $\mathrm{a}^3\Sigma_g^+$ state (6.4) [54] as illustrated in Figure 2.7. Molecular excitation from the ground state to $\mathrm{B}^1\Sigma_u^+$ (6.5) and $\mathrm{C}^1\Pi_u$ (6.6) singlet states have threshold approximately 12 eV [39], and the peak cross section is at clearly higher energies, which is shown in Figure 2.7. Atomic (6.7) and molecular ionization (6.8) have threshold at 13.6 eV and 16 eV [39], respectively, and similar energy dependence to excitations to singlet states as indicated in Figure 2.2. Processes with threshold energies higher than the difference between the energy of the absorbed photon and the surface

work function are possible only if the emitted electrons are accelerated to sufficient energy across the plasma sheath by the plasma potential. Typical plasma potentials in hydrogen ion sources are in the range of 1–10 V [108, 109]. In surface production H^- ion sources, the plasma electrode is usually biased positively in order to reduce the co-extracted electron current, which results in decreased potential difference between the plasma and the electrode [40, 44, 110, 111]. The transport of the emitted electrons from the surfaces to the plasma depends on the plasma sheath structure, magnetic field, and possible collisions, which can also change the electron energy distribution. The total effect of PEs on the plasma chemistry is a complex puzzle, and solving this would require the use of a global plasma model.

6.2 Plasma sheath model

In addition to plasma chemistry, the additional space charge due to the PE emission can affect the plasma sheath structure, which also determines the final energy of the emitted electrons entering the bulk plasma, thus affecting it's properties. PEs effect on the plasma sheath structure is predicted using a modified version of the one-dimensional analytical, collisionless model introduced by McAdams et al. and presented in detail in Reference [81]. The influence of the PE emission on the plasma sheath is originally discussed in Publication [PV].

The model is modified to include PE emission from the wall by substituting the H^- current density j_{H^-} with effective current density

$$j_{\text{eff}} = j_{H^-} + \int_0^{h\nu-\phi} j_{\text{PE}}(E_{\text{PE}}) \sqrt{\frac{m_e}{m_{H^-}}} \sqrt{\frac{E_{H^-}}{E_{\text{PE}}}}\, \mathrm{d}E_{\text{PE}}, \tag{6.9}$$

where j_{PE} is the PE current density, m_e electron mass, m_{H^-} negative hydrogen ion mass, E_{PE} PE energy, and E_{H^-} negative hydrogen ion energy. A uniform energy distribution ranging from zero to the maximum energy, which corresponds to the difference between the energy of the absorbed photon $h\nu$ and the surface work function ϕ, is used for PEs with $h\nu = 10$ eV corresponding to the average energy for the predominant part of the spectrum and $\phi = 2$ eV corresponding to approximate work function of a cesiated surface. The actual energy distribution of the emitted electrons is unknown. The measured PE current corresponds to the total emission caused by wide range of photon energies. The energy of the emitted electrons also depends on the photon interaction with electrons deeper (than the Fermi level) in the conduction band and on the processes taking place within the material after the actual photon–electron interaction. The measured VUV spectra (e.g. in Figure 2.9) together with the QEs reported in the literature cannot be used to derive the interaction probability nor the PE energy distribution, because the spectra are not calibrated for spectral response. Thus, an approximation, such

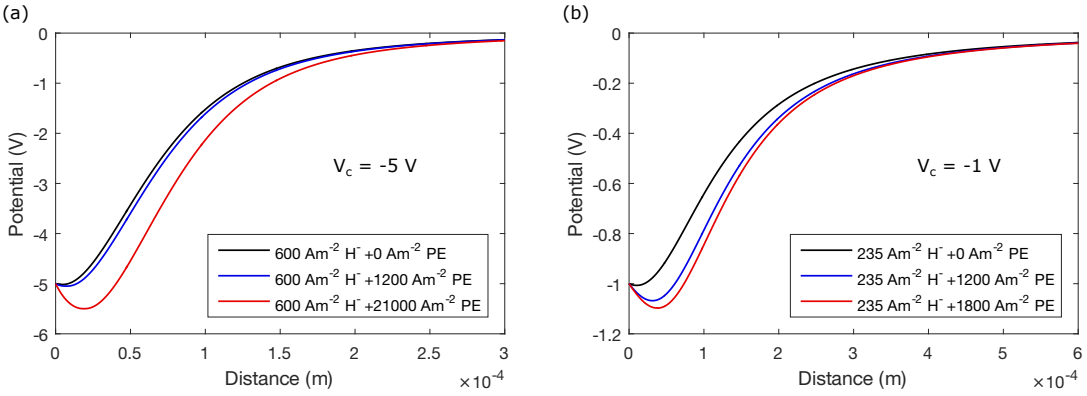

FIGURE 6.2 Sheath potentials for various negative hydrogen ion and photoelectron emission current densities with cathode potentials of (a) -5 V (b) -1 V.

as a uniform distribution, must be applied. Following Reference [81] a constant energy of 0.7 eV is assumed for surface produced negative hydrogen ions and the plasma density, electron temperature and positive ion temperature are set to 3.5×10^{17} m^{-3}, 2 eV and 0.8 eV, respectively. It is assumed that there are no volume produced negative ions.

The potential difference between the emitting surface and the plasma, i.e. the cathode potential, plays a major role in the significance of the PE emission on the sheath properties. In Figure 6.2 the plasma sheath potential is plotted for two different cathode potentials with various PE emission currents. The black line shows the sheath structure at the threshold H^- emission current density creating a virtual cathode. The red line presents the sheath structure with PE current density in addition to H^- current density needed for the depth of the virtual cathode to reach 10 % of the cathode potential. The blue line presents the sheath structure with a constant PE current density of 1200 Am^{-2} demonstrating that the PE emission has a more significant impact on the sheath structure with lower cathode potential. In H^- ion sources, the positive bias in the plasma electrode results in a decrease of the potential difference between the plasma and the electrode, which presumably affects the significance of the PE emission. The smaller the potential difference is, the lower PE current density is needed to alter the sheath structure, and thus influence the flux of negative ions. If the PE emission increases the depth of the virtual cathode, it can be considered as a potential limitation for the surface production of negative ions.

The influence of the cathode potential is further illustrated in Figure 6.3, where the virtual cathode depth is plotted as a function of the cathode potential. The negative hydrogen ion density corresponds to the threshold, when the virtual cathode is formed, and the additional PE current density, therefore, determines the depth of the virtual cathode.

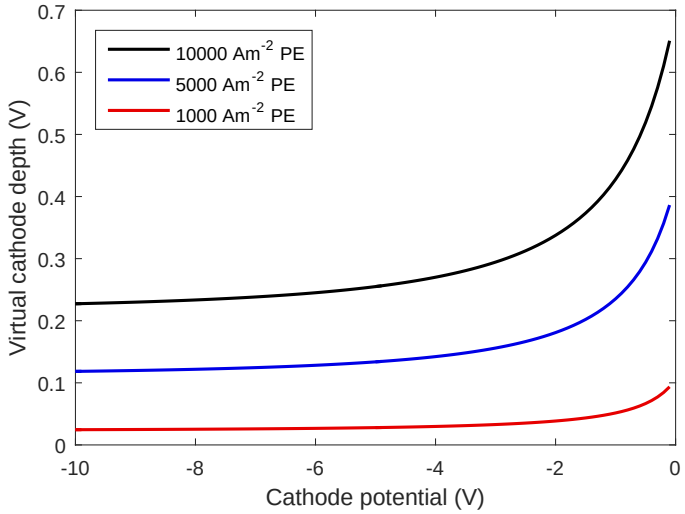

FIGURE 6.3 Virtual cathode depth as a function of cathode potential. With H^- current density corresponding to the threshold value required for the formation of the virtual cathode, the depth of the virtual cathode is determined by the additional photoelectron current density.

The influence of the negative ion energy is evaluated by plotting the sheath potential with different E_{H^-} in Figure 6.4, which can be compared to Figure 6.2 (a) where $E_{H^-} = 0.7$ eV. For different negative ion energies, the corresponding threshold value required for the formation of the virtual cathode is calculated, and the depth of the virtual cathode is again determined by the additional PE emission. With increasing negative ion energy, the current density required for the formation of the virtual cathode increases. On the other hand, when the negative ion energy increases, the influence of the PE emission on the virtual cathode becomes more significant as shown in Figure 6.4.

The influence of PE emission from cesium coated molybdenum surface on the

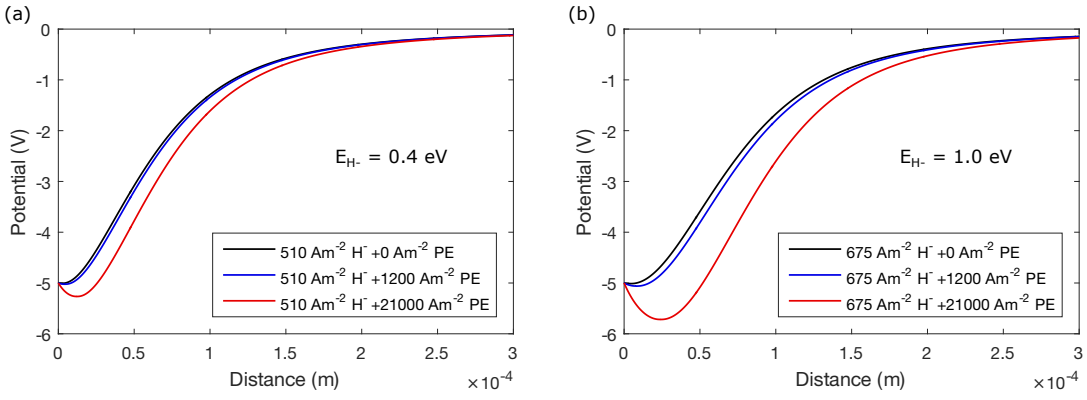

FIGURE 6.4 Sheath potentials for various negative hydrogen ion and photoelectron emission current densities with H^- energies of (a) 0.4 eV (b) 1.0 eV.

adjacent plasma sheath has been studied by a PIC code in References [112, 113]. It was concluded that the PE emission does not significantly influence the plasma sheath. However, only molecular emission was taken into consideration in the model, and the cathode potential used in the study was 4 V.

The realization of a PE emission density required to create a significant influence on the plasma sheath structure depends on the mechanical design of the plasma device, plasma heating method affecting the VUV emission spectrum, and the discharge power affecting the VUV emission intensity. The experimental results presented here suggest that the total PE current from cesiated plasma chamber walls could be as high as 3.5 A per kW of discharge power. For example, in a prototype surface production ion source (ELISE) being developed for neutral beam injection for ITER, the plasma is heated with the maximum RF power of 360 kW distributed evenly between 4 RF-drivers and the illuminated plasma grid area is 0.9 m^2 [111]. Direct extrapolation from 3.5 AkW^{-1} yields a total PE current density of 140–420 Am^{-2}, if 10–30 % of the emitted light is incident on the grid, which is an estimate based on the geometry of the ion source. In large-area surface production negative ion sources, there is a transverse magnetic field in front of the plasma grid, which suppresses the PE emission. However, the beam extraction field penetrates to the conical part of the plasma grid. The magnetic field at the conical part is not parallel to the surface of the plasma grid and the PEs are able to escape from the surface and they will be extracted. On the other hand, the corresponding estimate for a Penning type ion source with up to 3.85 kW of discharge power dissipated in < 1 cm^3 sized plasma contained in a chamber with a surface area of 2.48×10^{-4} m^2 [114], yields a PE current density of 54 kAm^{-2} if it is assumed that the power efficiency of the Penning discharge equals that of the filament- and microwave-driven plasma sources discussed here. In the ion sources used for the PE emission measurements, the light emission depends linearly on discharge power. However, this cannot automatically be assumed to hold for high power ion sources. It can be concluded, that if the order of magnitude for the PE current density reaches 1 kAm^{-2} and the cathode potential is low, the PE emission can be significant for the plasma sheath structure.

7 DISCUSSION

The experimental studies presented in this thesis give an understanding on the order of magnitude of the low temperature hydrogen plasma induced PE emission. It is suggested that the total PE emission from metal surfaces is in the order of 1 A per kW of discharge power. The given result corresponds to ion source relevant conditions. For a perfectly clean surface the emission might be different and, hence, the result is to be treated as an order of magnitude estimate. The value given here is the upper limit for the PE emission, which does not take into account the diffusion of the emitted electrons in the magnetic fields applied to ion sources. The effect of the magnetic field on the PE emission depends on the field strength, topology and direction with respect to the emitting surface. Nevertheless, this work gives a long-awaited answer to the question on the role of the photoelectric effect in hydrogen ion sources. The validity of the result can be reviewed by calculating the effective QE from the measured PE emission. If 10–30 % of the discharge power is dissipated through VUV emission with an average energy of 10 eV, the PE emission measured from metal surfaces yields a QE of 3–10 %, which is consistent with the measured values for the QE found from literature (see Figure 2.11). A thin layer of alkali metal on the surface can increase the emission up to 2–3.5 times, but a thick layer decreases the emission. Cesium has been reported to increase the extracted negative ion beam current 2–4 times [45, 115, 116]. However, the surface production of negative ions cannot be distinguished from the volume production, which complicates the interpretation of the result. The linear prediction on the total PE emission can be used as a guideline, for example, in numerical simulation models where plasma–surface interaction is taken into account. However, for more accurate results, the PE emission should be measured using the particular plasma source, since power dissipation and VUV light emission may vary between different plasma devices.

The PE emission might have a considerable influence on various plasma processes

and especially on the plasma sheath structure. PEs effect can be expected to be important particularly in tandem-type ion sources, when intense VUV photon flux, emitted from the hot and dense part of the plasma at the driver region, impinges on a surface in the cold and rarefied part of the plasma at the extraction region. In Penning type ion sources, the PE emission can reach large current densities, when a high discharge power is efficiently dissipated in a fingertip sized plasma. However, the role of PEs in plasmas is not yet known well enough. It is not possible to distinguish the population of electrons in the plasma produced by PE emission from other electron sources and, hence, the reciprocal significance of electrons from different sources can only be estimated. Further work with a global model would increase the knowledge on the importance of the photoelectric effect on the performance of ion sources. Also the effect of the magnetic field on the diffusion of the emitted electrons can be studied more thoroughly in the future.

The results obtained with rubidium, indicating a work function comparable to cesium, raise a question whether rubidium could be used as an alternative to cesium in negative ion sources. As similar PE emission results were obtained with cesium and rubidium it might be expected that the surface production of H^- could also be similar between the two alkali metals. Elements other than cesium with low ionization potentials (alkali and alkaline earth metals) have been tested in the early days of H^- ion source development. However, cesium was concluded to surpass other alkali elements under optimal conditions [49, 117, 118, 119]. Although cesium has a slightly lower work function, and thus is presumably more suitable to enhance H^- surface production, rubidium might have some advantages. From practical point of view, rubidium is less reactive, and thus safety hazards are reduced in comparison to cesium operation. As rubidium is lighter than cesium, it presumably causes less material erosion by sputtering, which limits the lifetime of H^- Penning ion sources, for example [120]. So-called scaled Penning ion sources have been developed to reduce the sputtering damage on the cathode, anode and extraction electrodes caused by positive cesium ions, and thus increase the lifetime of the source [121, 122].

When the role of surface processes is better understood, the ion beam generation could possibly be optimized by choosing the plasma chamber wall material and structure and plasma heating method accordingly. For example, future studies could include surface patterning to enhance the effective area of the surface producing negative ions. In negative ion sources, microfabrication of the converter surface, e.g. with a metallic dendrite surface [123], would not only increase the surface area significantly, but also could modify the electric field on the surface to aid the transport of surface produced negative ions through the plasma sheath.

REFERENCES

[1] V. Skalyga, I. Izotov, S. Golubev, A. Sidorov, S. Razin, A. Vodopyanov, O. Tarvainen, H. Koivisto, and T. Kalvas, *Rev. Sci. Instrum.* **87**, 02A716 (2016).

[2] R. F. Welton, M. P. Stockli, S. N. Murray, D. Crisp, J. Carmichael, R. H. Goulding, B. Han, O. Tarvainen, T. Pennisi, and M. Santana, *AIP Conf. Proc.* **1097**, 181 (2009).

[3] L. Celona, L. Allegra, A. Amato, G. Calabrese, A. Caruso, G. Castro, F. Chines, G. Gallo, S. Gammino, O. Leonardi, et al., Proc. IPAC2016, Busan, Korea, WEPMY035 (2016).

[4] R. Gobin, D. Bogard, P. Cara, N. Chauvin, S. Chel, O. Delferrière, F. Harrault, P. Mattei, A. Mosnier, F. Senée, et al., *Rev. Sci. Instrum.* **85**, 02A918 (2014).

[5] R. S. Hemsworth and T. Inoue, *IEEE Trans. Plasma Sci.* **33**, 1799 (2005).

[6] P. Heikkinen and E. Liukkonen, *AIP Conf. Proc.* **600**, 89 (2001).

[7] R. J. Van de Graaff, *Nucl. Instrum. Meth.* **8**, 195 (1960).

[8] R. Hemsworth, H. Decamps, J. Graceffa, B. Schunke, M. Tanaka, M. Dremel, A. Tanga, H. P. L. De Esch, F. Geli, J. Milnes, et al., *Nucl. Fusion* **49**, 045006 (2009).

[9] R. McAdams, *Rev. Sci. Instrum.* **85**, 02B319 (2014).

[10] S. Henderson, W. Abraham, A. Aleksandrov, C. Allen, J. Alonso, D. Anderson, D. Arenius, T. Arthur, S. Assadi, J. Ayers, et al., *Nucl. Instr. Meth. Phys. Res. A* **763**, 610 (2014).

[11] T. J. Ruth, *Rep. Prog. Phys.* **72**, 016701 (2008).

[12] E. Ahedo, *Plasma Phys. Control. Fusion* **53**, 124037 (2011).

[13] N. Gascon, M. Dudeck, and S. Barral, *Phys. Plasmas* **10**, 4123 (2003).

[14] H. B. Profijt, S. E. Potts, M. C. M. van de Sanden, and W. M. M. Kessels, *J. Vac. Sci. Technol. A* **29**, 050801 (2011).

[15] V. M. Donelly and A. Kornblit, *J. Vac. Sci. Technol. A* **31**, 050825 (2013).

[16] J. Komppula and O. Tarvainen, *Phys. Plasmas* **22**, 103516 (2015).

[17] J. Komppula, O. Tarvainen, S. Lätti, T. Kalvas, H. Koivisto, V. Toivanen, and P. Myllyperkiö, *AIP Conf. Proc.* **1515**, 66 (2013).

[18] J. Komppula, O. Tarvainen, T. Kalvas, H. Koivisto, R. Kronholm, J. Laulainen, and P. Myllyperkiö, *J. Phys. D: Appl. Phys.* **48**, 365201 (2015).

[19] U. Fantz, S. Briefi, D. Rauner, and D. Wünderlich, *Plasma Sources Sci. Technol.* **25**, 045006 (2016).

[20] S. R. Walther, K. N. Leung, and W. B. Kunkel, *J. Appl. Phys.* **64**, 3424 (1988).

[21] O. Waldmann and B. Ludewigt, *Rev. Sci. Instrum.* **82**, 113505 (2011).

[22] R. J. Goldston and P. H. Rutherford, *Introduction to Plasma Physics*, Institute of Physics Publishing, London (1995).

[23] J. A. Bittencourt, *Fundamentals of Plasma Physics*, Springer-Verlag New York, New York, USA (2004).

[24] A. A. Fridman and L. A. Kennedy, *Plasma Physics and Engineering*, Taylor & Francis Routledge, New York, London (2004).

[25] M. A. Lieberman and A. J. Lichtenberg, editors, *Principles of Plasma Discharges and Materials Processing*, John Wiley & Sons, Inc., Hoboken, New Jersey (2005).

[26] M. C. Williamson, A. J. Lichtenberg, and M. A. Lieberman, *J. Appl. Phys.* **72**, 3924 (1992).

[27] S. Gammino, L. Celona, G. Ciavola, F. Maimone, and D. Mascali, *Rev. Sci. Instrum.* **81**, 02B313 (2010).

[28] O. Tarvainen and S. X. Peng, *New J. Phys.* **18**, 105008 (2016).

[29] R. Cimino, I. R. Collins, M. A. Furman, M. Pivi, F. Ruggiero, G. Rumolo, and F. Zimmermann, *Phys. Rev. Lett.* **93**, 014801 (2004).

[30] V. Baglin, J. Bojko, O. Gröbner, B. Henrist, N. Hilleret, C. Scheuerlein, and M. Taborelli, Proceedings of EPAC 00 (2000).

[31] I. G. Brown, editor, *The Physics and Technology of Ion Sources*, WILEY-VCH Verlag GmbH & Co. KGaA, Weinheim (2004).

[32] M. Li, S. K. Dew, and M. J. Brett, *J. Phys. D: Appl. Phys.* **32**, 2056 (1999).

[33] V. A. Godyak, V. P. Meytlis, and H. R. Strauss, *IEEE Trans. Plasma Sci.* **23**, 728 (1995).

[34] V. A. Godyak, *IEEE Trans. Plasma Sci.* **34**, 755 (2006).

[35] S. Aleiferis and P. Svarnas, *Rev. Sci. Instrum.* **85**, 123504 (2014).

[36] J. Bretagne, G. Delouya, C. Gorse, M. Capitelli, and M. Bacal, *J. Phys. D: Appl. Phys.* **18**, 811 (1985).

[37] T. Kalvas, *Development and use of computational tools for modelling negative hydrogen ion source extraction system*, PhD thesis, University of Jyväskylä, Jyväskylä, Finland (2013).

[38] Y. K. Kim and M. E. Rudd, *Phys. Rev. A* **50**, 3954 (1994).

[39] J.-S. Yoon, M.-Y. Song, J.-M. Han, S. H. Hwang, W.-S. Chang, and B. Lee, *J. Phys. Chem. Ref. Data* **37**, 913 (2008).

[40] M. Bacal, A. Hatayama, and J. Peters, *Rev. Sci. Instrum.* **33**(6), 1845 (2005).

[41] M. Nishiura, *J. Plasma Fusion Res.* **80**, 757 (2004).

[42] M. Bacal, A. A. Ivanov Jr., M. Glass-Maujean, Y. Matsumoto, M. Nishiura, M. Sasao, and M. Wada, *Rev. Sci. Instrum.* **75**(5), 1699 (2004).

[43] K. Tsumori, H. Nakano, M. Kisaki, K. Ikeda, K. Nagaoka, M. Osakabe, Y. Takeiri, O. Kaneko, M. Shibuya, E. Asano, et al., *AIP Conf. Proc.* **1515**, 149 (2013).

[44] K. Tsumori, K. Ikeda, H. Nakano, M. Kisaki, S. Geng, M. Wada, K. Sasaki, S. Nishiyama, M. Goto, G. Serianni, et al., *Rev. Sci. Instrum.* **87**, 02B936 (2016).

[45] L. Schiesko, P. McNeely, U. Fantz, P. Franzen, and NNBI Team, *Plasma Phys. Control. Fusion* **53**, 085029 (2011).

[46] B. Rasser, J. N. M. van Wunnik, and J. Los, *Surf. Sci.* **118**, 697 (1982).

[47] R. Friedl, *Experimental investigations on the caesium dynamics in H_2/D_2 low temperature plasmas*, PhD thesis, Max-Planck-Institut für Plasmaphysik (IPP), Garching, Germany (2013).

[48] Yu. I. Belchenko, G. I. Dimov, and V. G. Dudnikov, *Nucl. Fusion* **14**, 113 (1974).

[49] V. G. Dudnikov, *Rev. Sci. Instrum.* **63**, 2660 (1992).

[50] B. S. Lee and M. Seidl, *Appl. Phys. Lett.* **61**, 2857 (1992).

[51] U. Fantz, *Plasma Sources Sci. Technol.* **15**, S137 (2006).

[52] U. Fantz and D. Wünderlich, *At. Data Nucl. Data Tables* **92**, 853 (2006).

[53] P. M. Stone, Y.-K. Kim, and J. P. Desclaux, *J. Res. Natl. Inst. Stand. Technol.* **107**, 327 (2002).

[54] R. K. Janev, D. Reiter, and U. Samm, *Collision Processes in Low-Temperature Hydrogen Plasmas* volume Juel-4105 of *Berichte des Forschungszentrums Jülich*, Forschungszentrum, Zentralbibliothek, Jülich (2003).

[55] A. Einstein, *Ann. Phys.* **322**, 132 (1905).

[56] Nobel Prize, The Nobel Prize in Physics 1921, https://www.nobelprize.org/nobel_prizes/physics/laureates/1921/, retrieved 3 November 2017.

[57] M. Cardona and L. Ley, *Photoemission in Solids I General Principles* volume 26 of *Topics in Applied Physics*, Springer-Verlag, Berlin Heidelberg New York (1978).

[58] B. Feuerbacher, B. Fitton, and R. F. Willis, editors, *Photoemission and the electronic properties of surfaces*, John Wiley & Sons, Chichester (1978).

[59] H. B. Michaelson, *J. Appl. Phys.* **48**, 4729 (1977).

[60] R. G. Wilson, *J. Appl. Phys.* **37**, 3161 (1966).

[61] R. H. Fowler, *Phys. Rev.* **38**, 45 (1931).

[62] B. Feuerbacher and B. Fitton, *J. Appl. Phys.* **43**, 1563 (1972).

[63] D. H. Dowell, F. K. King, R. E. Kirby, J. F. Schmerge, and J. M. Smedley, *Phys. Rev. ST AB* **9**, 063502 (2006).

[64] G. D. Alton, *Surf. Sci.* **175**, 226 (1986).

[65] P. W. van Amersfoort, *Formation of negative ions on a metal surface*, PhD thesis, FOM-Institute for Atomic and Molecular Physics, Amsterdam (1985).

[66] W. M. Haynes and D. R. Lide, editors, *CRC Handbook of Chemistry and Physics*, CRC Press, Taylor & Francis Group, Boca Raton, FL , 91st edition (2010).

[67] K. L. Jensen, N. A. Moody, D. W. Feldman, E. J. Montgomery, and P. G. O'Shea, *J. Appl. Phys.* **102**, 074902 (2007).

[68] R. G. Wilson, *J. Appl. Phys.* **37**, 4125 (1966).

[69] L. W. Swanson and R. W. Strayer, *J. Chem. Phys.* **48**, 2421 (1968).

[70] T. A. Callcott and A. U. Mac Rae, *Phys. Rev.* **178**, 966 (1969).

[71] O. Tarvainen, *Nucl. Instr. Meth. Phys. Res. A* **601**, 270 (2009).

[72] D. C. Faircloth, S. R. Lawrie, A. P. Letchford, C. Gabor, M. Whitehead, T. Wood, and M. Perkins, *AIP Conf. Proc.* **1390**, 205 (2011).

[73] U. Fantz, P. Franzen, and D. Wünderlich, *Chem. Phys.* **398**, 7 (2012).

[74] R. Gutser, D. Wünderlich, U. Fantz, and the N-NBI Team, *Plasma Phys. Control. Fusion* **53**, 105014 (2011).

[75] D. Faircloth, S. Lawrie, A. Letchford, C. Gabor, M. Perkins, M. Whitehead, T. Wood, O. Tarvainen, J. Komppula, T. Kalvas, et al., *AIP Conf. Proc.* **1515**, 359 (2013).

[76] R. Friedl and U. Fantz, *AIP Conf. Proc.* **1655**, 020004 (2015).

[77] H. Yamaoka, M. Sasao, M. Wada, and H. J. Ramos, *Nucl. Instr. Meth. Phys. Res. B* **36**, 227 (1989).

[78] A. Hatayama, *Rev. Sci. Instrum.* **79**, 02B901 (2008).

[79] F. Taccogna, P. Minelli, S. Longo, M. Capitelli, and R. Schneider, *Phys. Plasmas* **17**, 063502 (2010).

[80] R. McAdams and M. Bacal, *Plasma Sources Sci. Technol.* **19**, 042001 (2010).

[81] R. McAdams, A. J. T. Holmes, D. B. King, and E. Surrey, *Plasma Sources Sci. Technol.* **20**, 035023 (2011).

[82] R. McAdams, D. B. King, A. J. T. Holmes, and E. Surrey, *Rev. Sci. Instrum.* **83**, 02B109 (2012).

[83] H. Amemiya, B. M. Annaratone, and J. E. Allen, *J. Plasma Phys.* **60**, 81 (1998).

[84] T. Kalvas, O. Tarvainen, J. Komppula, M. Laitinen, T. Sajavaara, H. Koivisto, A. Jokinen, and M. P. Dehnel, *AIP Conf. Proc.* **1515**, 349 (2013).

[85] K. R. Kendall, M. McDonald, D. R. Mosscrop, P. W. Schmor, D. Yuan, G. Dammertz, B. Piosczyk, and M. Olivo, *Rev. Sci. Instrum.* **57**, 1277 (1986).

[86] C. Courteille, A. M. Bruneteau, and M. Bacal, *Rev. Sci. Instrum.* **66**, 2533 (1995).

[87] T. Kuo, R. Baartman, G. Dutto, S. Hahto, J. Ärje, and E. Liukkonen, *Rev. Sci. Instrum.* **73**, 986 (2002).

[88] T. Kuo, D. Yuan, K. Jayamanna, M. McDonald, R. Baartman, P. Schmor, and G. Dutto, *Rev. Sci. Instrum.* **67**, 1314 (1996).

[89] W. Kraus, U. Fantz, P. Franzen, M. Fröschle, B. Heinemann, C. Martens, R. Riedl, and D. Wünderlich, *AIP Conf. Proc.* **1515**, 129 (2013).

[90] Y. An, B. Jung, and Y. S. Hwang, *Rev. Sci. Instrum.* **81**, 02A702 (2010).

[91] O. D. Cortázar, A. Megía-Macías, A. Vizcaíno-de Julián, O. Tarvainen, J. Komppula, and H. Koivisto, *Rev. Sci. Instrum.* **85**, 02A902 (2014).

[92] S. Aleiferis, P. Svarnas, I. Tsiroudis, S. Béchu, M. Bacal, and A. Lacoste, *IEEE Trans. Plasma Sci.* **42**, 2828–9 (2014).

[93] A. Lacoste, T. Lagarde, S. Béchu, Y. Arnal, and J. Pelletier, *Plasma Sources Sci. Technol.* **11**, 407–412 (2002).

[94] S. Béchu, A. Soum-Glaude, A. Bès, A. Lacoste, P. Svarnas, et al., *Phys. Plasmas* **20**, 101601 (2013).

[95] S. Aleiferis, J. Laulainen, P. Svarnas, O. Tarvainen, M. Bacal, and S. Béchu, *AIP Conf. Proc.* **1869**, 030045 (2017).

[96] H. Koivisto, P. Heikkinen, V. Hänninen, A. Lassila, H. Leinonen, V. Nieminen, J. Pakarinen, K. Ranttila, J. Ärje, and E. Liukkonen, *Nucl. Instrum. Methods B* **174**, 379 (2001).

[97] O. Tarvainen, T. Kalvas, H. Koivisto, V. Toivanen, J. H. Vainionpää, A. Virtanen, and J. Ärje, Proc. HIAT09, Venice, Italy, WE-08 (2009).

[98] H. Henneken, F. Scholze, M. Krumrey, and G. Ulm, *Metrologia* **37**, 485 (2000).

[99] J. Komppula, *VUV-diagnostics of low temperature hydrogen plasmas*, PhD thesis, University of Jyväskylä, Jyväskylä, Finland (2015).

[100] T. Kalvas, O. Tarvainen, H. Koivisto, and K. Ranttila, Proc. ECRIS-2014, Nizhny Novgorod, Russia, WEOMMH04 (2014).

[101] A. G. Drentje, *Rev. Sci. Instrum.* **74**, 2631 (2003).

[102] C. M. Lyneis, Proceedings of International Conference on ECR ion sources and their Applications, East Lansing (1987).

[103] O. Tarvainen, *Studies of electron cyclotron resonance ion source plasma physics*, PhD thesis, University of Jyväskylä, Jyväskylä, Finland (2005).

[104] B. L. Henke, E. M. Gullikson, and J. C. Davis, *At. Data Nucl. Data Tables* **54**, 181 (1993).

[105] M. P. Seah and W. A. Dench, *Surf. Interface Anal.* **1**, 2 (1979).

[106] R. Friedl, *Rev. Sci. Instrum.* **87**, 043901 (2016).

[107] E. J. Montgomery, *Characterization of quantum efficiency and robustness of cesium-based photocathodes*, PhD thesis, University of Maryland, College Park, Maryland, USA (2009).

[108] S. Aleiferis, *Experimental study of H^- negative ion production by electron cyclotron resonance plasmas*, PhD thesis, University of Patras, University of Grenoble, (2016).

[109] Y. S. Hwang, G. Cojocaru, D. Yuan, M. McDonald, K. Jayamanna, G. H. Kim, and G. Dutto, *Rev. Sci. Instrum.* **77**, 03A509 (2006).

[110] S. Christ-Koch, U. Fantz, M. Berger, and NNBI Team, *Plasma Sources Sci. Technol.* **18**, 025003 (2009).

[111] U. Fantz, P. Franzen, B. Heinemann, and D. Wünderlich, *Rev. Sci. Instrum.* **85**, 02B305 (2014).

[112] D. Wünderlich and the NNBI team, 30th ICPIG (2011).

[113] D. Wünderlich, U. Fantz, and the NNBI team, 32nd ICPIG (2015).

[114] D. Faircloth and S. Lawrie, private communication (2013).

[115] M. Bacal and M. Wada, *Appl. Phys. Rev.* **2**, 021305 (2015).

[116] T. Inoue, H. Tobari, N. Takado, M. Hanada, M. Kashiwagi, A. Hatayama, M. Wada, and K. Sakamoto, *Rev. Sci. Instrum.* **79**, 02C112 (2008).

[117] Yu. I. Belchenko, G. I. Dimov, and V. G. Dudnikov, *Bull. Acad. Sci. USSR* **37**, 91 (1973).

[118] C. F. A. van Os, R. M. A. Heeren, and P. W. van Amersfoot, *Appl. Phys. Lett.* **51**, 1495 (1987).

[119] K. N. Leung, S. R. Walther, and W. B. Kunkel, *Phys. Rev. Lett.* **62**, 764 (1989).

[120] J. Lettry, J. Alessi, D. Faircloth, A. Gerardin, T. Kalvas, H. Pereira, and S. Sgobba, *Rev. Sci. Instrum.* **83**, 02A728 (2012).

[121] D. Faircloth, S. Lawrie, T. Rutter, M. Whitehead, and T. Wood, Proceedings of IPAC2015, Richmond, VA, USA, THPF104 (2015).

[122] T. Rutter, D. Faircloth, D. Turner, and S. Lawrie, *Rev. Sci. Instrum.* **87**, 02B131 (2016).

[123] L. Fu, T. Tamanna, W.-J. Hu, and A. Yu, *Chem. Pap.* **68**, 1283 (2014).

ORIGINAL PAPERS

PI

PHOTOELECTRON EMISSION FROM METAL SURFACES INDUCED BY VUV-EMISSION OF FILAMENT DRIVEN HYDROGEN ARC DISCHARGE PLASMA

by

Janne Laulainen, Taneli Kalvas, Hannu Koivisto, Jani Komppula, and Olli Tarvainen

AIP Conference Proceedings **1655**, 020007 (2015)

Photoelectron Emission from Metal Surfaces Induced by VUV-emission of Filament Driven Hydrogen Arc Discharge Plasma

J. Laulainen, T. Kalvas, H. Koivisto, J. Komppula and O. Tarvainen

University of Jyväskylä, Department of Physics, Finland

Abstract. Photoelectron emission measurements have been performed using a filament-driven multi-cusp arc discharge volume production H^- ion source (LIISA). It has been found that photoelectron currents obtained with Al, Cu, Mo, Ta and stainless steel (SAE 304) are on the same order of magnitude. The photoelectron currents depend linearly on the discharge power. It is shown experimentally that photoelectron emission is significant only in the short wavelength range of hydrogen spectrum due to the energy dependence of the quantum efficiency. It is estimated from the measured data that the maximum photoelectron flux from plasma chamber walls is on the order of 1 A per kW of discharge power.

Keywords: Negative ion source, arc discharge, photoelectron emission
PACS: 29.25.Ni, 52.50.Nr,52.25.Tx

INTRODUCTION

In volume production negative ion sources negative hydrogen ions are produced by electron-molecule and electron-ion collision processes in the plasma discharge [1]. The predominant production channel of negative hydrogen ions is dissociative attachment of a cold electron to a vibrationally excited H_2 molecule in the ground electronic $X^1\Sigma_g^+$ state:

$$e_{cold} + H_2(X^1\Sigma_g^+; v'') \rightarrow H_2^-(^2\Sigma_u^+) \rightarrow H(1s) + H^-. \quad (1)$$

An effective source of vibrationally excited molecules with $v'' > 8$ is radiative decay from singlet states, excited by collisions of ground state molecules with energetic primary electrons [2]:

$$e_{hot} + H_2 \rightarrow H_2(B^1\Sigma_u^+ \text{ or } C^1\Pi_u^+) \rightarrow H_2(X^1\Sigma_g^+; v'') + h\nu. \quad (2)$$

Also the plasma chamber walls contribute to negative ion yield by affecting the production of vibrationally excited molecules [1, 3]. In filament driven arc discharge ion sources the only source of hot electrons capable of ionizing or exciting neutral atoms or molecules from their ground states is thermionic emission from the hot biased filament. Sources of cold electrons required for effective dissociative electron attachment are thermally emitted electrons, whose energy is dissipated in consecutive inelastic collisions, electrons produced by ionization and electrons incident from the plasma chamber walls by secondary electron emission and photoelectron (PE) emission. This study concentrates on the PE emission from the plasma chamber walls by vacuum ultraviolet (VUV) radiation.

Light is emitted by hydrogen plasma as a consequence of electronic transitions from excited states to lower states of neutral atoms or molecules. Typical VUV-emission spectrum from hydrogen plasma is presented in Fig. 1 (a). The VUV-part of the spectrum is important for PE emission, because for common metals the quantum efficiency increases in the VUV-range with decreasing wavelength of the incident radiation (Fig. 1 (b)). An intensive source of light in hydrogen plasma is the Lyman-alpha line at 121.6 nm corresponding to the transition from the first excited state to the ground state ($2P \rightarrow 1S$) of atomic hydrogen. Lyman-band ($B^1\Sigma_u^+ \rightarrow X^1\Sigma_g^+$) at 92–184 nm and Werner-band ($C^1\Pi_u \rightarrow X^1\Sigma_g^+$) at 84–158 nm correspond to two lowest singlet transitions of hydrogen molecule. The molecular continuum at 165–400 nm corresponds to the lowest triplet transition of molecules ($a^3\Sigma_g^+ \rightarrow b^3\Sigma_u^+$). It has been previously measured that in a filament-driven arc discharge 15–30 % of the discharge power is dissipated via light emission in the VUV-range of 120–250 nm [4]. Taking into account the quantum efficiencies of PE emission this implies that plasma dynamics and their contribution to H^- production may be affected by surface processes on plasma chamber walls induced by radiation exceeding the surface work function of the wall material. This paper is dedicated to estimating the maximum PE flux from the plasma chamber walls based on experimental data and discussing the possible effects of the emitted photoelectrons on plasma properties.

Fourth International Symposium on Negative Ions, Beams and Sources (NIBS 2014)
AIP Conf. Proc. 1655, 020007-1–020007-7; doi: 10.1063/1.4916416

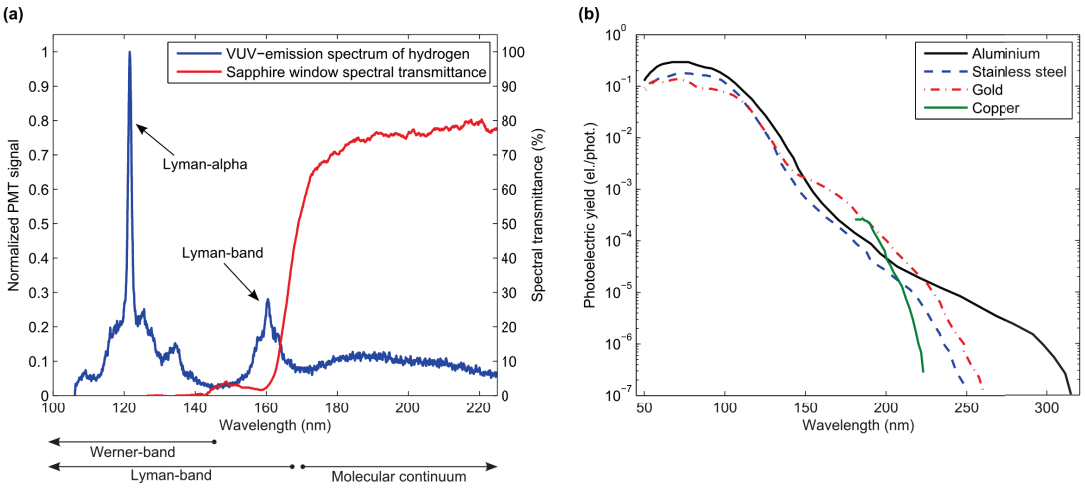

FIGURE 1. **(a)** Typical VUV-emission spectrum of the LIISA ion source and the spectral transmittance of the sapphire window. The spectrum is not corrected for spectral transmittance. **(b)** Photoelectron yield quantum efficiencies for aluminium, stainless steel, gold [5] and copper [6].

MEASUREMENT SETUP

The experimental setup is presented in Fig. 2. The LIISA (Light Ion Ion Source Apparatus) ion source is a TRIUMF-type DC (tantalum) filament-driven multi-cusp arc discharge volume production ion source. LIISA is designed to provide up to 3 mA of H^- at 5.9 keV injection energy to the JYFL K130 cyclotron [7]. The typical beam requirement of approximately 1 mA is reached with 70 V / $<$ 10 A discharge voltage / current. The optimum pressure for H^- beam current is $3.5 \cdot 10^{-3}$ mbar measured in the plasma chamber. The cylindrical plasma chamber is tantalum-coated copper with 9.8 cm diameter and 32 cm length. A cross-sectional view of the ion source is presented in Fig. 2. The PE currents were measured as a function of neutral gas pressure and discharge power. The plasma chamber pressure was varied between $5 \cdot 10^{-4}$ mbar and $1 \cdot 10^{-2}$ mbar and the arc discharge power between 200 W and 1000 W by adjusting the arc current and the arc voltage independently. The dependence of the extracted beam current and VUV-emission on these parameters has been reported in Ref. [4].

The PE currents are measured with a device designed for this work and shown in Fig. 2. The PE ammeter can be equipped with multiple targets and filters mounted to rotatable discs. Different filters can be used to limit the wavelength range of the radiation incident on the target. The PE currents presented in this paper have been measured with an unfiltered view from the plasma to the target and by filtering the incident radiation with a sapphire window. The spectral transmittance of the sapphire window is presented in Fig. 1 (a) with the VUV-emission spectrum of hydrogen plasma. The sapphire window was used to filter out the short wavelength VUV-radiation in order to demonstrate that the PE emission is significant only in the short wavelength range of hydrogen VUV-emission spectrum. The cathode current is measured from the target with a picoammeter (Keithley 485). The emitted electrons are collected with an anode ring located approximately 3 mm from the target and biased to 150 V. The device is protected from plasma particles with an electric deflector, and the light entering the device is collimated with a replaceable collimator. During the measurements the pressure inside the PE ammeter was $\sim 10^{-5}$ mbar. The background signal was measured from a plastic target and with an aluminium plate placed on the rotatable disc housing the filters and, thus, blocking all light. The PE ammeter was placed on the axis of the beamline approximately 1.5 m from the ion source and was looking into the plasma through the extraction aperture. The line-of-sight plasma volume was limited by the 9.5 mm diameter puller electrode aperture and the (6 mm / 8 mm diameter) collimator between the target and the plasma. The target materials used in this study are metals which are typically found in negative hydrogen ion sources as chamber materials (Al, Cu, SS) [8, 9, 10], filament materials (Ta) [7, 11], plasma grid materials (Mo) [12] or so-called collar materials (SS, Mo) [13, 14]. The effect of Al, Cu and SS wall materials and Ta covered walls on the volume production of negative hydrogen ions has been studied in [3, 15, 16].

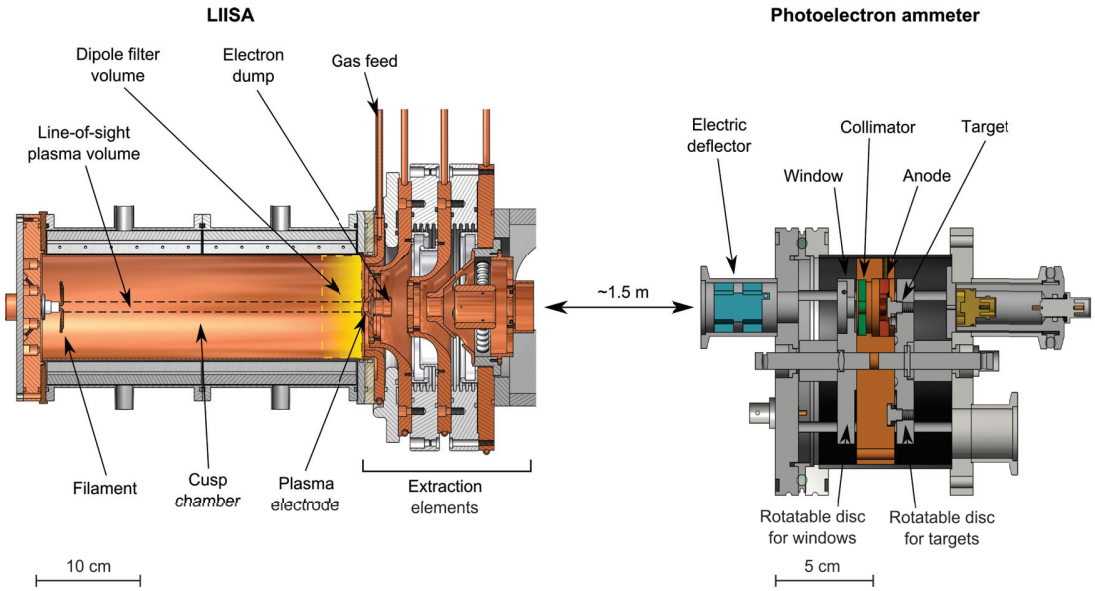

FIGURE 2. LIISA ion source and the photoelectron current measurement device.

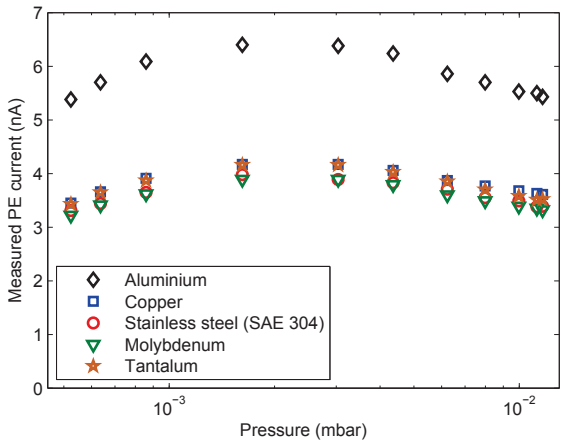

FIGURE 3. Measured photoelectron currents as a function of neutral hydrogen pressure without filter. The discharge power was 500 W (50 V / 10 A).

EXPERIMENTAL RESULTS

The PE currents measured from Al, Cu, stainless steel (SAE 304), Mo, and Ta without filter are presented in Fig. 3. The PE currents are measured as a function of neutral hydrogen pressure with constant discharge power (50 V / 10 A i.e. 500 W). The PE currents measured from Cu, SS, Mo, and Ta are approximately equal while the signal from Al is approximately 20–50 % higher. The dependence of the VUV-light emission on the pressure has been concluded to be weak [4], and similar behaviour is seen in the PE signals. The change in PE current is less than 20 % in the given pressure range. The optimum pressure for PE emission corresponds to the optimum pressure for H^- production ($3.5 \cdot 10^{-3}$ mbar).

The PE currents from different metals measured as a function of discharge power without filter are presented in

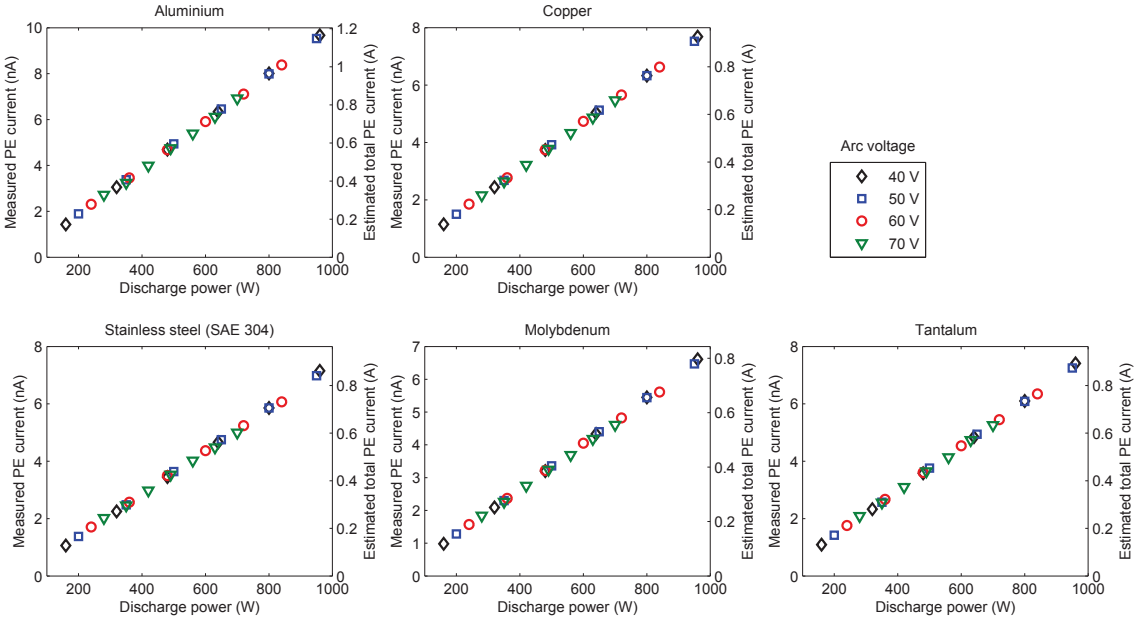

FIGURE 4. Measured PE currents and estimated total PE currents as a function of discharge current and voltage at $3.8 \cdot 10^{-3}$ mbar pressure without filter.

Fig. 4. The PE currents are measured with various combinations of discharge current and voltage at constant plasma chamber pressure of $3.8 \cdot 10^{-3}$ mbar. The PE currents depend linearly on the discharge power without a preference to neither, the discharge voltage nor current. The Lyman-band and Lyman-alpha light emission has been reported to exhibit similar behaviour. The linear dependence on the discharge power can be explained by the good confinement of hot electrons and their energy dissipation via inelastic collisions as discussed in Ref. [4]. The molecular continuum emission has a notable dependence on the discharge current. However, such trend is not observed in Fig. 4, which implies that the molecular continuum range is insignificant to PE emission from metal surfaces in comparison to shorter wavelength radiation.

A comparison between PE currents from Al measured as a function of discharge power without a filter and through a sapphire window at $4.2 \cdot 10^{-3}$ mbar pressure are presented in Fig. 5. When all wavelengths shorter than 150 nm are filtered out with the sapphire window, the PE current decreases by three orders of magnitude. Similar behaviour was observed for the other targets as well. The spectral transmittance of the sapphire window (Fig. 1 (a)) is not 100 % at wavelengths longer than 150 nm, but this has only a small effect on the measured PE current. It is concluded that the decrease in the PE current is due to lower quantum efficiency (Fig. 1 (b)) at longer wavelengths.

The total PE flux from the plasma chamber walls presented in Figs. 4 and 5 is estimated from the measured data by assuming that the light emission profile is homogeneous and isotropic across the plasma chamber profile. Monte Carlo methods were used to calculate the probability for a single photon to reach the target surface. In reality, the spatial distribution of the plasma light emission rate depends on the inhomogeneous plasma density and temperature profiles. Without accurate information about the density and temperature profiles the total PE flux can only be estimated. The assumption used for estimating the total PE flux yields the maximum value. It can be argued that in the line-of-sight volume the plasma density does not change significantly in the axial direction. Thus, the error caused by assuming a constant axial profile is small, because the measured signal corresponds to the average light emission over the axial distance on the line-of-sight. The estimated total PE flux depends on the radial plasma profile because it defines the ratio of observed emission volume to the total emission volume. In the radial direction the plasma density profile is typically almost uniform decaying only near the plasma chamber wall due to the multi-cusp field [17, 18]. The measurement was limited to line-of-sight in the axial direction at the plasma center as illustrated in Fig. 2. Comparing different radial emission profiles to radially homogeneous plasma it can be estimated that the total VUV-emission, and hence the PE current, is at least 50 % of the given maximum [4].

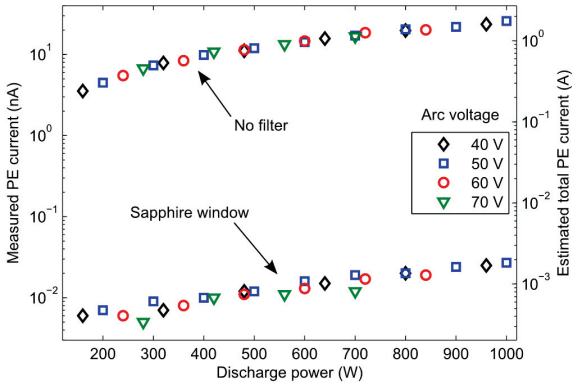

FIGURE 5. Difference between PE currents from aluminium without filter and with sapphire window at $4.2 \cdot 10^{-3}$ mbar pressure.

The effect of reflection and scattering of VUV-light from metal surfaces on the measured results can be considered insignificant. In the beam line geometry, scattering is possible only from a small area of the extraction einzel lens or tantalum-coated back plate of the plasma chamber. Also the error due to the picoammeter can be considered insignificant compared to the approximations made for the estimation of the total PE flux.

PE emission is very sensitive to surface contaminants because the penetration depth of VUV-photons and the escape depth of electrons is very short. Furthermore, the surface roughness affects the effective area of the surface, which is directly related to the measured signal. The experimental results are well repeatable after following a standard cleaning procedure of the samples, which includes abrading the surface with sandpaper and wiping with ethanol. Difference between PE currents measured from different Al targets is less than 5 %. However, a significant change in the PE current is caused by VUV-induced surface effects. Samples were cleaned in atmospheric pressure, and thus a natural oxide layer was formed on the surface of the metal, which is known to change the work function and the PE quantum efficiency of the surface [19]. Typical vacuum contaminants, such as residual gases, water vapour and pump oil, are also present on the sample surface. VUV-light is known to destroy organic compounds, in which case free radicals, which can react chemically with the surface, are formed. Consequently, the measurements described in this paper were performed as quickly as possible in order to minimize the effect of VUV-induced surface aging. The change in PE currents due to surface aging was 10 % at the most. Conditions and materials used in these experiments are similar to typical ion sources i.e. all phenomena due to surface contaminants are present in ion sources as well. However, in ion sources the surfaces emitting electrons are in direct contact with the plasma which has a cleaning effect that most likely affects the initial conditioning phase of the surfaces and hence the PE emission.

DISCUSSION

It has been estimated from the measured data that the maximum PE flux from plasma chamber walls is on the order of 1 A per kW of discharge power. Taking into account the surface area of the LIISA plasma chamber this corresponds to PE emission of 0.9 mAcm^{-2} per kW on average. Since the PE emission is linearly proportional to the arc discharge power, the numerical results are given normalized to kW of the discharge power. The PE currents obtained with different metals are on the same order of magnitude. The estimated maximum PE current corresponds to almost 10 % of the arc current of 14 A at 70 V discharge voltage. The arc current consists of thermionic emission of electrons from the filament and the flux of positive ions from the plasma to the filament. The PE flux from the wall to the plasma is limited by the cusp magnetic field, since the cross field diffusion of the emitted electrons in transverse magnetic field is significantly slower than their propagation along the field lines.

The same value for the total PE flux can be obtained independently from the experiments described in this paper by using the measured photon emission rate [4] and known quantum efficiency. The total PE current produced by plasma volume V can be estimated from

$$I\,\mathrm{d}E = \Phi(E)\eta(E)Ve\,\mathrm{d}E \tag{3}$$

where Φ is the volumetric photon emission rate, η the quantum efficiency, V the plasma volume, and e the elementary charge. The total VUV-emission power at the Lyman-alpha and Werner-band parts of the spectrum is the most significant and the most emissive part of the spectrum [4], and the quantum efficiency of common metals is several orders of magnitude higher at short wavelength range of the spectrum (Fig. 1 (b)). As discussed in the previous section, the PE emission is predominantly caused by radiation at short wavelength range of hydrogen VUV-spectrum. Thus, the total PE emission can be approximated by taking into account only a limited wavelength range. The measured photon emission from LIISA is $\Phi = 5.1 \cdot 10^{16}$ s^{-1}cm^{-3} per kW at 122 nm (FWHM 20 nm) [4] and the corresponding quantum efficiency of Al at this wavelength is approximately $5 \cdot 10^{-2}$ [5]. Substituting the given numbers into Eq. (3) yields approximately 1.0 A per kW total PE current from the plasma chamber walls, which correlates well with the result reported in this paper.

Based on the VUV-diagnostics it has been deduced that the arc discharge power is well dissipated to the plasma in filament driven arc discharge ion sources with cusp-confinement [4]. It has been concluded that the total path length of hot electrons emitted from the filament is long enough for multiple inelastic collisions with neutrals, which is the main energy dissipation process. This means that only electrons with low energy are escaping the plasma to the plasma chamber surface. For low energy electrons the secondary electron emission yield is small [20], and therefore the secondary electron emission can be considered insignificant in filament driven ion sources in comparison to PE emission.

Although the effect of the electrons, emitted from the surfaces, on the total electron density might be considered insignificant [21], they may have a considerable local effect on plasma properties. Photoelectrons can be beneficial for dissociative electron attachment or they can destroy already existing negative hydrogen ions in $e + H^-$ collisions. The role of photoelectrons depends strongly on the plasma parameters and the energy of the emitted electrons, which is determined by the initial kinetic energy of the electrons and by the potential difference in the plasma sheath. Photoelectrons are emitted from metal surfaces with all energies from zero up to the maximum energy [22]. The maximum energy of the photoelectrons corresponds to the difference between the energy of the absorbed photon and the surface work function. For common metals used in this study the work function is in the order of 4–5 eV [23]. This is for clean surfaces, and the real work function of technical surfaces covered with their natural oxide and contaminants, typically found in ion sources, can be different. The emitted electrons are further accelerated by the plasma sheath potential. For example, the plasma potential in the TRIUMF source has been measured to be about 5 V [18]. However, extracted negative ions are predominantly created near the (biased) plasma electrode due to short survival length of the negative ions [24]. Typically the optimal plasma electrode bias is close to the plasma potential [1], which minimizes the potential difference across the sheath. If the flux of the electrons emitted from the walls is high enough, the space charge of the emitted electrons (and negative ions) is not fully compensated by incoming positive ions, which can lead into formation of a virtual cathode [25, 26]. In surface production H^- ion sources the negative ion formation is based on resonant tunneling of electrons from the surface material to hydrogen atoms or protons impinging a metallic surface [24]. Surface produced negative ions are retarded by the virtual cathode, and therefore, the virtual cathode could limit the flux of negative ions that can be transported across the sheath and finally extracted.

Surface production efficiency can be significantly enhanced by covering the surface with a thin layer (ideally a sub-monolayer) of cesium, which decreases the work function of the surface. The cesium layer increases the efficiency of other surface processes as well, including PE emission. The effect of PE emission from cesium coated molybdenum surface to the adjacent plasma sheath has been studied by computer simulations [27]. It was concluded that the potential in the plasma sheath is not affected by the photoelectrons, but a small potential decrease in the plasma volume was observed. In the simulations [27] only molecular continuum radiation was taken into consideration. However, in this paper it is shown that PE emission is predominantly caused by radiation at shorter wavelengths. Thus, it is possible that the PE emission has a greater effect on the sheath structure than previously estimated.

ACKNOWLEDGMENTS

This work has been supported by the EU 7$^{\text{th}}$ framework programme “Integrating Activities – Transnational Access”, project number: 262010 (ENSAR) and by the Academy of Finland under the Finnish Centre of Excellence Programme 2012–2017 (Nuclear and Accelerator Based Physics Research at JYFL).

REFERENCES

1. M. Bacal, A. Hatayama, and J. Peters, *Review of Scientific Instruments* **33**, 1845 (2005).
2. M. Nishiura, *Journal of Plasma and Fusion Research* **80**, 757–762 (2004).
3. M. Bacal, A. A. Ivanov Jr., M. Glass-Maujean, Y. Matsumoto, M. Nishiura, M. Sasao, and M. Wada, *Review of Scientific Instruments* **75**, 1699 (2004).
4. J. Komppula, O. Tarvainen, S. Lätti, T. Kalvas, H. Koivisto, V. Toivanen, and P. Myllyperkiö, *AIP Conference Proceedings* **1515**, 66 (2013).
5. B. Feuerbacher, and B. Fitton, *Journal of Applied Physics* **43**, 1563 (1972).
6. D. H. Dowell, F. K. King, R. E. Kirby, J. F. Schmerge, and J. M. Smedley, *Physical Review ST Accelerators and Beams* **9**, 063502 (2006).
7. T. Kuo, R. Baartman, G. Dutto, S. Hahto, J. Ärje, and E. Liukkonen, *Review of Scientific Instruments* **73**, 986 (2002).
8. T. Kalvas, O. Tarvainen, J. Komppula, M. Laitinen, T. Sajavaara, H. Koivisto, A. Jokinen, and M. P. Dehnel, *AIP Conference Proceedings* **1515**, 349 (2013).
9. K. R. Kendall, M. McDonald, D. R. Mosscrop, P. W. Schmor, D. Yuan, G. Dammertz, B. Piosczyk, and M. Olivo, *Review of Scientific Instruments* **57**, 1277 (1986).
10. C. Courteille, A. M. Bruneteau, and M. Bacal, *Review of Scientific Instruments* **66**, 2533 (1995).
11. T. Kuo, D. Yuan, K. Jayamanna, M. McDonald, R. Baartman, P. Schmor, and G. Dutto, *Review of Scientific Instruments* **67**, 1314 (1996).
12. W. Kraus, U. Fantz, P. Franzen, M. Fröschle, B. Heinemann, C. Martens, R. Riedl, and D. Wünderlich, *AIP Conference Proceedings* **1515**, 129 (2013).
13. R. F. Welton, et al., *AIP Conference Proceedings* **1097**, 181 (2009).
14. Y. An, B. Jung, and Y. S. Hwang, *Review of Scientific Instruments* **81**, 02A702 (2010).
15. K. N. Leung, K. W. Ehlers, and R. V. Pyle, *Applied Physics Letters* **47**, 227 (1985).
16. O. Fukumasa, and S. Saeki, *Journal of Physics D* **20**, 237 (1987).
17. S. Asano, K. Tsumori, T. Okuyama, Y. Suzuki, M. Osakabe, Y. Oka, Y. Takeiri, and O. Kaneko, *Review of Scientific Instruments* **70**, 2338 (1999).
18. Y. S. Hwang, G. Cojocaru, D. Yuan, M. McDonald, K. Jayamanna, G. H. Kim, and G. Dutto, *Review of Scientific Instruments* **77**, 03A509 (2006).
19. J. A. Ramsey, and G. F. J. Garlick, *British Journal of Applied Physics* **15**, 1353 (1964).
20. V. Baglin, J. Bojko, O. Gröbner, B. Henrist, N. Hilleret, C. Scheuerlein, and M. Taborelli, *Proceedings of EPAC 00* (2000).
21. A. G. Drentje, *Review of Scientific Instruments* **74**, 2631 (2003).
22. L. A. DuBridge, *Physical Review* **43**, 727 (1933).
23. R. C. Weast, editor, *CRC Handbook of Chemistry and Physics*, CRC Press, Inc., 1977-1978, 58th edn.
24. D. Wünderlich, R. Gutser, and U. Fantz, *Plasma Sources Science and Technology* **18**, 045031 (2009).
25. R. McAdams, D. B. King, A. J. T. Holmes, and E. Surrey, *Review of Scientific Instruments* **83**, 02B109 (2012).
26. H. Amemiya, B. M. Annaratone, and J. E. Allen, *Journal of Plasma Physics* **60**, 81–93 (1998).
27. D. Wünderlich, and the NNBI team, *30th ICPIG* (2011).

PII

PHOTOELECTRON EMISSION FROM METAL SURFACES INDUCED BY RADIATION EMITTED BY A 14 GHZ ELECTRON CYCLOTRON RESONANCE ION SOURCE

by

Janne Laulainen, Taneli Kalvas, Hannu Koivisto, Jani Komppula, Risto Kronholm, and Olli Tarvainen

Review of Scientific Instruments **87**, 02A506 (2016)

REVIEW OF SCIENTIFIC INSTRUMENTS **87**, 02A506 (2016)

Photoelectron emission from metal surfaces induced by radiation emitted by a 14 GHz electron cyclotron resonance ion source

Janne Laulainen,[a] Taneli Kalvas, Hannu Koivisto, Jani Komppula, Risto Kronholm, and Olli Tarvainen
Department of Physics, University of Jyvaskyla, P.O. Box 35, FI-40014 Jyvaskyla, Finland

(Presented 25 August 2015; received 21 August 2015; accepted 19 October 2015; published online 3 November 2015)

Photoelectron emission measurements have been performed using a room-temperature 14 GHz ECR ion source. It is shown that the photoelectron emission from Al, Cu, and stainless steel (SAE 304) surfaces, which are common plasma chamber materials, is predominantly caused by radiation emitted from plasma with energies between 8 eV and 1 keV. Characteristic X-ray emission and bremsstrahlung from plasma have a negligible contribution to the photoelectron emission. It is estimated from the measured data that the maximum conceivable photoelectron flux from plasma chamber walls is on the order of 10% of the estimated total electron losses from the plasma. [http://dx.doi.org/10.1063/1.4935012]

I. INTRODUCTION

Wall conditions can have a significant effect on the performance of electron cyclotron resonance ion sources (ECRISs) intended for high charge state production.[1,2] Electron donors can improve the electron density of the plasma and low energy electrons emitted from the wall can have a significant effect on the plasma potential. The beneficial effect of wall coating was discovered when currents of highly charged oxygen ion beams increased by a factor of 2 after the plasma chamber had been covered by a silicon oxide layer.[3] Carbon contamination on the plasma chamber walls has been seen to affect the plasma potential and the oxygen ion beam current significantly.[4] It is commonly believed that wall coating changes the plasma properties due to alteration of the secondary electron emission yield. Another possible process that can affect the electron emission from plasma chamber walls is photoelectric effect.

ECR plasmas emit radiation on the entire electromagnetic spectrum from radio waves to X-rays. Photons impinging a metal surface on the plasma chamber wall can lead to emission of photoelectrons (PEs) when the energy of the photons exceeds the surface work function of the wall material. Photons carrying enough energy to cause PE emission from common metals are in the ultraviolet (UV) and X-ray parts of the spectrum. UV and X-ray photons are created in ECR plasmas due to electronic transitions from excited states to lower states of ions and neutrals and due to plasma bremsstrahlung. In ionizing plasmas, the volumetric photon emission rate is directly proportional to the density of free electrons, ions, and neutral particles and to the rate coefficient of the excitation reactions which depends on the electron energy distribution. A considerable part of the radiation emitted by ECRISs comes also from the walls due to wall bremsstrahlung and recombination of highly charged ions. As highly charged ions become neutralized at the walls by removal of electrons from the surface, the captured electrons mostly go into highly excited states creating a "hollow ion" with empty core states, which then leads to photon emission.[5]

Energy and material dependent quantum efficiency (QE) describe the average number of electrons emitted per incident photon. Vacuum-ultraviolet (VUV) is essential for PE emission since common metals have high QE at the VUV-part of the emission spectrum.[6] Previous work with light ion sources suggests that PE emission could contribute to properties of hydrogen ion source plasmas.[7] ECR plasmas emit less intense VUV-radiation compared to light ion sources, since typical ECRISs operate at lower neutral gas pressure. However, ECR plasmas emit characteristic X-rays and bremsstrahlung, and common metals have high QE at the X-ray parts of the emission spectrum as well.[8]

II. MEASUREMENT SETUP

The measurement setup is presented in Figure 1. The experimental data presented in this article were taken with the room-temperature AECR-U type JYFL 14 GHz ECRIS[9,10] operated with a single frequency (14.085 GHz) in continuous mode.

The PE ammeter was placed on a radial diagnostics port at approximately 0.4 m distance from the plasma. The line-of-sight plasma volume was limited by the diagnostics port (∅ = 5.2 mm) and the collimator (∅ = 6 mm). The line-of-sight is between the poles of the permanent magnet sextupole, i.e., the X-ray spectrum at the target is dominated by the characteristic radiation from the plasma and PE emission induced by radiation from the walls is not well observed.

The PE ammeter can be equipped with multiple targets and filters mounted to rotatable discs. Different filters can be used to limit the wavelength range of the radiation incident

Note: Contributed paper, published as part of the Proceedings of the 16th International Conference on Ion Sources, New York, New York, USA, August 2015.

[a]janne.p.laulainen@student.jyu.fi

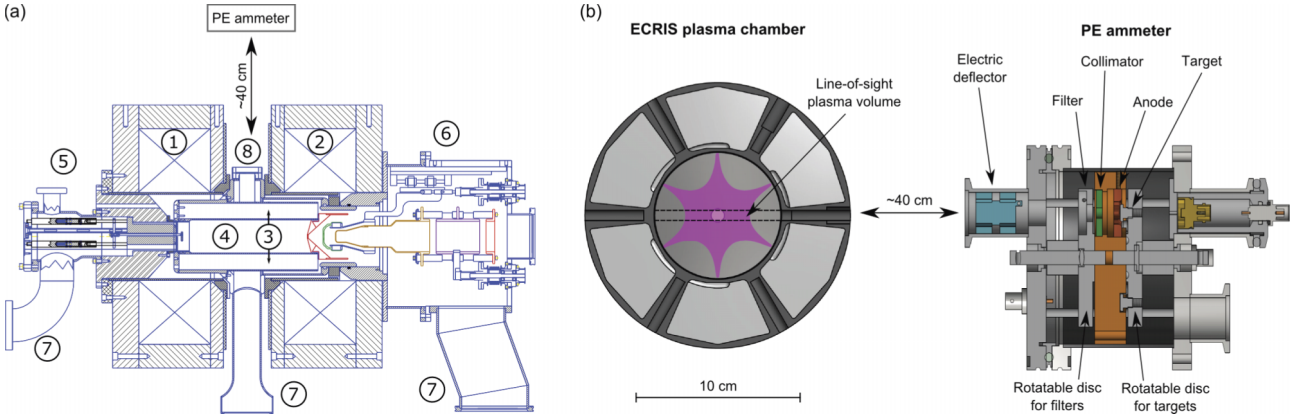

FIG. 1. (a) The JYFL 14 GHz ECRIS. (1) Injection and (2) extraction coils, (3) NdFeB sextupole, (4) plasma chamber ($\ell = 270$ mm, $\varnothing = 76$ mm), (5) iron plug, biased disc, gas, and microwave injection, (6) extraction system, (7) pumping, (8) vacuum gauge and PE ammeter. (b) ECRIS plasma chamber and the PE current measurement device.

on the target. The cathode current is measured from the target with a picoammeter (Keithley 485). The emitted electrons are collected with an anode ring located approximately 3 mm from the target and biased to 150 V. The device is protected from plasma particles with an electric deflector, and the light is collimated with a 6 mm diameter aperture. The target materials used in this study are metals which are typically found in ion sources as chamber materials (Al, Cu, and stainless steel).[11–13] A 1 μm thick mylar film, which is transparent for energies higher than 1 keV, was used to study the X-ray part of the spectrum. A sapphire window, which is transparent in the wavelength range of 150 nm–5 μm, was used to study the VUV-part of the spectrum.

III. RESULTS

The PE currents measured from Al, Cu, and stainless steel without filters are presented in Figure 2. The PE currents are measured as a function of microwave power with different magnetic field strengths using residual gas at $1 \cdot 10^{-6}$ mbar pressure. The PE current increases linearly with increasing microwave power in the given power range. There are no significant differences between different metals.

The total PE emission from plasma chamber walls is estimated using a Monte Carlo code, which tracks single electron trajectories in the ion source magnetic field.[14] The particles are launched isotropically from random locations with $B < B_{\mathrm{ECR}}$, where B_{ECR} is the resonance field for 10 keV electrons. Electrons are tracked 1 μs or until they hit the wall and the plasma density profile is produced from the electron population. Photons are emitted isotropically with an intensity directly proportional to the plasma density, and the probability for a single photon to hit the target is calculated. The total PE current is estimated by comparing the number of photons hitting the target to the total photon flux from the plasma. The estimated total PE current yields the maximum value from the total area of the plasma chamber wall. However, the PE flux from the wall to the plasma is limited by the magnetic field, since the cross field diffusion of the emitted electrons in transverse magnetic field is significantly slower than their propagation along the field lines. Due to the assumptions made in the calculations, the given total PE currents are an order of magnitude estimates.

Different optical filters were used to find out the predominant wavelength range contributing to the measured PE emission. Filtering the radiation emitted by the residual gas plasma with the 1 μm mylar filter dropped the PE current signal to zero. Thus, it is concluded that the intensity of the X-ray emission from the plasma is too weak to cause any significant PE emission. However, the K_α for C (277 eV), N (392.4 eV), and O (524.9 eV) are filtered out with the 1 μm mylar filter. Similarly, when a sapphire window was placed between the plasma and the target, the PE current was too low to be measured. Hence, it is concluded that PE emission is

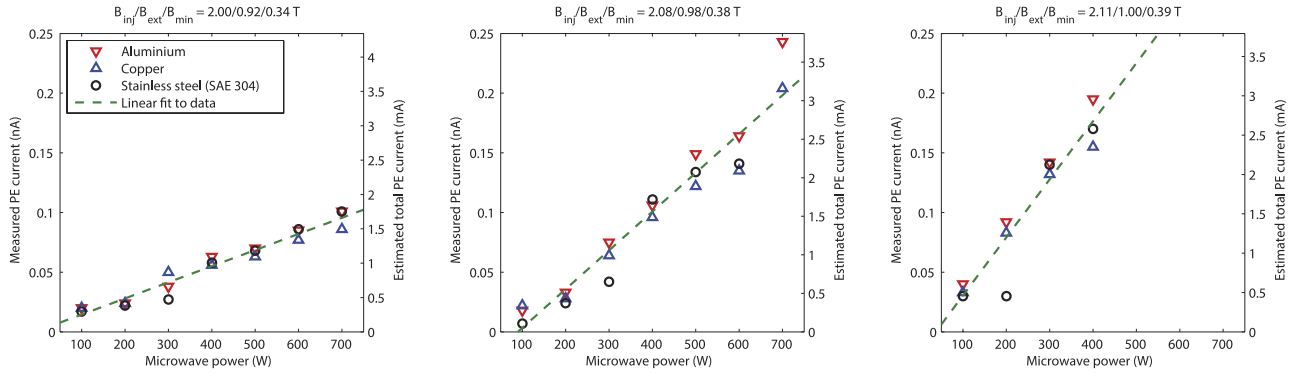

FIG. 2. Photoelectron current from different materials as a function of microwave power measured with residual gas at $1 \cdot 10^{-6}$ mbar pressure (injection).

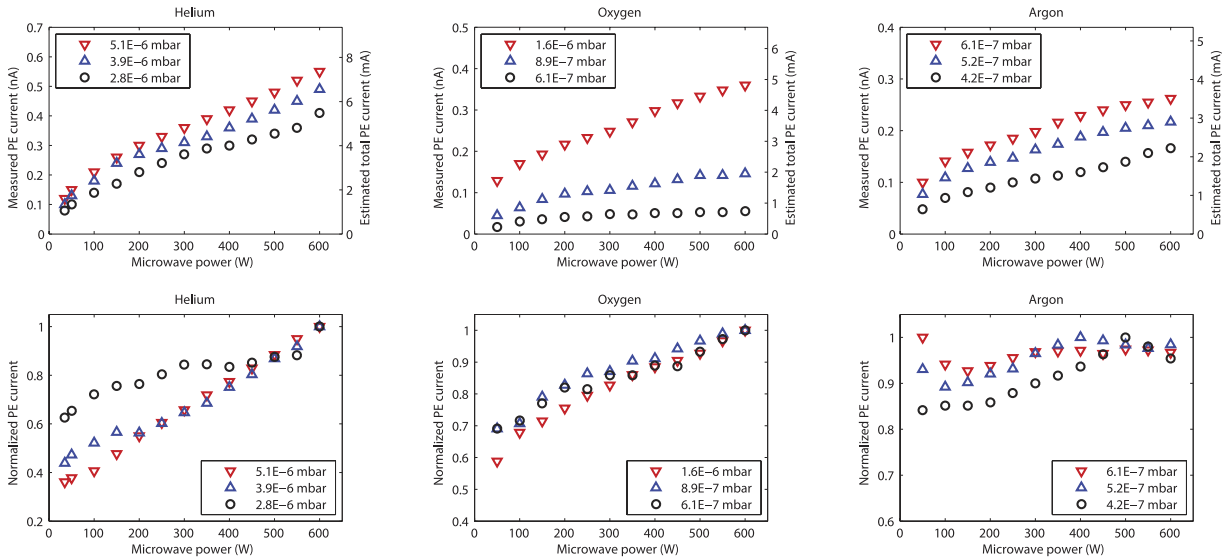

FIG. 3. Photoelectron current from aluminium with different gases measured with magnetic field values $B_{inj}/B_{ext}/B_{min} = 2.00/0.92/0.34$ T. The upper pictures show the absolute values and estimated total currents and, in the lower pictures, the measured photoelectron current is normalized with the biased disc current.

predominantly caused by radiation emitted with energies between 8 eV and 1 keV.

Higher magnetic field (coil current) corresponds to higher PE emission. The PE currents from Al, Cu, and stainless steel were measured with different values of the magnetic field at the injection B_{inj}, extraction B_{ext}, and minimum-B B_{min}. Linear fits to measured data in Figure 2 correspond to average total PE currents of 2 mA per kW of injected microwave power, 5 mA per kW, and 7 mA per kW for 2.00/0.92/0.34 T, 2.08/0.98/0.38 T, and 2.11/1.00/0.39 T magnetic fields, respectively. The increase of the PE emission with increasing magnetic field values can be caused by increased plasma density or by increased excitation rate to electronic states emitting at 8 eV–1 keV energies due to a shift of the electron energy distribution.

The PE current from Al was measured using different gases and neutral gas pressures. The results with He, O_2, and Ar plasma are presented in Figure 3. The indicated neutral particle pressures are gas calibrated readings of an ionization gauge located outside the plasma chamber and connected to it through a radial diagnostics port. The given pressure values are measured without igniting the plasma. The results indicate that the pressure dependence is significant. Measurements were performed also with Ne, Kr, and Xe showing similar results.

The measured PE currents have also been normalized with the biased disc current, which can be considered as an indicator of the plasma density at a constant magnetic field. Biased disc voltage was −120 V. The normalized PE currents are not constant as a function of microwave power, which suggests that not only the electron density but also the excitation rate changes as a function of microwave power, which is possibly due to a shift of the electron energy distribution.

IV. DISCUSSION

The same Monte Carlo code that was used to estimate the total PE current has been used to estimate the total electron flux that exit the plasma.[14] According to the simulation 5.1% of electrons with 10 keV kinetic energy exit the plasma through the extraction aperture. It can be assumed that a corresponding fraction of the electrons reach the plasma–beam boundary (meniscus) when the extraction high voltage is applied. The extracted ion current is typically on the order of 1 mA. Due to ambipolar diffusion the electron current towards the extraction aperture is assumed to be the same. Thus, the simulated total electron current from the plasma is on the order of 20 mA, which is roughly an order of magnitude higher than the estimated maximum PE current in typical operating pressure.

Electrons are emitted from all metal surfaces inside the plasma chamber, but due to the magnetic field structure of the ECRIS, only part of the emitted electrons are transmitted to the plasma. Electrons are most probably transmitted to the plasma from the area where plasma can touch the walls, which covers approximately 5% of the total plasma chamber area. Hence, the total PE currents are overestimated by a factor of 20. On the other hand, the measurements in this study also underestimate the PE emission, since the contribution of direct wall bremsstrahlung and radiation emitted due to recombination of highly charged ions near the plasma chamber walls was not completely taken into account. It is probable that PE emission is not an important process in relation to the electron density of ECR plasmas, but the PE flux should be compared to the total secondary electron flux in order to conclude its importance.

ACKNOWLEDGMENTS

This work has been supported by the EU 7th framework programme “Integrating Activities — Transnational Access,” Project No. 262010 (ENSAR) and by the Academy of Finland under the Finnish Centre of Excellence Programme 2012–2017 (Nuclear and Accelerator Based Physics Research at JYFL).

[1]R. Geller, *Electron Cyclotron Resonance Ion Sources and ECR Plasmas* (Institute of Physics Publishing, London, 1996).
[2]A. G. Drentje, Rev. Sci. Instrum. **74**, 2631 (2003).

[3]C. M. Lyneis, in Proceedings of International Conference on ECR Ion Sources and their Applications, East Lansing, 1987.
[4]O. Tarvainen, "Studies of electron cyclotron resonance ion source plasma physics," Ph.D. thesis, Department of Physics, Univerity of Jyväskylä, 2005.
[5]D. C. Parks, R. Bastasz, R. W. Schmieder, and M. Stöckli, J. Vac. Sci. Technol., B: Microelectron. Nanometer Struct. **13**, 941 (1995).
[6]R. B. Cairns and J. A. R. Samson, J. Opt. Soc. Am. **56**, 1568 (1966).
[7]J. Laulainen, T. Kalvas, H. Koivisto, J. Komppula, and O. Tarvainen, AIP Conf. Proc. **1655**, 020007 (2015).
[8]H. Henneken, F. Scholze, M. Krumrey, and G. Ulm, Metrologia **37**, 485 (2000).
[9]H. Koivisto *et al.*, Nucl. Instrum. Methods Phys. Res., Sect. B **174**, 379 (2001).
[10]O. Tarvainen, T. Kalvas, H. Koivisto, V. Toivanen, J. H. Vainionpää, A. Virtanen, and J. Ärje, in Proceedings of HIAT09, WE-08, Venice, Italy, 2009.
[11]T. Kalvas, O. Tarvainen, J. Komppula, M. Laitinen, T. Sajavaara, H. Koivisto, A. Jokinen, and M. P. Dehnel, AIP Conf. Proc. **1515**, 349 (2013).
[12]K. R. Kendall, M. McDonald, D. R. Mosscrop, P. W. Schmor, D. Yuan, G. Dammertz, B. Piosczyk, and M. Olivo, Rev. Sci. Instrum. **57**, 1277 (1986).
[13]C. Courteille, A. M. Bruneteau, and M. Bacal, Rev. Sci. Instrum. **66**, 2533 (1995).
[14]T. Kalvas, O. Tarvainen, H. Koivisto, and K. Ranttila, in Proceedings of ECRIS-2014, WEOMMH04, Nizhny Novgorod, Russia, 2014.

PIII

PHOTOELECTRON EMISSION EXPERIMENTS WITH ECR-DRIVEN MULTI-DIPOLAR NEGATIVE ION PLASMA SOURCE

by

Janne Laulainen, Taneli Kalvas, Hannu Koivisto, Risto Kronholm, Olli Tarvainen, Spyridon Aleiferis, and Panagiotis Svarnas

AIP Conference Proceedings **1869**, 020012 (2017)

Photoelectron Emission Experiments with ECR-driven Multi-dipolar Negative Ion Plasma Source

J. Laulainen[1,a)], T. Kalvas[1], H. Koivisto[1], R. Kronholm[1], O. Tarvainen[1], S. Aleiferis[2] and P. Svarnas[2]

[1]*University of Jyvaskyla, Department of Physics, Finland*

[2]*High Voltage Laboratory, Department of Electrical and Computer Engineering, University of Patras, Rion-Patras 26504, Greece*

[a)]Corresponding author: janne.p.laulainen@student.jyu.fi

Abstract. Photoelectron emission measurements have been performed using a 2.45 GHz ECR-driven multi-dipolar plasma source in a low pressure hydrogen discharge. Photoelectron currents induced by light emitted from ECR zone and H^- production region are measured from Al, Cu, Mo, Ta, and stainless steel (SAE 304) surfaces as a function of microwave power and neutral hydrogen pressure. The total photoelectron current from the plasma chamber wall is estimated to reach values up to 1 A for 900 W of injected microwave power. It is concluded that the volumetric photon emission rate in wavelength range relevant for photoelectron emission is a few times higher in arc discharge.

INTRODUCTION

It has been theoretically shown that in low temperature hydrogen plasmas at least 10% of heating power is dissipated via photon emission when at least 1% of the heating power is dissipated in ionization [1]. It has also been demonstrated experimentally that a significant fraction of plasma heating power is dissipated via vacuum ultraviolet (VUV) emission in arc discharge [2], ECR [3] and RF hydrogen plasmas [4]. Photons in the VUV range (wavelength < 150 nm) carry enough energy to induce a significant emission of photoelectrons (PE) when they impinge on a metal surface (typical work function 4–5 eV) on the plasma chamber wall [5]. Additional electrons produced by PE emission might have a considerable effect on plasma properties and especially on the formation of the plasma sheath. PE emission measurements with a filament driven hydrogen arc discharge ion source 'LIISA' have been reported earlier in Ref. [5]. In this paper PE emission measurements with the ECR-driven multi-dipolar plasma source 'Prometheus I' are reported and the results are compared to those obtained from the arc discharge.

A major difference between arc discharges and ECR discharges is the electron energy distribution (EED). In arc discharge plasmas, the EED spans from very low energies up to the energy corresponding to the cathode bias forming a rather uniform distribution [6]. In ECR plasmas, the EED is often considered Maxwellian. Although, two electron populations with temperatures of 1–5 eV and ≥ 10 eV can typically be identified [7]. The EED might have a notable effect on PE emission as the volumetric dissociation rate through electronic excitation to triplet states depends strongly on the EED. The dissociation rate itself affects the atomic to molecular hydrogen fraction in the discharge and, therefore, plays a crucial role on plasma emission spectrum. Even small changes in the light emission spectrum might have a considerable effect on the PE emission since the quantum efficiency for common metals is heavily dependent on photon energy [8, 9]. PE emission is predominantly caused by Lyman-alpha and Werner-band emission, because the quantum efficiency of common metals increases in the VUV range with decreasing wavelength of the incident radiation. The dissociation rate has been observed to be considerably higher in microwave-driven ion sources [3], whereas the EED in arc discharge leads to dominance of molecular excitation.

Fifth International Symposium on Negative Ions, Beams and Sources (NIBS 2016)
AIP Conf. Proc. 1869, 020012-1–020012-7; doi: 10.1063/1.4995718
Published by AIP Publishing. 978-0-7354-1549-2/$30.00

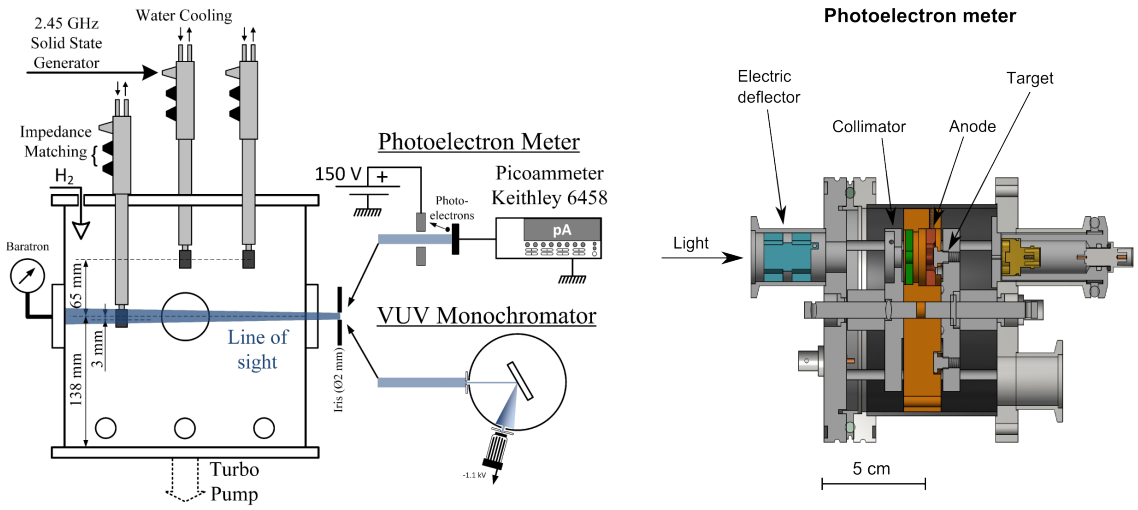

FIGURE 1. Setup for photoelectron emission measurements with 'Prometheus I' ion source and details of the photoelectron meter.

MEASUREMENT SETUP

The experimental setup is presented in Figure 1. The experimental data presented in this article were taken with the ECR-driven multi-dipolar plasma source Prometheus I [10] in a low pressure hydrogen discharge. The plasma is sustained by a 2D network of ECR plasma sources [11, 12]. Each elementary source consists of two parts: a cylindrical samarium-cobalt (Sm_2Co_{17}) permanent magnet, magnetized along its axis, and a coaxial line parallel to the magnetization vector, with an open end at the rear of the magnet. The sources are driven individually at 2.45 GHz by five solid state power supplies (0–180 W/elementary source). A tuner embedded on the main body of each source is used for impedance matching in order to minimize microwave power reflection (maximum accepted reflected power of 5 W). A turbo-molecular pump adapted under the bottom flange pumps the source down to $2 \cdot 10^{-6}$ Torr. High purity hydrogen is introduced by a digital mass flow controller (MKS 1179B) from the top flange to obtain a working pressure between 1 and 20 mTorr. The pressure is accurately monitored with an absolute pressure transducer (MKS Baratron 627D). The cubic plasma chamber (24 cm edge) is made from stainless steel (SS), and the central viewport that was used in the studies is located 138 mm above the bottom of the chamber.

The magnetic field of the source plays two roles for the application of negative ion production. Firstly, the necessary resonance zone with 875 G magnetic field intensity is created to satisfy the ECR condition. The ECR zone of Prometheus I is depicted in Ref. [10]. The second function is to confine hot electrons in the vicinity of the magnets

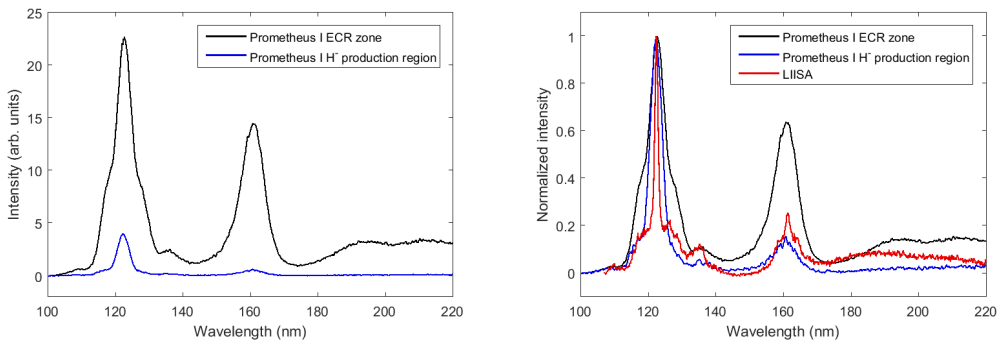

FIGURE 2. Measured VUV spectra of hydrogen plasmas in 'Prometheus I' and 'LIISA' ion sources.

and, in this respect, work as the magnetic filter of the source. The elementary sources are vertically movable, and in the experiments the source was used in two configurations. In the first, the photoelectron meter is looking to the H^- production region, 65 mm below the midplane of the ECR zones. In the second, the meter is looking to the ECR zones, 3 mm above the midplane of the ECR zones.

The spectra of the hydrogen plasma was measured from the central viewport in both configurations in order to obtain fundamental information of the VUV emission. In Figure 2, the VUV spectra measured from Prometheus I is presented and, for comparison, a corresponding spectrum from LIISA is also plotted. The apparent broadening of the Prometheus I VUV spectra in comparison to the one measured from the LIISA ion source is due to the different measurement geometry. In the case of Prometheus I the distance from the plasma to the entrance slit of the monochromator is 28 cm, which is significantly less than in the case of LIISA (1.5 m). Moreover, the light emission from the LIISA ion source is collimated by the extraction aperture far from the monochromator entrance slit as described in Ref. [2] whereas the iris in Prometheus I setup is located in the close proximity of the slit. Hence, the angular spread of the photons incident on the monochromator is larger for the Prometheus I setup, which results to decreased wavelength resolution of the VUV spectrum. The geometrical effects of the light source on VUV spectroscopy are described thoroughly in Ref. [13]. In the ECR zone, the electron temperature is higher, which results to higher Lyman-band and Werner-band emission compared to the H^- production region. In the H^- production region, Lyman-alpha dominates, which indicates higher dissociation degree compared to the ECR zone. In the ECR discharge, the EED has to be determined locally, since the heating power is dissipated to the plasma predominantly on the ECR surface and, consequently, the hot electron density is higher in the ECR zone. In arc discharge with a good magnetic confinement, plasma is heated more evenly by the thermally emitted electrons. A parametric study of VUV emission in Prometheus I is reported in Ref. [14].

The photoelectron meter is described in detail in Ref. [5]. Its cross sectional view is presented in Figure 1. On the first disc facing the plasma, a 2 mm collimator was adapted to limit the photon flux incident on the sample. The light that passes the collimator illuminates the sample (photocathode) which is grounded through a picoammeter (Keithley 6458) measuring the PE current. The sample is placed 120 mm away from the chamber wall or 240 mm away from the center of the ECR zone. The emitted electrons are collected with an anode ring located approximately 3 mm from the target and biased to +150 V with respect to the cathode i.e. laboratory ground. An aluminium plate, adapted on the first rotating disc, protects the sample from the VUV light when measurements are not being made. Samples are cleaned in atmospheric pressure, but they are covered with their natural oxides, which can give rise to VUV induced surface modification that can change the PE emission [15]. The measurements are performed in ion source relevant conditions, and within two hours of exposure the measured PE current was observed to vary less than 6%. The sample, which is adapted on a second rotating disc, can be changed during measurements without compromising the vacuum in order to study different materials. A parametric study is realized with materials typically used in negative hydrogen

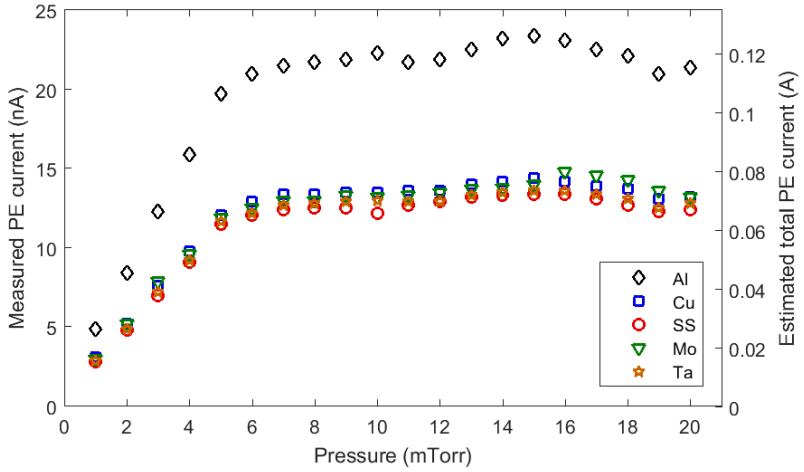

FIGURE 3. Photoelectron currents from different metal samples when the photoelectron meter is looking to the H^- production region. The power is maintained constant at 900 W (180 W/elementary source) and the pressure is varied.

ion sources as chamber materials (Al, Cu, SS) [16, 17, 18], filament materials (Ta) [19, 20], plasma grid materials (Mo) [21] or so-called collar materials (SS, Mo) [22, 23].

In the photoelectron meter, photons strike the sample with normal incidence whereas, in actual discharge chamber their angle of incidence covers a large solid angle. The mean free path for 10 eV VUV photons, corresponding to the dominant Lyman-alpha emission of hydrogen plasmas, varies in the range of 8–13 nm for the materials used in this study [24] while typical escape depth of photoelectrons is 1–3 nm [25]. Because the penetration depth of the photons exceeds the electron escape depth, it could be expected that the angle of incidence affects the quantum efficiency of the photoelectron emission at Lyman-alpha wavelength. However, it was confirmed with atomic-force microscopy that the peak-to-peak roughness of the sample surface exceeds 100 nm, which effectively randomizes the photon angle of incidence. Similar to the samples manufactured for this work, technical surfaces in ion sources are rough in the nanoscale and, thus, it is concluded that angular effects in photoelectric yield are probably insignificant in this case.

EXPERIMENTAL RESULTS

The measured PE emission and estimated total PE emission for Al, Cu, SS (SAE 304), Mo, and Ta samples for both source configurations is presented in Figures 3–6. In Figures 3 and 5, the variation of the PE current as a function of the filling gas pressure is plotted, while the power is maintained constant at 900 W (180 W/elementary source). In Figures 4 and 6, the PE current from all the samples is presented as a function of the microwave power per elementary source for four selected pressures. Much more light is emitted from the ECR zone compared to H^- production region and, thus, there is almost an order of magnitude difference in PE emission. The PE currents measured from Cu, SS, Mo, and Ta are approximately equal while the signal from Al is consistently about 50% higher. The fact that Al always has the highest PE current is most probably due to higher quantum efficiency in the VUV range.

The line-of-sight plasma volume covers only a few percent of the total plasma chamber volume. In order to estimate the total PE current from the internal surface of Prometheus I, the measurements need to to be extrapolated.

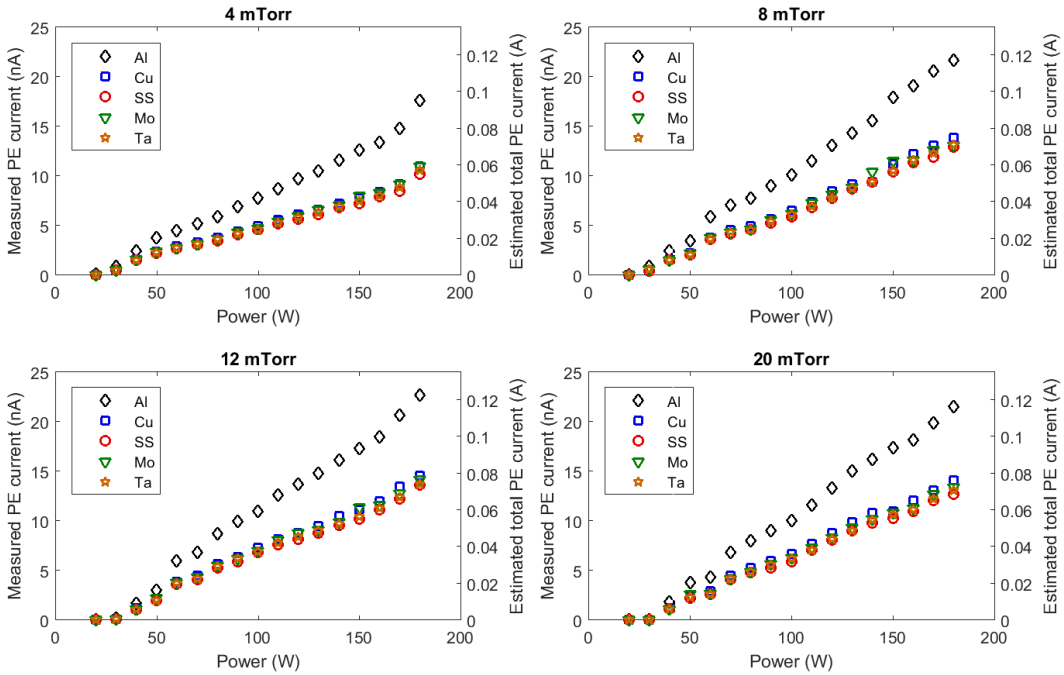

FIGURE 4. Photoelectron currents from different metal samples when the photoelectron meter is looking to the H^- production region. The power is varied in selected pressures.

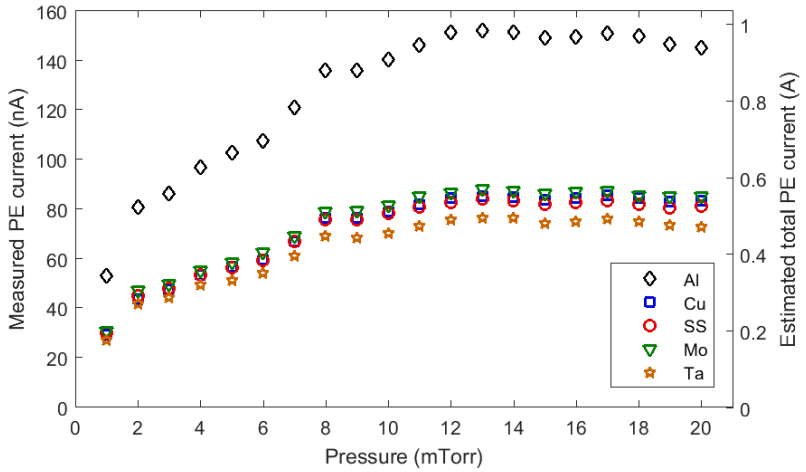

FIGURE 5. Photoelectron currents from different metal samples when the photoelectron meter is looking to the ECR zone. The power is maintained constant at 900 W (180 W/elementary source) and the pressure is varied.

Monte Carlo methods were used to calculate the probability for a single photon to reach the target surface. The total PE current is obtained by dividing the measured current with the given probability. In the simulations, the light emission profile is assumed homogeneous and isotropic across the plasma chamber profile. In reality, the spatial distribution of the plasma light emission rate depends on the inhomogeneous plasma density and temperature profiles. Without accurate information about the density and temperature profiles in the entire plasma volume the total PE flux can only be estimated. However, in the H^- production region, the plasma properties (as measured with a horizontally movable probe) show only low variation along the source width (typically: cold electron density 25%, cold electron temperature 15%, plasma potential 2%, and floating potential 15%) [26]. The estimated total PE current for the H^- production region is in the order of 0.1 A, which can be considered as the lower limit for the total PE emission. The estimated total PE emission reaches values of 1 A, when the ECR zone is in the line-of-sight, and this can be considered as a possible maximum current. The lower and upper limits are obtained assuming that the whole plasma chamber volume emits light corresponding to H^- production region and ECR zone, respectively.

DISCUSSION

It has been estimated from the measured data that the maximum PE current from the total internal surface of Prometheus I is on the order of 1 A for 900 W of injected microwave power. Taking into account the surface area of the Prometheus I plasma chamber this corresponds to PE emission of 0.3 $mAcm^{-2}$ per kW. This value can be compared to the previous measurement with the arc discharge source LIISA in which the PE current density is estimated to be three times higher for the same total power [5]. On the other hand, based on the PE measurements, the volumetric photon emission rate in wavelength range relevant for PE emission is concluded to be five times higher in the arc discharge. This indicates that the power efficiency is better in arc discharge compared to ECR discharge. However, the PE flux from the wall to the plasma is limited by the cusp magnetic field of LIISA, since the cross field diffusion of the emitted electrons in transverse magnetic field is significantly slower than their propagation along the field lines. In Prometheus I, the transverse magnetic field intensity is lower near the plasma chamber walls, and the emitted electrons are accelerated towards the plasma by the positive plasma potential. Secondary electron emission can be considered insignificant in comparison to PE emission, since the secondary electron emission yield is small for low energy electrons [27]. In Prometheus I, high energy electrons are captured near the ECR zone due to the magnetic field and electrons escaping from the plasma are also decelerated by the positive plasma potential.

The role of additional electrons to the plasma properties depends strongly on the energy of the electrons. Photoelectrons are emitted with all energies from zero up to the maximum energy, which corresponds to the difference between the energy of the absorbed photon and the surface work function. For common metals used in this study the

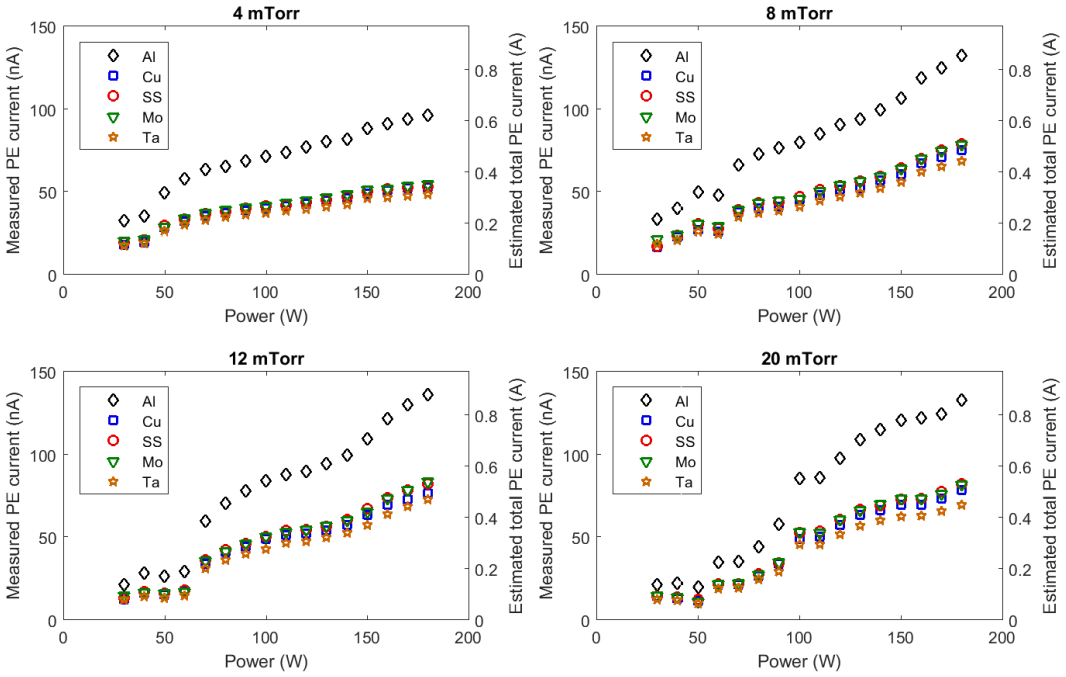

FIGURE 6. Photoelectron currents from different metal samples when the photoelectron meter is looking to the ECR zone. The power is varied in selected pressures.

work function is in the order of 4–5 eV. This is for clean surfaces, and the real work function of technical surfaces covered with their natural oxide and contaminants, typically found in ion sources, can be different. The emitted electrons are further accelerated by the plasma potential, which has been measured to be about 4–9 V (depending on the source parameters) in Prometheus I [28] and, thus, their final energies can reach approximately 15 eV. These electrons can contribute to various plasma processes, with threshold energies below 15 eV. These processes include dissociative electron attachment ($e_{cold} + H_2(X^1\Sigma_g^+; v'') \rightarrow H_2^-(^2\Sigma_u^+) \rightarrow H(1s) + H^-$) where low energy electrons (< 5 eV) are required, molecular excitation from the ground state ($X^1\Sigma_g^+; v'' = 0$) to $B^1\Sigma_u^+$ and $C^1\Pi_u^+$ singlet states (threshold energies approximately 12 eV [29]), excitation from the ground state to $a^3\Sigma_g^+$ and repulsive $b^3\Sigma_u^+$ triplet states (threshold about 12 eV and 8 eV, respectively [30]), and electron detachment ($e + H^- \rightarrow 2e + H$) which has a high cross section for energies higher than ~ 2 eV [30]. Altogether, the role of photoelectrons is not well known. For the source Prometheus I, which is characterized by an excess of vibrational states and a lack of cold electrons [28], it is possible that an additional source of electrons could only be beneficial.

There is a parametric correlation between PE emission and H^- production, as deduced from the correlation of negative ion density (by means of laser photodetachment) and VUV emission measurements under the same operating conditions [26]. This is probably due to the fact that PE emission is directly proportional to photon emission rate, which correlates to vibrational excitation and ionization. It has also been observed in probe measurements that the hot electron temperature is always about 15 eV in Prometheus I [28]. Thus, the parametric dependence of the PE emission is determined only by the variation of electron density.

ACKNOWLEDGMENTS

This work has been supported by the EU 7th framework programme “Integrating Activities – Transnational Access”, project number: 262010 (ENSAR) and by the Academy of Finland under the Finnish Centre of Excellence Programme 2012–2017 (Nuclear and Accelerator Based Physics Research at JYFL).

REFERENCES

[1] J. Komppula and O. Tarvainen, Phys. Plasmas **22**, p. 103516 (2015).
[2] J. Komppula, O. Tarvainen, S. Lätti, T. Kalvas, H. Koivisto, V. Toivanen, and P. Myllyperkiö, AIP Conf. Proc. **1515**, p. 66 (2013).
[3] J. Komppula, O. Tarvainen, T. Kalvas, H. Koivisto, R. Kronholm, J. Laulainen, and P. Myllyperkiö, J. Phys. D: Appl. Phys. **48**, p. 365201 (2015).
[4] U. Fantz, S. Briefi, D. Rauner, and D. Wünderlich, Plasma Sources Sci. Technol. **25**, p. 045006 (2016).
[5] J. Laulainen, T. Kalvas, H. Koivisto, J. Komppula, and O. Tarvainen, AIP Conf. Proc. **1655**, p. 020007 (2015).
[6] J. Bretagne, G. Delouya, C. Gorse, M. Capitelli, and M. Bacal, J. Phys. D: Appl. Phys. **18**, p. 811 (1985).
[7] S. Aleiferis and P. Svarnas, Rev. Sci. Instrum. **85**, p. 123504 (2014).
[8] B. Feuerbacher and B. Fitton, J. Appl. Phys. **43**, p. 1563 (1972).
[9] D. H. Dowell, F. K. King, R. E. Kirby, J. F. Schmerge, and J. M. Smedley, Phys. Rev. Accel. Beams **9**, p. 063502 (2006).
[10] S. Aleiferis, P. Svarnas, I. Tsiroudis, S. Béchu, M. Bacal, and A. Lacoste, IEEE Trans. Plasma Sci. **42**, 2828–9 (2014).
[11] A. Lacoste, T. Lagarde, S. Béchu, Y. Arnal, and J. Pelletier, Plasma Sources Sci. Technol. **11**, 407–412 (2002).
[12] S. Béchu *et al.*, Phys. Plasmas **20**, p. 101601 (2013).
[13] A. McPherson, N. Rouze, W. B. Westerveld, and J. S. Risley, Appl. Opt. **25**, 298–310 (1986).
[14] S. Aleiferis, J. Laulainen, P. Svarnas, O. Tarvainen, M. Bacal, and S. Béchu, In these proceedings.
[15] J. A. Ramsey and G. F. J. Garlick, Br. J. Appl. Phys. **15**, p. 1353 (1964).
[16] T. Kalvas, O. Tarvainen, J. Komppula, M. Laitinen, T. Sajavaara, H. Koivisto, A. Jokinen, and M. P. Dehnel, AIP Conf. Proc. **1515**, p. 349 (2013).
[17] K. R. Kendall, M. McDonald, D. R. Mosscrop, P. W. Schmor, D. Yuan, G. Dammertz, B. Piosczyk, and M. Olivo, Rev. Sci. Instrum. **57**, p. 1277 (1986).
[18] C. Courteille, A. M. Bruneteau, and M. Bacal, Rev. Sci. Instrum. **66**, p. 2533 (1995).
[19] T. Kuo, R. Baartman, G. Dutto, S. Hahto, J. Ärje, and E. Liukkonen, Rev. Sci. Instrum. **73**, p. 986 (2002).
[20] T. Kuo, D. Yuan, K. Jayamanna, M. McDonald, R. Baartman, P. Schmor, and G. Dutto, Rev. Sci. Instrum. **67**, p. 1314 (1996).
[21] W. Kraus, U. Fantz, P. Franzen, M. Fröschle, B. Heinemann, C. Martens, R. Riedl, and D. Wünderlich, AIP Conf. Proc. **1515**, p. 129 (2013).
[22] R. F. Welton *et al.*, AIP Conf. Proc. **1097**, p. 181 (2009).
[23] Y. An, B. Jung, and Y. S. Hwang, Rev. Sci. Instrum. **81**, p. 02A702 (2010).
[24] B. L. Henke, E. M. Gullikson, and J. C. Davis, At. Data Nucl. Data Tables **54**, p. 181 (1993).
[25] M. P. Seah and W. A. Dench, Surf. Interface Anal. **1**, p. 2 (1979).
[26] S. Aleiferis, O. Tarvainen, P. Svarnas, M. Bacal, and S. Béchu, J. Phys. D: Appl. Phys. **49**, p. 095203 (2016).
[27] V. Baglin, J. Bojko, O. Gröbner, B. Henrist, N. Hilleret, C. Scheuerlein, and M. Taborelli, Proceedings of EPAC 2000 p. 217 (2000).
[28] S. Aleiferis, "Experimental Study of the Production of H^- Negative Ions by Electron Cyclotron Resonance Plasmas," Ph.D. thesis, University of Patras, University of Grenoble 2016.
[29] J.-S. Yoon, M.-Y. Song, J.-M. Han, S. H. Hwang, W.-S. Chang, and B. Lee, J. Phys. Chem. Ref. Data **37**, p. 913 (2008).
[30] R. K. Janev, D. Reiter, and U. Samm, *Collision Processes in Low-Temperature Hydrogen Plasmas* (2003).

PIV

HYDROGEN PLASMA INDUCED PHOTOELECTRON EMISSION FROM LOW WORK FUNCTION CESIUM COVERED METAL SURFACES

by

Janne Laulainen, Spyridon Aleiferis, Taneli Kalvas, Hannu Koivisto, Risto Kronholm, and Olli Tarvainen

Physics of Plasmas **24**, 103502 (2017)

Hydrogen plasma induced photoelectron emission from low work function cesium covered metal surfaces

J. Laulainen,[1,a)] S. Aleiferis,[2] T. Kalvas,[1] H. Koivisto,[1] R. Kronholm,[1] and O. Tarvainen[1]
[1]*Department of Physics, University of Jyvaskyla, Jyvaskyla, Finland*
[2]*High Voltage Laboratory, Department of Electrical and Computer Engineering, University of Patras, Rion-Patras 26504, Greece*

(Received 28 July 2017; accepted 27 August 2017; published online 14 September 2017)

Experimental results of hydrogen plasma induced photoelectron emission from cesium covered metal surfaces under ion source relevant conditions are reported. The transient photoelectron current during the Cs deposition process is measured from Mo, Al, Cu, Ta, Y, Ni, and stainless steel (SAE 304) surfaces. The photoelectron emission is 2–3.5 times higher at optimal Cs layer thickness in comparison to the clean substrate material. Emission from the thick layer of Cs is found to be 60%–80% lower than the emission from clean substrates. *Published by AIP Publishing.* [http://dx.doi.org/10.1063/1.4998005]

I. INTRODUCTION

Negative hydrogen and deuterium ion sources are used in many applications, for example, neutral beam injection into fusion devices,[1] charge exchange injection into storage rings, e.g., in spallation neutron sources[2] and isotope production with cyclotrons.[3] H^-/D^- ions are produced *via* two predominant channels, dissociative electron attachment in the plasma volume and the surface production.[4] Surface production of negative hydrogen ions is based on electron tunneling from the conduction band of a metal to the affinity level of a hydrogen atom.[5] Cesium is commonly used in negative ion sources to enhance the surface production of negative ions by lowering the work function and thereby increasing the tunneling probability.[6–8] However, lowering the work function can also enhance the photoelectron (PE) emission induced by the plasma light emission, the effect of which has not been studied as extensively.

Theoretical calculations based on fundamental conservation laws and reaction cross sections show that at least 10% of plasma heating power is dissipated *via* photon emission in low temperature hydrogen plasmas.[9] The theoretical result is supported by experimental evidence showing that low temperature hydrogen plasmas are strong sources of vacuum ultraviolet (VUV) radiation with up to 15%–30% of the discharge power radiated at wavelengths of 120–250 nm in filament-driven arc discharge,[10] up to 8% of the injected microwave power at 80–250 nm in ECR discharge,[11] and up to 21% of RF power at 117–280 nm in RF discharge.[12]

Electrons in the conduction band of a metal follow the Fermi-Dirac distribution which can be used to derive the following relation for the quantum efficiency Y of the PE emission:[13]

$$\begin{aligned} Y &\propto \frac{(h\nu-\phi)^2}{(U_0-h\nu)^{1/2}}, && \text{when } h\nu \geq \phi, \\ &= 0, && \text{when } h\nu < \phi, \end{aligned} \tag{1}$$

where $h\nu$ is the energy of the photon, ϕ is the work function, and U_0 is the potential step at the surface–vacuum boundary. However, this relationship is accurate only for photon energies near the threshold, when electrons are emitted close to the surface and the quantum efficiency is not affected by the electron transport inside the metal lattice. Typical work functions of common metals are on the order of 4–5 eV. Adsorption of electropositive Cs atoms on a metal surface takes place by transfer of a valence electron to the conduction band of the metal.[14] As the Cs coverage on the surface increases, the work function decreases reaching a minimum value at 0.5–0.7 monolayer thickness. Beyond this, repulsive forces between dipole bonds lead to an increasing work function saturating to a value corresponding to bulk Cs at one monolayer thickness. An area density of 5.5×10^{14} Cs atoms per cm^2 corresponds to one monolayer.[15] The minimum work function ϕ_{min} of a cesiated metal surface can be estimated using a semiempirical expression[14]

$$\phi_{min} = 2.707 - 0.24\phi_0, \tag{2}$$

where ϕ_0 is the work function of uncesiated metal. Higher ϕ_0 results to lower ϕ_{min}, which is due to stronger electric field on the surface. The functional dependence of the work function on surface coverage θ can be estimated using a semiempirical expression[14]

$$\begin{aligned} \phi(\theta) \simeq\ & \phi_0 + \frac{6\,\Delta\phi_{min}}{(3-\theta_{min})\theta_{min}}\theta - \frac{3\,\Delta\phi_{min}(\theta_{min}+1)}{(3-\theta_{min})\theta_{min}^2}\theta^2 \\ & + \frac{2\,\Delta\phi_{min}}{(3-\theta_{min})\theta_{min}^2}\theta^3, \end{aligned} \tag{3}$$

where $\Delta\phi = \phi_{min} - \phi_0$ is the work function change and θ_{min} is the relative coverage corresponding to the minimum work function. Work function values suggested by Eq. (3), which have been shown to be in good accuracy with experimental data,[14] are plotted in Fig. 1 for different substrates (used in the experiments) with variable ϕ_0[16,17] with a choice of $\theta_{min} = 0.5$.

a)janne.p.laulainen@student.jyu.fi

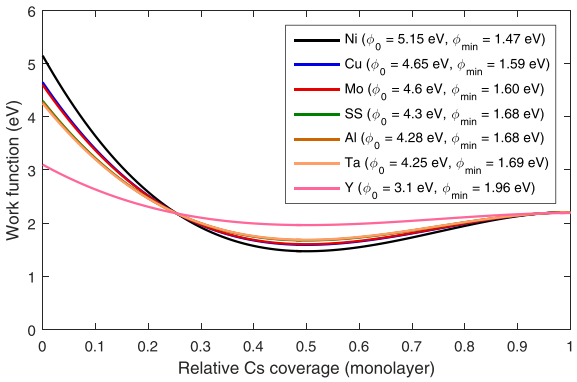

FIG. 1. Semiempirical relationship for the work function as a function of relative Cs coverage in monolayers on different substrates.

Quantified values for the work function of Cs covered metals are usually measured in ultra-high vacuum conditions.[17–20] However, in ion sources the surface is unavoidably exposed to higher neutral particle fluxes, plasma bombardment, and UV radiation which can affect the formation of the Cs layer. Furthermore, the high reactivity of Cs leads to formation of compounds, e.g., CsOH and Cs_2O, with the impurities present in all low temperature ion source plasmas. The thickness of the Cs layer and the level of surface impurities are determined by the balance between their deposition and adsorption rates. Hence, the surface conditions can have significant temporal variation especially in pulsed high power discharges.[21,22] Usually a continuous evaporation of Cs into the source is used to keep the surfaces "clean."[23–25] There are experimental results from a Penning type ion source showing notable transient lines of Cs compounds in the VUV spectra after plasma ignition.[26] It has been suggested that the involvement of Cs compounds in the Cs dynamics of the ion source is significant or even dominating in ion sources for neutral beam injection.[23] Therefore, work function values derived from the measurements performed at ultra-high vacuum conditions do not apply directly to ion sources, and the minimum work function measured under ion source relevant conditions is typically higher.[27] However, a work function of less than 1.91 eV, which is below the work function of solid Cs, has been measured with a 650 nm laser from a negative ion source converter surface.[28]

As the work function decreases with the build-up of the Cs layer, the PE quantum efficiency increases, since a wider range of hydrogen VUV emission spectrum is able to induce PE emission. Thus, an increase in the PE emission is expected with a buildup of a thin Cs layer. It has been shown that low temperature hydrogen plasma induced PE emission from clean metals is predominantly caused by radiation at wavelengths shorter than 150 nm,[29] i.e., Lyman-alpha (121.6 nm) and Werner-band (84–158 nm) emission, which is due to the wavelength dependence of the quantum efficiency first increasing towards shorter wavelengths and then decreasing at wavelengths below 50 nm.[30] The Lyman-alpha and Werner-band range have also been found to dominate the plasma emission spectral power in the filament-driven arc discharge.[10] It is not known how Cs deposition on a metal surface affects the quantum efficiency at this wavelength range, which motivates to study how hydrogen plasma induced PE emission is affected by the Cs deposition. The objective of the experiment is to quantify the change in hydrogen plasma induced PE emission as a function of the Cs coverage of a metal surface in ion source relevant conditions.

II. EXPERIMENTAL SETUP

The experimental setup is presented in Fig. 2. The measurements were performed with a filament-driven multi-cusp arc discharge plasma generator, which is a commonly used technology in volume production H^- ion sources, e.g., LIISA H^- ion source at JYFL.[31] The vacuum chamber is evacuated down to 10^{-8} mbar background pressure with a 880 ls^{-1} turbomolecular pump before introducing 99.9999% purity hydrogen into the discharge volume. 70 V/4 A arc discharge voltage/current (280 W discharge power) and a plasma chamber (hydrogen) pressure of 2×10^{-2} mbar were used in the measurements. It has been shown earlier that the PE current measured from clean metal samples increases linearly with the discharge power.[29] A VUV emission spectrum measured from the hydrogen plasma with a spectrometer consisting of a monochromator (McPherson model 234/302), holographic grating, and photomultiplier tube (ET Enterprises 9406B) is presented in Fig. 3.

The PE emission is measured from a remote sample, which is illuminated by light emitted from the arc discharge.

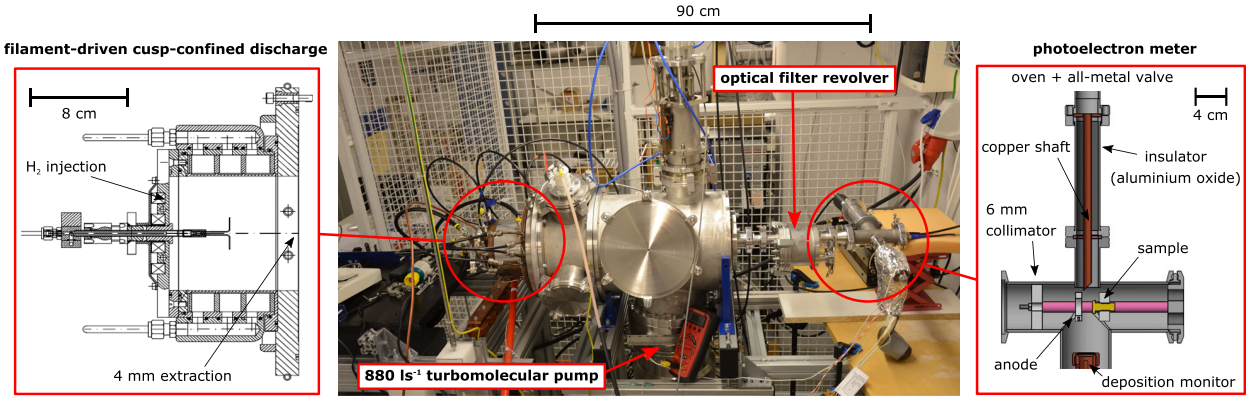

FIG. 2. The experimental setup with cross-sectional views of the plasma generator and the photoelectron meter.

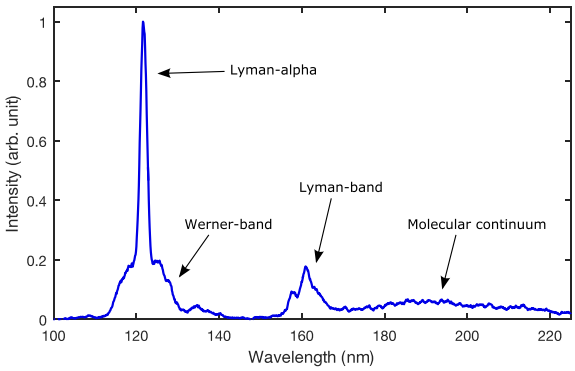

FIG. 3. VUV emission spectrum of the hydrogen plasma generator. The spectrum is not calibrated for spectral response.

It is not possible to measure the PE emission inside the plasma chamber, because the measured current would be affected by particle currents from various sources (plasma losses, secondary electron emission, etc.) making it impossible to determine the origin of electrons in the plasma. The PE current was measured with an updated version of a previous apparatus[29] with an integrated Cs oven and a deposition monitor. The light emitted by the hydrogen plasma passes through the extraction aperture (∅ 4 mm) of the plasma chamber and travels through the collimator (∅ 6 mm) and illuminates the sample (4 cm behind the collimator, 90 cm away from the plasma generator). The PE current is measured from the sample with a SRS SR570 preamplifier and National Instruments data acquisition system. The emitted electrons are collected with an anode ring located approximately 10 mm from the target and biased to +150 V with respect to the grounded cathode. The vacuum system includes an optical filter revolver that can be used to limit the wavelength range incident on the sample. A bandpass filter corresponding to Lyman-alpha (eSource Optics 25122FNB, 122 nm, FWHM 20 nm) was used to study the predominant part of the spectrum for PE emission. The transmittance of the filter is in the order of a few percent. The photons are impinging on the macroscopic sample surface on normal incidence. The angle of incidence does not affect the measured PE current since the peak-to-peak roughness of the sample surface is over 100 nm, which exceeds the mean free path for VUV photons and the escape depth of the PEs and, therefore, effectively randomizes the photon angle of incidence in the microscale.[32] It is not possible to estimate reliably the molecular/atomic hydrogen flux reaching the sample due to the gas feed and pumping arrangement. The sample temperature can be considered to be close to the ambient temperature. The sample is mechanically and chemically cleaned before the measurements. Metals chosen for substrate materials are typically used in negative hydrogen ion sources as chamber materials [Al, Cu, stainless steel (SS)],[33–35] filament materials (Ta),[31,36] plasma grid materials (Mo)[37] or so-called collar materials (SS, Mo).[38,39] Also Ni and Y were chosen as high and low work function materials, respectively.

The Cs oven is based on the Los Alamos design.[21] Cs is evaporated from the oven consisting of a flexible bellows, where the 1 g Cs ampoule is placed and broken inside the vacuum by bending the bellows, and an all-metal valve. The oven is connected to the vacuum system with a thermal insulator and Cs is supplied through a copper shaft. The oven is heated up to 200 °C and kept at a constant temperature as Cs evaporates onto the metal sample in the PE detector. An Inficon XTM/2 deposition monitor, placed next to the sample, was used to verify the accumulation of Cs, but absolute layer thickness on the sample was not measured.

III. RESULTS AND DISCUSSION

Figure 4 presents the PE current measured from the Mo sample while Cs is deposited on the sample surface. As Cs starts to evaporate, a significant increase in the PE current is observed. As the thickness of the Cs coverage grows, the PE current exhibits a double hump structure before starting to decrease. The PE current eventually saturates to a value, lower than the signal from a clean substrate that corresponds to bulk Cs. The PE current measured with the Lyman-alpha filter shows similar behavior as a function of Cs coverage on the substrate compared to the current measured without a filter.

The observations can be qualitatively explained by the decreasing work function of the surface, and by comparison of the photon penetration depth within the Cs layer and the metal substrate to the escape depth of the PEs. It is clearly noticeable that the work function change, illustrated in Fig. 1, alone does not explain the observed behavior of the PE emission. The mean free path for 10 eV VUV photons, which is the average energy for the predominant part of the spectrum, is 10 nm in Mo while the penetration depth in Cs is 13 μm.[40] This means that photons interact predominantly with the Mo substrate even at a considerable Cs layer thickness. With a thin layer of Cs, the work function is lowered and thus the PE yield is higher, as long as the emitted electrons are able to propagate through the Cs layer with sufficient energy. Typical escape depth of PEs with energies of a few eV is 1–3 nm.[41] If the Cs layer is too thick, the PE current is limited by the short escape depth of the electrons, although the work function is lower for bulk Cs in comparison to Mo. The weaker PE emission from bulk Cs compared

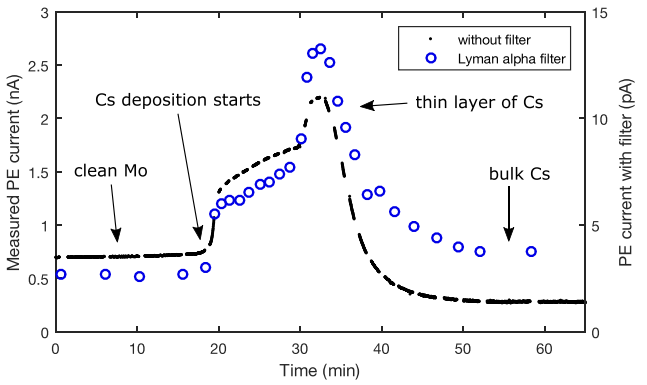

FIG. 4. Measured photoelectron current from the Mo sample as a function of time (i.e., Cs coverage on the surface) by exposing the sample to the whole emission spectrum of the hydrogen plasma (left axis) and by applying the Lyman-alpha filter (right axis). Gaps in the data correspond to filtered measurements.

to clean Mo can be attributed to at least two factors. One is the long mean free path of photons in Cs *versus* the short escape depth of PEs and the other is the lower density of conduction band electrons in Cs (Fermi energy 1.59 eV[42]) in comparison to Mo (Fermi energy 5.32 eV[43]) It was confirmed with the deposition monitor that the observed transition was indeed caused by a thin layer of Cs, since a change in the PE signal was observed before measuring any detectable signal with the deposition monitor, which has a resolution of 0.01 nm. The measurements are repeatable with less than 12% variation in the maximum gain with optimal Cs layer thickness as measured with Mo and Al samples in four independent measurements per sample. The repeatability includes variable evaporation rates, which presumably affects the concentration of Cs compounds on the sample surface. Uneven Cs distribution on the substrate can create patches with different PE quantum efficiency causing nonhomogeneity of the PE emission.[44,45] These patches can be caused by local nonuniformity of the substrate due to different crystal faces, roughness, contamination, etc. However, the characteristic dimension of the irradiated surface area (∅ 6 mm) is much larger than the surface roughness (peak-to-peak over 100 nm) and the dimensions of the possible patches. Thus, it can be expected that the patch effect is averaged over multiple measurements and included in the uncertainty probed by repeated measurements.

Figure 5 presents the measured absolute PE currents from different substrates [Mo, Al, Cu, Ta, SS (SAE 304), Y, and Ni] as Cs is deposited on the surface. The horizontal axes have been normalized with the Cs deposition rate for easier comparison, because even a small change in the oven temperature has a significant impact on the deposition rate. Clean substrate materials have variable work functions in the range of 3.1–5.15 eV,[16,17] while the mean free path for 10 eV VUV photons varies in the range of 8–13 nm.[40] The observed behavior in the PE current transition is similar for all the substrate materials. The PE current is 2–3.5 times higher at optimal Cs layer thickness compared to the clean substrate material. Y has the lowest work function of all the substrates (3.1 eV) and, thus, has the smallest change in the work function due to Cs deposition as suggested by Eq. (2). Y also has the smallest increase in PE current by Cs deposition. Ni,

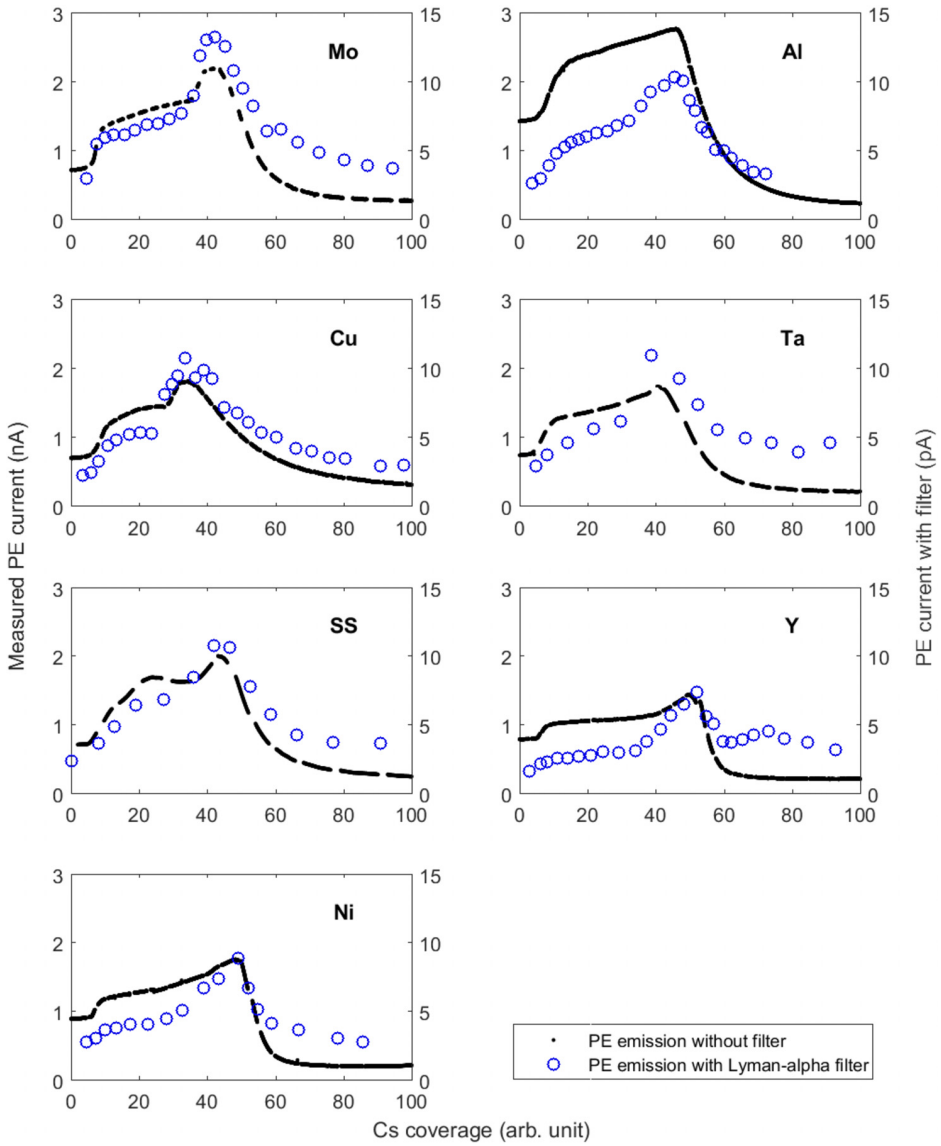

FIG. 5. Measured photoelectron currents from different substrates as a function of Cs coverage by exposing the sample to the whole emission spectrum of the hydrogen plasma (left axes) and by applying the Lyman-alpha filter (right axes).

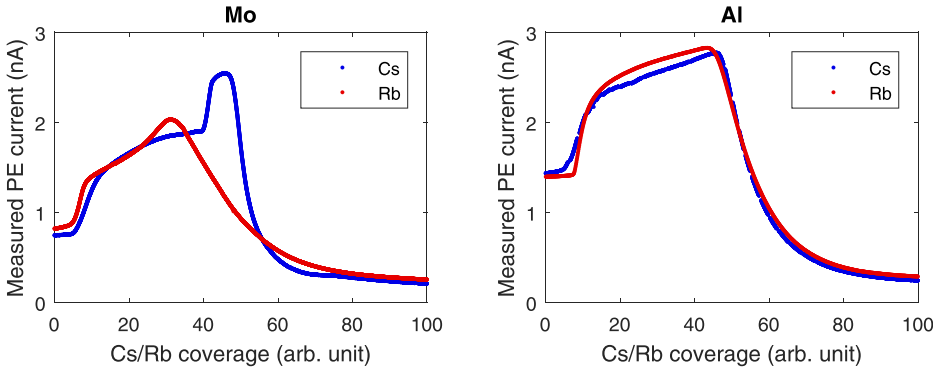

FIG. 6. Measured photoelectron currents from Mo and Al substrates as a function of Cs and Rb coverage.

which has the highest work function (5.15 eV), behaves similar to the other substrate materials, which have work functions between 4 and 5 eV. With all the substrates the PE current saturates to the same value, which is 60%–80% lower than the starting value, supporting the conclusion that the emission is from bulk Cs. The relative difference in the PE current measured with the Lyman-alpha filter in proportion to the PE current measured without a filter has somewhat different values for different metals. The ratio also changes as a function of the Cs coverage. This is believed to be due to the functional dependence of the PE emission quantum efficiency on the photon energy with varying work function.[30,46]

Rb was used as an alternative alkali metal to confirm the results obtained with Cs. The work function of Rb (2.16 eV) is almost as low as the work function of Cs (2.14 eV).[16] A comparison of PE emission from Mo and Al substrates as a function of Cs and Rb coverage is presented in Fig. 6. In four independent measurements for both alkali metals on Mo substrate, the increase factor in PE current from the clean substrate to maximum current was 3.4 for Cs and 2.6 for Rb on average. Based on two independent measurements with Rb on Al, it is concluded that the PE emission from Rb covered Al is practically the same as for Cs covered Al. The PE current saturates to the same value with both alkali metals, i.e., low temperature hydrogen plasma induced PE emission from bulk Cs and bulk Rb are identical. The comparison of the two alkali metals also suggests that their impurity compounds with different chemical properties play a minor role in determining the PE current.

The role of PEs in plasmas is not well known as they might have a considerable effect on various plasma processes depending on the intensity and the energy distribution of the emitted electrons. In addition to the energy of the absorbed photon, the final energy distribution of the emitted electrons is determined by the plasma sheath structure, i.e., (positive) plasma potential and a possible virtual cathode. A virtual cathode can be formed, if the emission of electrons (and negative ions) from the wall is high enough to prevent the compensation of the space charge by incoming positive ions.[47,48] If the virtual cathode exists, it limits the transport of the low energy PEs to the plasma, but does not change the energy of the PEs that reach the plasma as the sheath potential forms between the conducting chamber wall and bulk plasma. The emitted electrons may have an impact on the volumetric rates of the dissociative electron attachment ($e_{cold} + H_2(X^1\Sigma_g^+; v'') \rightarrow H_2^-(^2\Sigma_u^+) \rightarrow H(1s) + H^-$) which has a large cross section for vibrationally excited molecules at low electron energies (around 1 eV), electron detachment ($e + H^- \rightarrow 2e + H$) which has a large cross section for energies higher than ~2 eV,[49] molecular excitation from the ground state to $a^3\Sigma_g^+$ and repulsive $b^3\Sigma_u^+$ triplet states (threshold of about 12 and 8 eV, respectively[49]) excitation from the ground state ($X^1\Sigma_g^+; v'' = 0$) to $B^1\Sigma_u^+$ and $C^1\Pi_u^+$ singlet states (threshold approximately 12 eV[50]) and molecular ionization (threshold 16 eV[50]). Nevertheless, processes with threshold energies higher than the difference between the energy of the absorbed photon and the surface work function are possible only if the emitted electrons with energies ranging from 0 to $h\nu - \phi$ are accelerated to sufficient energy across the plasma sheath by the plasma potential.

In the filament-driven arc discharge, the total PE current from the plasma chamber walls has been estimated to be in the order of 1 A per kW of discharge power, which corresponds to almost 10% of the arc current of 14 A at 70 V discharge voltage.[29] A thin layer of alkali metal can increase the PE emission by a factor of 2–3.5 at optimal layer thickness. The results obtained in this study suggest that the PE emission especially from cesiated surfaces should be considered to be included in plasma simulations, in which the plasma surface interaction is taken into account.[51] This is especially true for surface production ion sources used for neutral beam injection, in which the Cs covered multiaperture extraction grid covers a large area exposed to VUV photons.[52,53] The formation of the virtual cathode requires few hundred Am^{-2} of negative ion current density and, due to lower space charge of electrons, it can be assumed that the PE current density needs to be higher by an order of magnitude to impact the sheath structure. Nevertheless, the effect of PEs on the plasma sheath structure may be significant for example in Penning type ion sources,[54] where a few kW discharge power is deposited into a small plasma volume ($<1\,cm^3$), which can lead to high PE emission density from the walls as a significant part of the injected power is dissipated *via* photon emission.[9–12] On the contrary, in neutral beam injection sources the current density can be expected to be smaller, but this does not exclude the PEs effect on the reaction rates.

ACKNOWLEDGMENTS

This work has been supported by the Academy of Finland under the Finnish Centre of Excellence Programme

2012–2017 (Nuclear and Accelerator Based Physics Research at JYFL) and the European Union's Horizon 2020 research and innovation programme under Grant Agreement No. 654002.

[1]R. Hemsworth, H. Decamps, J. Graceffa, B. Schunke, M. Tanaka, M. Dremel, A. Tanga, H. P. L. De Esch, F. Geli, J. Milnes *et al.*, Nucl. Fusion **49**, 045006 (2009).
[2]S. Henderson, W. Abraham, A. Aleksandrov, C. Allen, J. Alonso, D. Anderson, D. Arenius, T. Arthur, S. Assadi, J. Ayers *et al.*, Nucl. Instrum. Methods Phys. Res. A **763**, 610 (2014).
[3]T. J. Ruth, Rep. Prog. Phys. **72**, 016701 (2008).
[4]M. Bacal, Nucl. Fusion **46**, S250 (2006).
[5]B. Rasser, J. N. M. van Wunnik, and J. Los, Surf. Sci. **118**, 697 (1982).
[6]Y. I. Belchenko, G. I. Dimov, and V. G. Dudnikov, Nucl. Fusion **14**, 113 (1974).
[7]V. G. Dudnikov, Rev. Sci. Instrum. **63**, 2660 (1992).
[8]B. S. Lee and M. Seidl, Appl. Phys. Lett. **61**, 2857 (1992).
[9]J. Komppula and O. Tarvainen, Phys. Plasmas **22**, 103516 (2015).
[10]J. Komppula, O. Tarvainen, S. Lätti, T. Kalvas, H. Koivisto, V. Toivanen, and P. Myllyperkiö, AIP Conf. Proc. **1515**, 66 (2013).
[11]J. Komppula, O. Tarvainen, T. Kalvas, H. Koivisto, R. Kronholm, J. Laulainen, and P. Myllyperkiö, J. Phys. D: Appl. Phys. **48**, 365201 (2015).
[12]U. Fantz, S. Briefi, D. Rauner, and D. Wünderlich, Plasma Sources Sci. Technol. **25**, 045006 (2016).
[13]R. H. Fowler, Phys. Rev. **38**, 45 (1931).
[14]G. D. Alton, Surf. Sci. **175**, 226 (1986).
[15]P. W. van Amersfoort, "Formation of negative ions on a metal surface," Ph.D. thesis (FOM-Institute for Atomic and Molecular Physics, Amsterdam, 1985).
[16]H. B. Michaelson, J. Appl. Phys. **48**, 4729 (1977).
[17]R. G. Wilson, J. Appl. Phys. **37**, 3161 (1966).
[18]R. G. Wilson, J. Appl. Phys. **37**, 4125 (1966).
[19]L. W. Swanson and R. W. Strayer, J. Chem. Phys. **48**, 2421 (1968).
[20]T. A. Callcott and A. U. Mac Rae, Phys. Rev. **178**, 966 (1969).
[21]O. Tarvainen, Nucl. Instrum. Methods Phys. Res. A **601**, 270 (2009).
[22]D. C. Faircloth, S. R. Lawrie, A. P. Letchford, C. Gabor, M. Whitehead, T. Wood, and M. Perkins, AIP Conf. Proc. **1390**, 205 (2011).
[23]R. Friedl, "Experimental investigations on the caesium dynamics in H_2/D_2 low temperature plasmas," Ph.D. thesis (Max-Planck-Institut für Plasmaphysik (IPP), Garching, Germany, 2013).
[24]U. Fantz, P. Franzen, and D. Wünderlich, Chem. Phys. **398**, 7 (2012).
[25]R. Gutser, D. Wünderlich, U. Fantz, and the N-NBI Team. Plasma Phys. Controlled Fusion **53**, 105014 (2011).
[26]D. Faircloth, S. Lawrie, A. Letchford, C. Gabor, M. Perkins, M. Whitehead, T. Wood, O. Tarvainen, J. Komppula, T. Kalvas *et al.*, AIP Conf. Proc. **1515**, 359 (2013).
[27]R. Friedl and U. Fantz, AIP Conf. Proc. **1655**, 020004 (2015).
[28]H. Yamaoka, M. Sasao, M. Wada, and H. J. Ramos, Nucl. Instrum. Methods Phys. Res. B **36**, 227 (1989).
[29]J. Laulainen, T. Kalvas, H. Koivisto, J. Komppula, and O. Tarvainen, AIP Conf. Proc. **1655**, 020007 (2015).
[30]B. Feuerbacher and B. Fitton, J. Appl. Phys. **43**, 1563 (1972).
[31]T. Kuo, R. Baartman, G. Dutto, S. Hahto, J. Ärje, and E. Liukkonen, Rev. Sci. Instrum. **73**, 986 (2002).
[32]J. Laulainen, T. Kalvas, H. Koivisto, R. Kronholm, O. Tarvainen, S. Aleiferis, and P. Svarnas, AIP Conf. Proc. **1869**, 020012 (2017).
[33]T. Kalvas, O. Tarvainen, J. Komppula, M. Laitinen, T. Sajavaara, H. Koivisto, A. Jokinen, and M. P. Dehnel, AIP Conf. Proc. **1515**, 349 (2013).
[34]K. R. Kendall, M. McDonald, D. R. Mosscrop, P. W. Schmor, D. Yuan, G. Dammertz, B. Piosczyk, and M. Olivo, Rev. Sci. Instrum. **57**, 1277 (1986).
[35]C. Courteille, A. M. Bruneteau, and M. Bacal, Rev. Sci. Instrum. **66**, 2533 (1995).
[36]T. Kuo, D. Yuan, K. Jayamanna, M. McDonald, R. Baartman, P. Schmor, and G. Dutto, Rev. Sci. Instrum. **67**, 1314 (1996).
[37]W. Kraus, U. Fantz, P. Franzen, M. Fröschle, B. Heinemann, C. Martens, R. Riedl, and D. Wünderlich, AIP Conf. Proc. **1515**, 129 (2013).
[38]R. F. Welton, M. P. Stockli, S. N. Murray, D. Crisp, J. Carmichael, R. H. Goulding, B. Han, O. Tarvainen, T. Pennisi, and M. Santana, AIP Conf. Proc. **1097**, 181 (2009).
[39]Y. An, B. Jung, and Y. S. Hwang, Rev. Sci. Instrum. **81**, 02A702 (2010).
[40]B. L. Henke, E. M. Gullikson, and J. C. Davis, At. Data Nucl. Data Tables **54**, 181 (1993).
[41]M. P. Seah and W. A. Dench, Surf. Interface Anal. **1**, 2 (1979).
[42]N. W. Ashcroft and N. D. Mermin, *Solid State Physics* (Holt, Rinehart and Winston, 1976).
[43]A. Marikani, *Materials Science* (PHI Learning Private Limited, 2017).
[44]E. J. Montgomery, "Characterization of quantum efficiency and robustness of cesium-based photocathodes," Ph.D. thesis (University of Maryland, College Park, Maryland, USA, 2009).
[45]K. L. Jensen, P. G. O'Shea, and D. W. Feldman, Phys. Rev. ST Accel. Beams **13**, 080704 (2010).
[46]D. H. Dowell, F. K. King, R. E. Kirby, J. F. Schmerge, and J. M. Smedley, Phys. Rev. ST Accel. Beams **9**, 063502 (2006).
[47]R. McAdams, D. B. King, A. J. T. Holmes, and E. Surrey, Rev. Sci. Instrum. **83**, 02B109 (2012).
[48]H. Amemiya, B. M. Annaratone, and J. E. Allen, J. Plasma Phys. **60**, 81 (1998).
[49]R. K. Janev, D. Reiter, and U. Samm, *Collision processes in low-temperature hydrogen plasmas*, Vol. Juel-4105 of Berichte des Forschungszentrums Jülich. Forschungszentrum, Zentralbibliothek, Jülich (2003).
[50]J.-S. Yoon, M.-Y. Song, J.-M. Han, S. H. Hwang, W.-S. Chang, and B. Lee, J. Phys. Chem. Ref. Data **37**, 913 (2008).
[51]A. Hatayama, Rev. Sci. Instrum. **79**, 02B901 (2008).
[52]Y. Takeiri, Rev. Sci. Instrum. **81**, 02B114 (2010).
[53]B. Heinemann, H.-D. Falter, U. Fantz, P. Franzen, M. Froeschle, W. Kraus, C. Martens, R. Nocentini, R. Riedl, E. Speth, and A. Staebler, Fusion Eng. Des. **86**, 768 (2011).
[54]D. C. Faircloth, S. Lawrie, A. P. Letchford, C. Gabor, P. Wise, M. Whitehead, T. Wood, M. Westall, D. Findlay, M. Perkins *et al.*, Rev. Sci. Instrum. **81**, 02A721 (2010).

PV

PHOTOELECTRON EMISSION INDUCED BY LOW TEMPERATURE HYDROGEN PLASMAS

by

Janne Laulainen, Taneli Kalvas, Hannu Koivisto, Risto Kronholm, and Olli Tarvainen

Accepted for publication in AIP Conference Proceedings (2018)

Photoelectron Emission Induced by Low Temperature Hydrogen Plasmas

Janne Laulainen[1,a)], Taneli Kalvas[1], Hannu Koivisto[1], Risto Kronholm[1] and Olli Tarvainen[1]

[1] *University of Jyvaskyla, Department of Physics, Finland*

[a)] Corresponding author: janne.p.laulainen@student.jyu.fi

Abstract. Experimental results of low temperature hydrogen plasma induced photoelectron emission measurements comparing two different plasma heating methods are summarized. By exposing the samples to the vacuum ultraviolet radiation of a filament-driven multi-cusp arc discharge ion source and a 2.45 GHz microwave-driven ion source, it has been measured that the total photoelectron emission from various metal surfaces is on the order of 1 A per kW of plasma heating power, which can be increased by a factor of 2–3.5 with a thin layer of alkali metal. The possible effects of the photoelectrons on the plasma sheath structure are studied with a 1D collisionless model extended to include the contribution of photoelectron emission from the surface.

INTRODUCTION

Low temperature hydrogen plasmas of positive (H^+, H_2^+, D^+) and negative (H^-, D^-) ion sources are strong sources of vacuum ultraviolet (VUV) radiation dissipating up to 30 % of the heating power through VUV emission [1, 2, 3, 4]. Plasma induced photoelectron (PE) emission from metal surfaces is a source of free electrons potentially affecting the ion source plasma properties. We have carried out measurements aiming at quantifying the PE emission induced by low temperature hydrogen plasmas. The fundamental data can be used e.g. for improving numerical simulation models to predict the performances of various kinds of plasma devices.

Intense VUV radiation is emitted by hydrogen plasmas as a consequence of electronic transitions from excited states to lower states of neutral atoms and molecules. Typical VUV emission spectra of hydrogen plasmas are presented in Fig. 1. The Lyman-alpha line at 121.6 nm corresponds to the transition from the first excited state to the ground state of atomic hydrogen. The Werner-band originates from the resonant $C^1\Pi_u \rightarrow X^1\Sigma_g^+$ transitions in the singlet system of the hydrogen molecule, the dominant part of the emission being found at wavelengths shorter than 130 nm. The dominant part of Lyman-band emission originating from $B^1\Sigma_u^+ \rightarrow X^1\Sigma_g^+$ transitions is in the wavelength range of 130–170 nm. The molecular continuum from the $a^3\Sigma_g^+ \rightarrow b^3\Sigma_u^+$ transition of the triplet system is assigned to wavelengths longer than 170 nm. It has been experimentally shown that the PE emission is predominantly induced by VUV emission at wavelengths shorter than 150 nm [5] as indicated by the quantum efficiency of PE emission also plotted in Fig. 1.

This paper summarizes and compares the results of the PE emission measurements performed with a filament-driven multi-cusp arc discharge ion source presented in detail in ref. [5] and with a 2.45 GHz ECR-driven microwave ion source presented in detail in ref. [3]. A major difference between the two plasma heating methods is the resulting electron energy distribution function (EEDF). In arc discharge, the EEDF spans from very low energies up to the energy corresponding to the cathode bias forming a rather uniform distribution [6]. In ECR plasmas, the EEDF is often considered (bi-)Maxwellian [7]. The EEDF influences the VUV emission by affecting the volumetric rates of electronic excitations to singlet and triplet systems of the H_2 molecules and the resulting dissociation degree. Also, the effect of PEs on the plasma sheath structure is evaluated hereafter using a model developed by McAdams et al. [8], which is extended by including the PE current density to the surface emission.

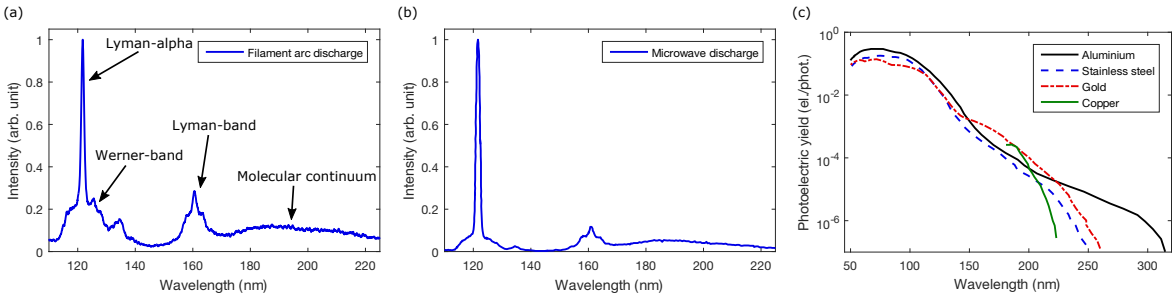

FIGURE 1. (a) Typical VUV emission spectrum of hydrogen plasma of a filament arc discharge (from Ref. [5]) and (b) of a microwave discharge (from Ref. [3]). The spectra are not corrected for spectral transmittance. (c) Photoelectric yield quantum efficiencies for aluminium, stainless steel, gold (from Ref. [9]) and copper (from Ref. [10]).

EXPERIMENTAL METHODS

Hydrogen plasma induced PE emission has been measured from clean (filament and microwave discharges) and cesiated (filament discharge) surfaces of molybdenum, aluminium, copper, tantalum, stainless steel (SAE 304), yttrium, and nickel, using a remote sample illuminated by the plasma light. The measurement setup is presented schematically in Fig. 2. The measurement geometry and conditions are described in detail in Ref. [5]. The distance between the sample and the plasma varied in the two setups, being approximately 1.5 m with the filament source and 0.5 m with the microwave source. Measuring the PE emission directly inside the plasma chamber is not possible, since the measured current would be affected by particle currents from various sources (plasma losses, secondary electron emission, etc.) making it impossible to determine the origin of collected charges. The PE current measured from a remote sample can be considered to give the lower limit for the PE emission inside the plasma chamber, because VUV can be partly absorbed between the sample and the plasma and exposure to VUV and hydrogen plasma can increase the quantum efficiency of the PE emission [10]. The samples, like all the surfaces in ion sources, are technical materials, which are rough in the nanoscale. The sample surface has to be large enough compared to the surface roughness and characteristic dimensions of the variation of different crystal faces etc. in order to measure the average emission. Sample preparation, which included mechanical and chemical cleaning, was performed in atmospheric pressure, and thus the surfaces were covered with their natural oxides and typical vacuum contaminants. The vacuum chamber was evacuated down to 10^{-8} mbar background pressure before introducing 99.9999 % purity hydrogen into the discharge volume. With the remote sample, VUV induced surface aging was observed to change the PE emission slightly.

Monte Carlo methods can be applied to derive an estimate for the total PE current (density), emitted from the walls of the plasma chamber, from the PE current measured with the remote sample. The probability for a single photon to reach the sample surface is calculated and the measured current is divided with the given probability. In the simulation, the light emission profile is assumed homogeneous and isotropic across the plasma chamber volume, which yields the maximum value for the PE emission. In reality, the spatial distribution of the plasma light emission rate depends on the plasma density and temperature profiles. For example, in microwave discharges, the light emission distribution depends on the magnetic field configuration, incident microwave power, and neutral gas pressure [11].

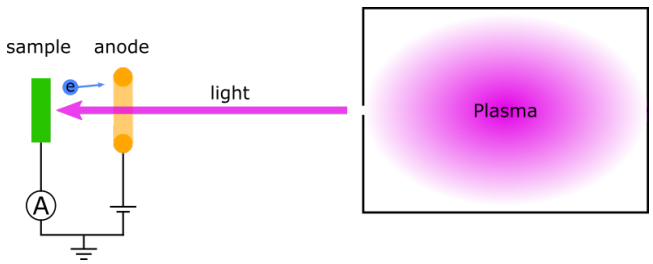

FIGURE 2. Schematic picture of the experimental setup for photoelectron emission measurements.

TABLE 1. Estimated total photoelectron emission. The presented range corresponds to measured PE current variations with different metals (Al, Ta, Mo, Cu, and stainless steel). The current density is determined by scaling the total PE current with the geometry of the particular ion source and, thus, depends directly on the surface area of the plasma chamber.

	PE current (AkW^{-1})	**PE current density ($AkW^{-1}m^{-2}$)**
filament arc discharge	0.8–1.2	7–11
microwave discharge	0.9–1.6	20–33

Without accurate information about the density and temperature profiles the total PE emission can only be estimated. It can be argued that the total VUV emission, and hence the PE emission, is most often at least 50 % of the given maximum [2].

EXPERIMENTAL RESULTS

Table 1 summarizes the estimated total PE currents and PE current densities per kW of injected power for filament and microwave discharges. In both cases, the PE current depends linearly on the discharge power. The presented range corresponds to measured PE current variations with different metals, and the current density is directly proportional to the surface area of the plasma chamber. In the case of microwave discharge the estimated total PE emission is slightly higher. The EEDF in the microwave source results to preferential excitation to the triplet states, which leads to higher dissociation rate in comparison to the arc discharge. The volumetric dissociation rate (via $b^3\Sigma_u^+$ state) is calculated to be $2.8–12 \times 10^{16}$ $cm^{-3}s^{-1}$ for the microwave source [3] and $1.8–4.2 \times 10^{15}$ $cm^{-3}s^{-1}A^{-1}$ for the filament source [12]. The higher dissociation rate and the subsequent Lyman-alpha emission can explain the higher PE emission observed in the microwave source due to high quantum efficiency at Lyman-alpha wavelength (Fig. 1). The VUV emission spectra measured from both ion sources are presented in Fig. 1, where it can be seen that in the spectrum of the microwave discharge the Lyman-alpha peak is higher than the Werner-band and Lyman-band emissions (relative intensities) in comparison to the filament discharge. It can be assumed, due to the higher power efficiency of the filament source in comparison to the microwave source [2, 3, 12], that the results presented in Table 1 correspond to the minimum difference between the different plasma heating methods.

The effect of alkali metal coverage (Cs and Rb) on the PE emission has been studied with a filament discharge [13]. As an example, Fig. 3 presents the measured PE current from Ta sample during and after Cs deposition. A thin layer of alkali metal increases the PE emission 2–3.5 times in comparison to clean substrate. Emission from thick layer of alkali metal is 60–80 % lower than the emission from clean substrate. Due to the long penetration depth of 10 eV photons in Cs (3.9 μm [14]) in comparison to Ta (8 nm [14]) it is argued that the photons interact predominantly with the Ta substrate even at considerable Cs layer thickness. The work function is lowered by the accumulation of the alkali metal, and thus the PE yield is higher, as long as the emitted electrons are able to propagate through the deposited layer with sufficient energy. The decreasing PE current at thicker layer can be attributed to the short escape depth of the PEs (1-3 nm for few eV electrons [15]) in comparison to the penetration depth of VUV photons. As the Cs deposition is seized the PE current starts to increase again reaching another maximum before saturation. The so

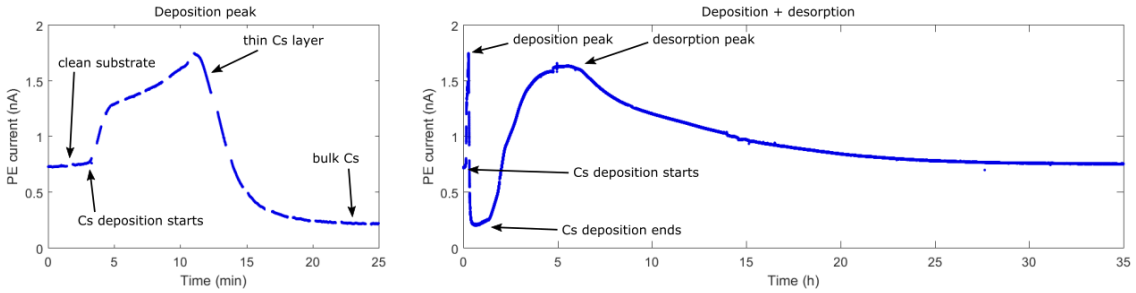

FIGURE 3. Measured photoelectron current from Ta sample with Cs deposition peak shown on the left and both deposition and desorption peaks on the right.

called desorption peak is also observed with photocathodes and is believed to be caused by diffusion and desorption of Cs [16]. In ion sources, the Cs layer is often replenished by constant evaporation. The aim is to sustain a sub-monolayer thickness. However, the minimum measured work function is typically higher than the tabulated values for pure Cs [17].

EXTENSION OF THE SHEATH MODEL

The PE emission may have an impact on the volumetric rates of various plasma processes depending on the intensity and the energy distribution of the emitted electrons. The evaluation of PEs effect on the reaction rates would require the use of a global model. In addition to the plasma chemistry, PE emission can affect the plasma sheath structure, which also determines the final energy of the emitted electrons. A virtual cathode can be formed, if the emission of electrons (and negative ions) from the wall is high enough to prevent the compensation of the space charge by incoming positive ions [8]. If the virtual cathode exists, it limits the transport of surface produced negative ions and the emitted PEs into the plasma depending on their energies. If the PE emission increases the depth of the virtual cathode, it can be considered as a potential limitation for the surface production of negative ions.

PEs effect on the plasma sheath structure is predicted using a one-dimensional analytical model of the sheath in a negative ion source [8]. The collisionless model does not take into account the magnetic field. The model is modified to include PE emission from the wall by substituting the H^- current density j_{H^-} with effective current density

$$j_{\mathrm{eff}} = j_{H^-} + \int_0^{h\nu-\phi} j_{\mathrm{PE}}(E_{\mathrm{PE}}) \sqrt{\frac{m_{\mathrm{e}}}{m_{H^-}}} \sqrt{\frac{E_{H^-}}{E_{\mathrm{PE}}}}\, \mathrm{d}E_{\mathrm{PE}}, \tag{1}$$

where j_{PE} is the PE current density, m_{e} electron mass, m_{H^-} negative hydrogen ion mass, E_{PE} PE energy, and E_{H^-} negative hydrogen ion energy. A uniform energy distribution ranging from zero to the maximum energy, which corresponds to the difference between the energy of the absorbed photon $h\nu$ and the surface work function ϕ, is used for PEs with $h\nu = 10$ eV and $\phi = 2$ eV corresponding to approximate work function of a cesiated surface. The actual energy distribution of the emitted electrons is unknown. The measured PE current corresponds to the total emission caused by wide range of photon energies. The energy of the emitted electrons also depends on the photon interaction with electrons deeper (than the Fermi level) in the conduction band and on the processes taking place within the material after the actual photon–electron interaction. The measured VUV spectra (e.g. in Fig. 1) together with the quantum efficiencies reported in the literature cannot be used to derive the interaction probability nor the PE energy distribution, because the spectra are not calibrated for spectral response. Thus, an approximation, such as a uniform distribution, must be used. Following Ref. [8] a constant energy of 0.7 eV is assumed for surface produced negative hydrogen ions and the plasma density, electron temperature and positive ion temperature are set to 3.5×10^{17} m^{-3}, 2 eV and 0.8 eV, respectively. It is assumed that there are no volume produced negative ions.

The potential difference between the emitting surface and the plasma, referred as the cathode potential, plays a major role in the significance of the PE emission on the sheath properties. In Fig. 4 the plasma sheath potential is plotted for different cathode potentials with various emission currents. The black line shows the sheath structure at the threshold H^- emission current density creating a virtual cathode. The red line presents the sheath structure with PE current density needed (in addition to H^- current density) for the depth of the virtual cathode to reach 10 % of

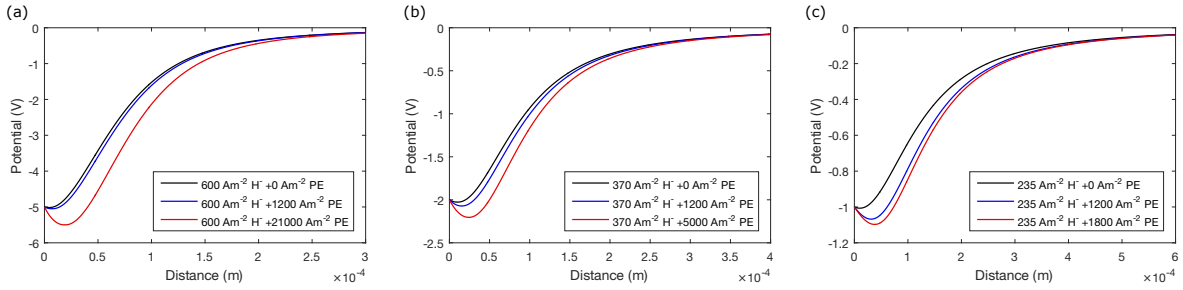

FIGURE 4. Sheath potentials for various H^- and photoelectron emission current densities with cathode potentials of (a) −5 V (b) −2 V (c) −1 V.

the cathode potential. The blue line presents the sheath structure with a constant PE current density of 1200 Am^{-2} demonstrating that the PE emission has a more significant impact on the sheath structure with lower cathode potentials. In H^- ion sources, the plasma electrode is usually biased positively, resulting in decreased potential difference between the plasma and the electrode, in order to reduce the co-extracted electron current [18], which presumably affects the significance of the PE emission.

Are the PE current densities in Fig. 4 realistic? The experimental results suggest that the total PE current from cesiated plasma chamber walls could be as high as 3.5 A per kW of discharge power. For example, in a surface production ion source used for neutral beam injection (ELISE), the plasma is heated with the maximum RF power of 360 kW and the illuminated plasma grid area is 0.9 m^2 [18]. Direct extrapolation from 3.5 AkW^{-1} yields a total PE current density of 140–420 Am^{-2}, if 10–30 % of the emitted light is incident on the grid. On the other hand, the corresponding estimate for a Penning type ion source with up to 3.85 kW of discharge power dissipated in < 1 cm^3 sized plasma contained in a chamber with a surface area of 2.48×10^{-4} m^2 [19], yields a PE current density of 54 kAm^{-2}. In the ion sources used for the PE emission measurements, the light emission depends linearly on discharge power. However, this cannot automatically be assumed to hold for high power ion sources. The realization of a PE emission density needed for a significant influence on the plasma sheath structure depends on the mechanical design of the plasma device, plasma heating method and the discharge power. It can be concluded, that if the order of magnitude for the PE current density reaches 1 kAm^{-2} and the cathode potential is low, the PE emission can be significant for the plasma sheath structure.

ACKNOWLEDGMENTS

This work has been supported by the Academy of Finland under the Finnish Centre of Excellence Programme 2012–2017 (Nuclear and Accelerator Based Physics Research at JYFL) and European Union's Horizon 2020 research and innovation programme under grant agreement No. 654002.

REFERENCES

[1] J. Komppula and O. Tarvainen, Phys. Plasmas **22**, p. 103516 (2015).
[2] J. Komppula, O. Tarvainen, S. Lätti, T. Kalvas, H. Koivisto, V. Toivanen, and P. Myllyperkiö, AIP Conf. Proc. **1515**, p. 66 (2013).
[3] J. Komppula, O. Tarvainen, T. Kalvas, H. Koivisto, R. Kronholm, J. Laulainen, and P. Myllyperkiö, J. Phys. D: Appl. Phys. **48**, p. 365201 (2015).
[4] U. Fantz, S. Briefi, D. Rauner, and D. Wünderlich, Plasma Sources Sci. Technol. **25**, p. 045006 (2016).
[5] J. Laulainen, T. Kalvas, H. Koivisto, J. Komppula, and O. Tarvainen, AIP Conf. Proc. **1655**, p. 020007 (2015).
[6] J. Bretagne, G. Delouya, C. Gorse, M. Capitelli, and M. Bacal, J. Phys. D: Appl. Phys. **18**, p. 811 (1985).
[7] V. A. Godyak, IEEE Trans. Plasma Sci. **34**, p. 755 (2006).
[8] R. McAdams, A. J. T. Holmes, D. B. King, and E. Surrey, Plasma Sources Sci. Technol. **20**, p. 035023 (2011).
[9] B. Feuerbacher and B. Fitton, J. Appl. Phys. **43**, p. 1563 (1972).
[10] D. H. Dowell, F. K. King, R. E. Kirby, J. F. Schmerge, and J. M. Smedley, Phys. Rev. ST AB **9**, p. 063502 (2006).
[11] O. D. Cortázar, A. Megía-Macías, A. Vizcaíno-de Julián, O. Tarvainen, J. Komppula, and H. Koivisto, Rev. Sci. Instrum. **85**, p. 02A902 (2014).
[12] J. Komppula and O. Tarvainen, Plasma Sources Sci. Technol. **24**, p. 045008 (2015).
[13] J. Laulainen, S. Aleiferis, T. Kalvas, H. Koivisto, R. Kronholm, and O. Tarvainen, Phys. Plasmas **24**, p. 103502 (2017).
[14] B. L. Henke, E. M. Gullikson, and J. C. Davis, At. Data Nucl. Data Tables **54**, p. 181 (1993).
[15] M. P. Seah and W. A. Dench, Surf. Interface Anal. **1**, p. 2 (1979).
[16] E. J. Montgomery, "Characterization of quantum efficiency and robustness of cesium-based photocathodes," Ph.D. thesis, University of Maryland, College Park, Maryland, USA. 2009.
[17] R. Friedl and U. Fantz, AIP Conf. Proc. **1655**, p. 020004 (2015).
[18] U. Fantz, P. Franzen, B. Heinemann, and D. Wünderlich, Rev. Sci. Instrum. **85**, p. 02B305 (2014).
[19] D. C. Faircloth and S. Lawrie, private communication (2013).